

Modeling Neural Switching via Drift-Diffusion Models

Nicholas Marco *

Department of Statistical Science, Duke University, Durham, NC, USA.

and

Jennifer M. Groh †

Department of Neurobiology, Duke University, Durham, NC, USA.

and

Surya T. Tokdar

Department of Statistical Science, Duke University, Durham, NC, USA.

October 2, 2024

*Corresponding Author: nicholas.marco@duke.edu

†Jennifer M. Groh has an additional primary appoint in the Department of Psychology and Neuroscience, and secondary appointments in the Departments of Computer Science and Biomedical Engineering.

Abstract

Neural encoding, or neural representation, is a field in neuroscience that focuses on characterizing how information is encoded in the spiking activity of neurons. Currently, little is known about how sensory neurons can preserve information from multiple stimuli given their broad receptive fields. Multiplexing is a neural encoding theory that posits that neurons temporally switch between encoding various stimuli in their receptive field. Here, we construct a statistically falsifiable single-neuron model for multiplexing using a competition-based framework. The spike train models are constructed using drift-diffusion models, implying an integrate-and-fire framework to model the temporal dynamics of the membrane potential of the neuron. In addition to a multiplexing-specific model, we develop alternative models that represent alternative encoding theories (normalization, winner-take-all, subadditivity, etc.) with some level of abstraction. Using information criteria, we perform model comparison to determine whether the data favor multiplexing over alternative theories of neural encoding. Analysis of spike trains from the inferior colliculus of two macaque monkeys provides tenable evidence of multiplexing and offers new insight into the timescales at which switching occurs.

Keywords: Point Process, Drift Diffusion Process, Integrate-and-fire Model, Neural Encoding, Spike Train, Multiplexing

1 Introduction

The primary function of sensory neurons is to encode information from stimuli into action potentials (spikes), which will be transmitted throughout the central nervous system. Neural coding theory posits that information is encoded in the firing rate (Adrian and Zotterman, 1926), neuronal variability (Stein et al., 2005), and the coordination between neurons (Ebitz and Hayden, 2021; Saxena and Cunningham, 2019). A central interest in neural coding theory is understanding how neurons encode information from multiple stimuli in the receptive field, which is defined as the area in which a neuron will fire if a stimulus is present. When multiple stimuli are in the receptive field of a neuron, it has been suggested that normalization (Carandini and Heeger, 2012), subadditivity (Goris et al., 2024), or winner-take-all (Chen, 2017) schemes occur; leading to questions of how information from distinct stimuli is preserved and how scalable these schemes are when multiple stimuli are present.

A theory known as multiplexing (Caruso et al., 2018; Mohl et al., 2020; Jun et al., 2022; Schmehl et al., 2024; Groh et al., 2024) posits that individual neurons can switch between encoding the different stimuli over time, causing a fluctuating pattern of the firing rate. Multiplexing is a scalable encoding scheme that offers a clear explanation of how information from the distinct stimuli is preserved. To gain insight into how multiple stimuli are encoded, neuroscientists have obtained extracellular recordings of neurons from various brain regions, under various triplets of conditions, such as the triplet shown in Figure 1. A triplet of conditions consists of a set of trials recorded under the A condition (A stimulus only), a set of trials recorded under the B condition (B stimulus only), and a set of trials recorded under the AB condition (A and B stimuli concurrently). Using the spike trains obtained under the A condition and the B condition as benchmarks, our aim is to determine whether the spike trains obtained under the AB condition provide supporting evidence for multiplexing.

To further this aim, Chen et al. (2024) created a statistical framework to determine if trial-wise spike count data supported multiplexing activity. As illustrated in Figure 2, the framework assumes that the A condition and B condition spike counts are Poisson

Sound Localization Task (Caruso et al. 2018)

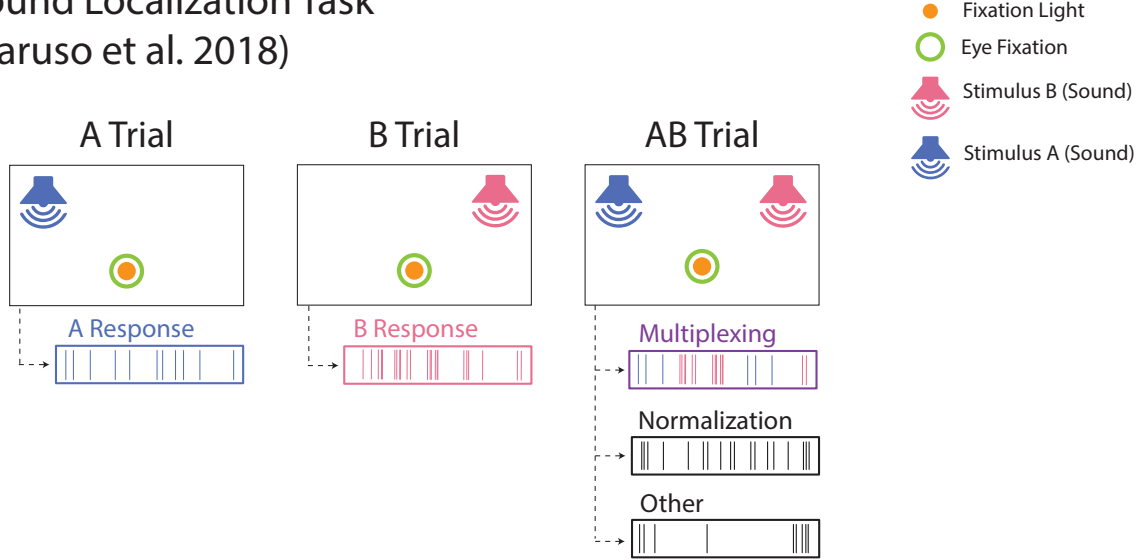
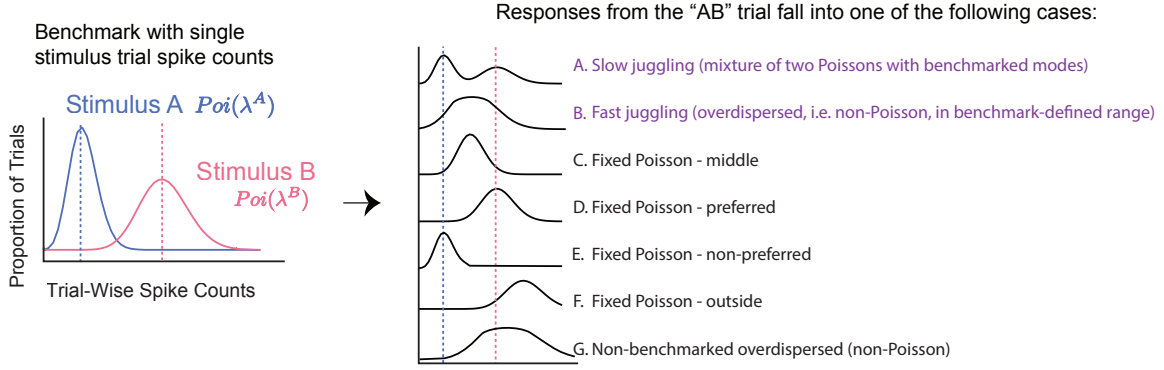


Figure 1: Diagram of the stimuli used in Caruso et al. (2018), along with synthetic spike trains illustrating possible neural encodings for the dual stimuli (AB condition).

distributed, and aims to categorize the AB response as one of seven different responses. The seven categories are indicated by the letters A through G in Figure 2, with purple representing the categories in which multiplexing is believed to possibly occur. However, a spike count analysis relies solely on the aggregate number of spikes within a trial; requiring a more granular level of analysis to determine whether multiplexing occurs on a time scale shorter than the duration of the trial. This is apparent in Figure 2, as both the IIGPP model (non-multiplexing) and the Competition model (multiplexing) can generate spike count distributions that would be classified as fast juggling (B) and non-benchmarked overdispersed (G). To achieve a more granular level of analysis, Glynn et al. (2021) developed the dynamic admixture point process (DAPP) model. The DAPP model used spike train data to model within-trial fluctuating patterns in neuronal firing rates under the AB condition. Although DAPP is capable of modeling fluctuating firing patterns, it is not a generative model specific to multiplexing; making it challenging to ascertain whether a neuron is multiplexing and providing minimal information about the time-scale of any potential switching. In addition, both the DAPP model and the trial-wise spike count

Conceptual Spike Count Approach (Chen et al. 2024):



Conceptual Spike Train Approach:

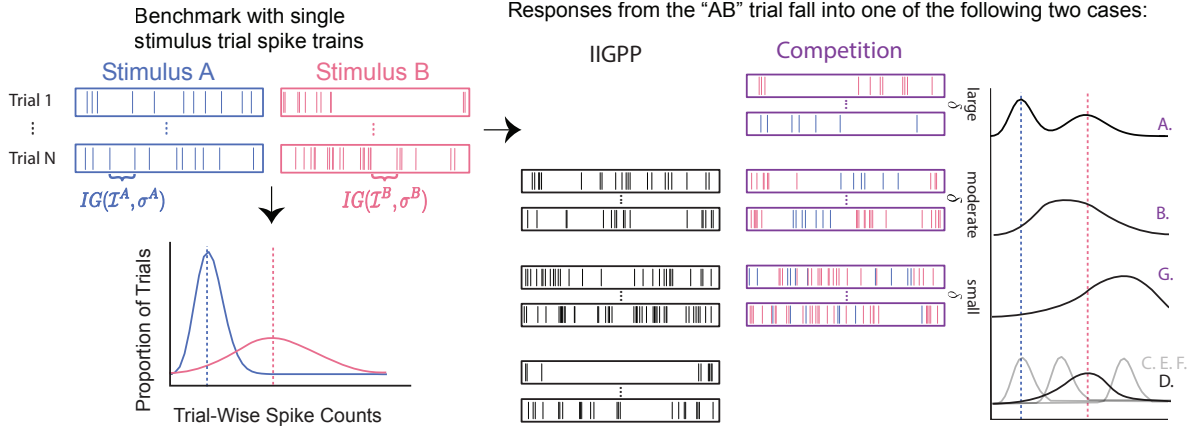


Figure 2: Illustrative differences in the spike count approach used in [Chen et al. \(2024\)](#) and the proposed spike train approach. The visualization of the spike train approach demonstrates how two distinct frameworks can result in identical spike count distributions, highlighting the necessity for a more granular approach.

framework rely on Poisson assumptions, which often necessitates discarding a considerable number of triplets before analysis of the data. Since neuronal variability is a central idea in neural coding theory, there is a crucial need for more flexible models; allowing for the analysis of bursty neurons (overdispersed spike count distribution) and regular neurons (underdispersed spike count distribution).

In this manuscript, we aim to construct a generative model for multiplexing allowing for direct inference into the timescale of switching. Specifically, we start by using the data generated under the single-stimulus trials to define probabilistic models for the neural

response to each stimuli. These single-stimulus models will help define the competition model for multiplexing, which will be fit using the spike trains recorded under the *AB* condition (dual stimuli). We will also fit an alternative model, which we will call the inhomogeneous inverse Gaussian point process (IIGPP) model, which represents a wide class of alternative neural coding theories (normalization, winner-takes-all, ect.) with a greater level of abstraction. Once we fit the competition model and the IIGPP model, we will conduct model comparison to gain insight into whether multiplexing can explain the observed spike trains under the *AB* condition over alternative theories. The overall conceptual approach can be visualized in Figure 2. Crucially, this model will be able to account for neural variability; allowing for more expressive models and the ability to model more of the triplets compared to previous statistical frameworks.

The manuscript begins with an overview of integrate-and-fire models and accumulator models, which then leads to the proposed generative model for multiplexing and the IIGPP model in Section 2. Novel MCMC methods to efficiently conduct posterior inference, as well as methods to conduct Bayesian model comparison between the IIGPP model and the competition model, can be found in Section 3. Section 4 continues with a simulation study evaluating the recovery of model parameters and posterior predictive distributions of scientific interest under various sample sizes. In Section 5, we use our statistical framework to gain insight into the behavior of neurons in various brain regions of macaque monkeys; comparing the results to the previous results of [Chen et al. \(2024\)](#). Lastly, we conclude this manuscript with a discussion in Section 6; comparing our framework to alternative frameworks and discussing potential improvements upon this framework.

2 Statistical Models for Spike Trains

2.1 Integrate-and-Fire Models

Integrate-and-fire models are mathematical models that characterize the temporal dynamics of the membrane potential of a neuron as a function of membrane conductance, passive leakage of the membrane potential, synaptic input to the neuron, and current injected into

the neuron by an intracellular electrode (Burkitt, 2006). Integrate-and-fire models typically model the temporal dynamics of the membrane potential through a set of differential equations with varying degrees of computational complexity and biophysical realism.

The use of leaky integrate-and-fire models (Geisler and Goldberg, 1966; Roy and Smith, 1969) and, more recently, generalized leaky integrate-and-fire models (Teeter et al., 2018; Liu and Wang, 2001) have been shown to be computationally scalable models that can accurately reproduce neural behavior. The general form of a leaky integrate-and-fire model can be expressed as the following stochastic differential equation:

$$dV(t) = [-g(t)(V(t) - V_0) + I(t)] dt + \sigma dW(t), \quad (1)$$

where $V(t)$ denotes the membrane voltage, V_0 denotes the resting potential, $g(t)$ represents the membrane conductance, $I(t)$ represents the input current, and $W(t)$ denotes a Wiener process (Burkitt, 2006; Paninski et al., 2009). The generation of an action potential, or spike, usually occurs when the membrane voltage crosses some voltage threshold V_{th} . Once the membrane voltage crosses the threshold, the membrane voltage returns to the resting potential ($V(t) = V_0$). As specified in Equation 1, the leaky integrate-and-fire model typically assumes that $g(\cdot)$ is a non-negative function and that $I(\cdot)$ is a positive function. If we simplify the model by assuming constant membrane conductance ($g(t) = g$) and constant input current ($I(t) = I$), then the model becomes an Ornstein–Uhlenbeck process (Uhlenbeck and Ornstein, 1930). Furthermore, if we assume that there is no membrane conductance ($g(t) = 0$), then we have a Wiener process with drift.

The leaky integrate-and-fire model specified in Equation 1 can also be used to model spike trains. Given a diffusion process representing the voltage process, the interspike interval times (ISIs), or the time between consecutive action potentials, can be modeled as first passage times. Although the leaky integrate-and-fire model induces a distribution on the ISIs, the distribution cannot be expressed in an analytic form. However, if we assume the simplified model with no membrane conductance and constant input current (perfect integrator model), we can express the distribution of the ISIs in analytic form. The perfect integrator model can be expressed as the following stochastic differential equation:

$$dV(t) = Idt + \sigma dW(t). \quad (2)$$

By using the perfect integrator model, it can be shown that the ISIs are Inverse Gaussian distributed with mean parameter $\mu = \frac{V_{th}-V_0}{I}$ and shape parameter $\lambda = \left(\frac{V_{th}-V_0}{\sigma}\right)^2$ (Folks and Chhikara, 1978). Let $\mathcal{S}_i := \{S_{i1}, \dots, S_{in_i}\}$ be the spike train of the i^{th} observation for $i = 1, \dots, N$. The i^{th} ISI can be defined as $X_{ij} := S_{ij} - S_{i(j-1)}$ for $i = 1, \dots, N$ and $j = 1, \dots, n_i$, where $S_{i0} = 0$. Assuming the perfect integrator model, we have $X_{ij} \sim IG\left(\frac{V_{th}-V_0}{I}, \left(\frac{V_{th}-V_0}{\sigma}\right)^2\right)$, where the probability density function of X_{ij} is

$$f(x_{ij} \mid I, \sigma, V_{th}, V_0) = \frac{V_{th} - V_0}{\sigma \sqrt{2\pi x_{ij}^3}} \exp\left(-\frac{((V_{th} - V_0) - Ix_{ij})^2}{2\sigma^2 x_{ij}}\right), \quad (3)$$

for $i = 1, \dots, N$ and $j = 1, \dots, n_i$.

Although intracellular activity of neurons can be captured using methods such as the patch-clamp method (Noguchi et al., 2021), extracellular recording techniques are much more common due to the relative ease of obtaining recordings and the relatively low cost (Chorev et al., 2009). In extracellular recordings, we typically are only able to obtain spike times and are unable to recover any information on the temporal dynamics of the neuron's membrane potential. Thus, the temporal dynamics of the membrane potential are considered to be a latent diffusion process that produces the spike trains obtained from the extracellular recordings.

As specified in Equation 3, it is apparent that some of the model parameters are unidentifiable. To construct an identifiable model, we assume that $V_{th} - V_0 = 1$. To allow time-inhomogeneous firing rates, we will allow the input current of the voltage process to change once an action potential occurs. Specifically, letting $V_{ij}(t)$ be the voltage process associated with X_{ij} , we assume that $dV_{ij}(t) = \mathcal{I}(S_{i(j-1)})dt + \sigma dW(t)$, where $S_{ij} := \sum_0^j X_{ij}$. Thus, we have that the probability density function of X_{ij} is

$$f(x_{ij} \mid \mathcal{I}(\cdot), \sigma, s_{i(j-1)}) = \frac{1}{\sigma \sqrt{2\pi x_{ij}^3}} \exp\left(-\frac{(1 - \mathcal{I}(s_{i(j-1)})x_{ij})^2}{2\sigma^2 x_{ij}}\right), \quad (4)$$

for $i = 1, \dots, N$ and $j = 1, \dots, n_i$. Although this construction allows for time-inhomogeneous firing rates, this construction is not as flexible as assuming voltage processes that have time-varying input currents (i.e. $dV_{ij}(t) = I_{ij}(t)dt + \sigma dW(t)$). However, by assuming a constant

voltage, we maintain a computationally tractable model while allowing for the possibility of time-inhomogeneous firing rates over the experimental time window.

Compared to using a Poisson process, the inverse Gaussian point process does not assume that the ISI coefficient of variation (ISI-CV) is equal to one. Therefore, we are able to model neurons that are burstier (ISI-CV > 1) or more regular (ISI-CV < 1) than neurons that can be represented by a Poisson process (Kass et al., 2014). Modeling neural spike trains with an inverse Gaussian point process is well-supported from a biophysical standpoint, as it can be formulated through an integrate-and-fire framework that models the temporal dynamics of a neuron’s membrane potential. As a result, the inhomogeneous inverse Gaussian point process framework will serve as the foundation for both the non-multiplexing and multiplexing models.

2.2 A Competition Model for Two Stimuli

Section 2.1 presented a suitable way to model the spike trains generated from a single stimulus condition. However, studies have shown that neurons can have a fluctuating spiking pattern when multiple stimuli are in the receptive field (Kayser et al., 2009; Caruso et al., 2018; Glynn et al., 2021; Schmehl et al., 2024; Shi et al., 2023). In this manuscript, we propose using the accumulator model framework to account for the fluctuating neuronal firing patterns found in spike trains recorded under the *AB* condition.

Accumulator models (Ratcliff and Smith, 2004; Gold and Shadlen, 2007; Ratcliff and McKoon, 2008; Paulon et al., 2021) are a class of models that are commonly used to model multicategory decision tasks. Accumulator models typically use diffusion processes to model the accumulation of evidence over time for different possible decisions. Under the accumulator model framework, each diffusion process has a corresponding boundary, and the first process to reach its corresponding boundary is the decision chosen. Typically, the decisions that were chosen in these multicategory decision studies are known from the experiment, and the goal is to make inference on the latent diffusion processes. In this manuscript, we propose modeling the fluctuating firing behavior of a neuron under the *AB* condition through a competition-style framework, similar to the accumulator model

framework.

In our experimental setup, we observe spike trains under three different conditions (A, B, AB) , consisting of combinations of two different stimuli (stimulus A and stimulus B). In this manuscript, we will let $\mathcal{H} \in \{A, B, AB\}$ denote one of the three conditions and let $\mathcal{S} \in \{A, B\}$ denote one of the two stimuli. Let $\mathcal{S}_i^{\mathcal{H}} = \{S_{i1}^{\mathcal{H}}, \dots, S_{in_i^{\mathcal{H}}}^{\mathcal{H}}\}$ be the i^{th} spike train generated under the condition \mathcal{H} for $i = 1, \dots, N^{\mathcal{H}}$ and $\mathcal{H} = A, B, AB$. Let $X_{ij}^{\mathcal{H}} := S_{ij}^{\mathcal{H}} - S_{i(j-1)}^{\mathcal{H}}$ be the corresponding interspike intervals. Using the model specified in Equation 4 for spike trains generated under a single stimulus, we have that the probability density function of $X_{ij}^{\mathcal{S}}$ is

$$f_{X^{\mathcal{S}}}(x_{ij}^{\mathcal{S}} \mid \mathcal{I}^{\mathcal{S}}(\cdot), \sigma^{\mathcal{S}}, s_{i(j-1)}^{\mathcal{S}}) = \frac{1}{\sigma^{\mathcal{S}} \sqrt{2\pi(x_{ij}^{\mathcal{S}})^3}} \exp \left(-\frac{(1 - \mathcal{I}^{\mathcal{S}}(s_{i(j-1)}^{\mathcal{S}})x_{ij}^{\mathcal{S}})^2}{2(\sigma^{\mathcal{S}})^2 x_{ij}^{\mathcal{S}}} \right), \quad (5)$$

for $i = 1, \dots, N^{\mathcal{S}}$, $j = 1, \dots, n_i^{\mathcal{S}}$, and $\mathcal{S} = A, B$. Given the two voltage processes for stimulus A and stimulus B , we can model the AB process as a competition between the two processes. Under our modeling assumptions, this corresponds to an action potential being generated once either the A voltage process or the B voltage process reaches the voltage threshold. Once either of the voltage processes reaches the voltage threshold, both the A and B voltage processes are reset to their resting potential, V_0 . Let $L_{ij} \in \{A, B\}$, which we will refer to as labels, be latent variables that represent which process generated the j^{th} spike in the i^{th} spike train generated by the AB process for $i = 1, \dots, N^{AB}$ and $j = 1, \dots, n_i^{AB}$. These labels are akin to the decisions chosen in multi-category decision studies; however, unlike the multi-category decision studies, the labels are not known and need to be inferred. Lastly, inhibition is introduced through the introduction of a time delay, similar to the offsets used in [Paulon et al. \(2021\)](#).

Although the voltage process that generates the first spike does not have inhibition, each voltage process after the first spike will include inhibition, which helps to control the periodicity of switching between the A and B firing rates. Specifically, if the voltage process corresponding to stimulus \mathcal{S} generated the previous spike, then the voltage process corresponding to stimulus \mathcal{S}^C ($\mathcal{S}^C := \{A, B\} \setminus \mathcal{S}$) will begin after a time delay of δ . If δ is large, there will be very little switching and the spike train will be generated primarily by

only one of the voltage processes. Alternatively, if δ is zero or close to zero, then switching between encodings will occur often, and there will be an almost additive effect on the total number of spikes generated in a trial under stimulus AB as visualized in Figure 2.

Although the modeling framework for the spike trains generated from the AB stimulus has been described in terms of the latent voltage processes, the model can be fully characterized through the distribution of the interspike intervals. Specifically, we have that the joint probability density function of the labels and ISIs corresponding to the first spike in the spike trains can be expressed as

$$f_{X^{AB},L}(x_{i1}^{AB}, L_{i1} = \mathcal{S} \mid \boldsymbol{\theta}) = f_{X^{\mathcal{S}}}(x_{i1}^{AB}) [1 - F_{X^{\mathcal{S}^C}}(x_{i1}^{AB})] \quad (6)$$

for $i = 1, \dots, N^{AB}$, where $f_{X^{\mathcal{S}}}(x) := f_{X^{\mathcal{S}}}(x \mid \mathcal{I}^{\mathcal{S}}(\cdot), \sigma^{\mathcal{S}}, s_{i(j-1)}^{\mathcal{S}})$ is defined in Equation 5, $F_{X^{\mathcal{S}}}(\cdot)$ is the cumulative density function of $X^{\mathcal{S}}$, and $\boldsymbol{\theta} := \{\mathcal{I}^A(\cdot), \mathcal{I}^B(\cdot), \sigma^A, \sigma^B, \delta\}$. Similarly, the joint probability density function of the labels and the rest of the ISIs can be expressed in a similar functional form, but with the inclusion of a time delay for one of the processes. Specifically, we have

$$f_{X^{AB},L}(x_{ij}^{AB}, L_{ij} = \mathcal{S} \mid \boldsymbol{\theta}, l_{i(j-1)}, s_{i(j-1)}^{AB}) = f_{X^{\mathcal{S}}}(x_{ij}^{AB} - \delta \mathbb{1}\{l_{i(j-1)} = \mathcal{S}^C\}) \times [1 - F_{X^{\mathcal{S}^C}}(x_{ij}^{AB} - \delta \mathbb{1}\{l_{i(j-1)} = \mathcal{S}\})], \quad (7)$$

for $i = 1, \dots, N^{AB}$ and $j = 2, \dots, n_i^{AB}$. From Equation 7, it is apparent that if the ISI is smaller than the time delay, then the label of the j^{th} spike must be equal to the value of the previous label (i.e. $l_{ij} = l_{i(j-1)}$). From Equation 7, we have that the likelihood function of ISIs recorded under the AB stimulus can be expressed as

$$f_{X^{AB}}(x_{ij}^{AB} \mid l_{i(j-1)}, l_{ij}, \boldsymbol{\theta}, s_{i(j-1)}^{AB}) = \frac{f_{X^{AB},L}(x_{ij}^{AB}, l_{ij} \mid \boldsymbol{\theta}, l_{i(j-1)}, s_{i(j-1)}^{AB})}{\int_0^\infty f_{X^{AB},L}(x, l_{ij} \mid \boldsymbol{\theta}, l_{i(j-1)}, s_{i(j-1)}^{AB}) dx}, \quad (8)$$

for $i = 1, \dots, N^{AB}$ and $j = 2, \dots, n_i^{AB}$. Similarly, using Equation 6, we can arrive at a similar expression for $f_{X^{AB}}(x_{i1}^{AB} \mid l_{i1}, \boldsymbol{\theta})$. Although the denominator in Equation 8 does not have an analytic form, we can obtain numerical approximations of the integral when the likelihood is explicitly needed.

Utilizing this framework to model spike trains generated under the AB condition allows us to model many of the phenomena observed in previous studies. [Chen et al. \(2024\)](#)

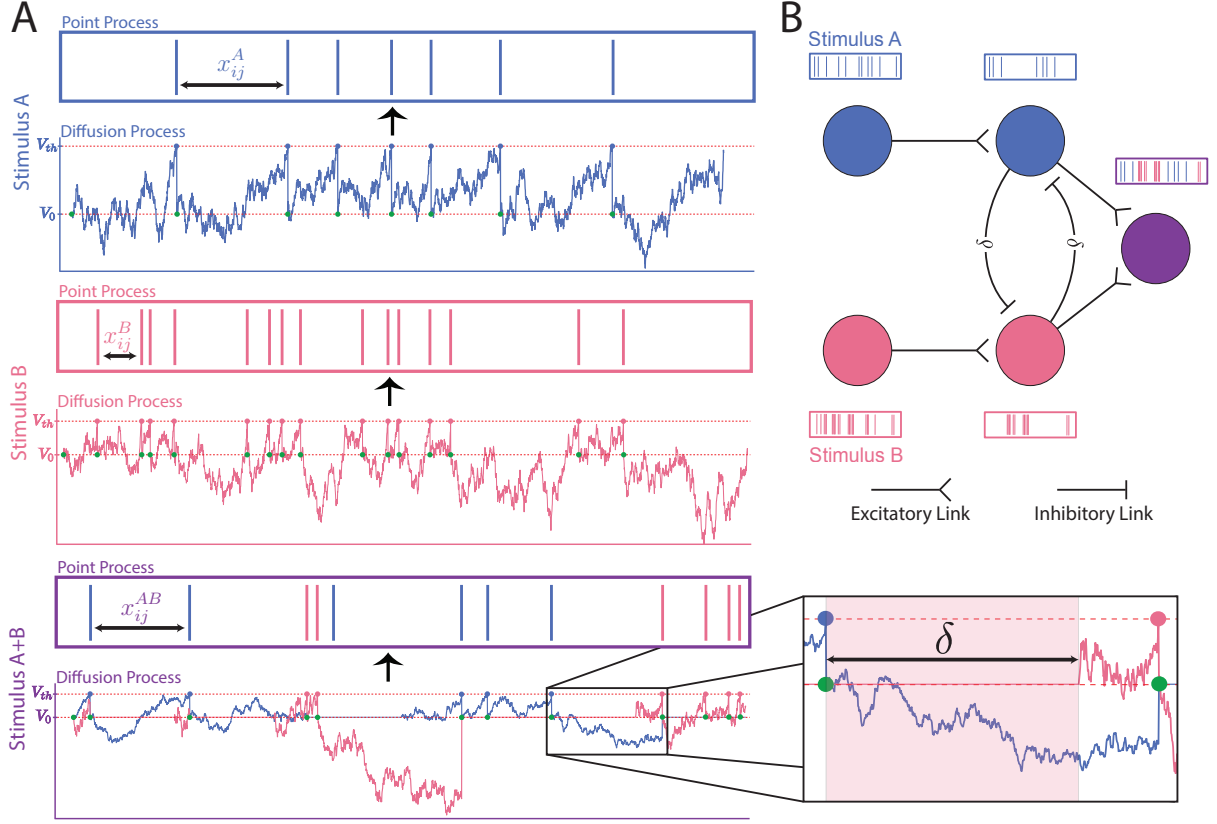


Figure 3: (Subfigure A) Illustration of how the latent drift diffusion processes relate to the observed spike trains. The start of the drift diffusion process is denoted by a green circle, while the hitting time is denoted by a red or blue circle depending on which stimulus the spike is encoding. (Subfigure B) Potential neural motif that could lead to the observed competition framework proposed in this manuscript.

classified the observed spike trains into four major categories: mixture, intermediate, single, and outside. The mixture category accounts for whole trial spike counts that are a mixture of the distributions of A whole trial spike counts and B whole trial spike counts; representing “slow switching”, which is characterized as neural switching across trials. In our proposed framework, this would be represented by models with a large δ , where the probability of switching within a trail would be relatively small. Intermediate spike trains represent trials in which the expected number of whole trial spike counts is between the expected whole trial spike count under stimulus A and the expected whole trial spike count under stimulus

B , potentially representing “fast switching”. Fast switching can be defined by switching between the two firing rates within a trial, creating an fluctuating firing rate. Intermediate spike trains can be represented with moderate values of δ , which would allow potential switching within the trials. Lastly, our model can also represent outside spike trains, which are defined by firing rates higher than those observed in A stimulus trials or B stimulus trials. When δ is close to zero, we get an almost additive effect of the firing rates in our model, which would be similar to the idea of neural summation (Carandini and Heeger, 1994).

Thus far, we have specified a formal statistical model for multiplexing using a competition framework. The specified competition framework also implies the neural circuit in Subfigure B of Figure 3. In this neural circuit, we have two neurons at the top level, each encoding their respective stimulus-specific signal. Each of these top-level neurons has an excitatory link to the next layer of neurons, which have mutual inhibitory links between the second layer of neurons. In this second layer, if one neuron fires, then it inhibits the other neuron from firing, which is controlled by the δ parameter in our model. Lastly, these second-layer neurons are connected to a final neuron through an excitatory link, which would have a fluctuating firing rate; encoding for both the A stimulus and the B stimulus over time.

2.3 Model Specification

Using the modeling framework specified in Section 2.1 to model the spike trains observed under condition A and condition B , and utilizing the competition framework specified in Section 2.2 to model the spike trains observed under the AB condition, we can specify a statistical model for the spike trains observed from the “triplets” of conditions. From the experiment, we observe the spike trains $\mathcal{S}_1^A, \dots, \mathcal{S}_{N^A}^A, \mathcal{S}_1^B, \dots, \mathcal{S}_{N^B}^B, \mathcal{S}_1^{AB}, \dots, \mathcal{S}_{N^{AB}}^{AB}$ and can calculate the corresponding ISIs $X_{ij}^{\mathcal{H}} := S_{ij}^{\mathcal{H}} - S_{i(j-1)}^{\mathcal{H}}$ for $i = 1, \dots, N^{\mathcal{H}}, j = 1, \dots, n_i^{\mathcal{H}}$, and $\mathcal{H} = A, B, AB$. Let $\mathcal{T} = [0, T]$ be the experimental time window of interest. To allow for a time-inhomogeneous point process, we will utilize B-splines (Eilers and Marx, 1996), which will allow for a flexible yet computationally efficient model. Let $\mathbf{b}(t) := [b_1(t), \dots, b_P(t)]^\top \in$

\mathbb{R}^P be the set of basis functions, without including an intercept term, evaluated at $t \in \mathcal{T}$. The input current, which depends on the time of the previous spike, can be specified as $\mathcal{I}^\mathcal{S}(s) = I^\mathcal{S} \exp\left(\left(\boldsymbol{\phi}^\mathcal{S}\right)^\top \mathbf{b}(s)\right)$, where $\boldsymbol{\phi}^\mathcal{S} \in \mathbb{R}^P$ are the spline coefficients that model the time-heterogeneity of the firing rate under stimulus $\mathcal{S} \in \{A, B\}$. Given this construction, when $\boldsymbol{\phi}^\mathcal{S} = \mathbf{0}$, we can see that the firing rate is time-homogeneous, and that $I^\mathcal{S}$ represents the time-homogeneous firing rate. Thus, the likelihood function of data observed under the single-stimulus conditions can be expressed as

$$f_{X^\mathcal{S}}(x_{ij}^\mathcal{S} \mid \boldsymbol{\theta}, s_{i(j-1)}^\mathcal{S}) = \frac{1}{\sigma^\mathcal{S} \sqrt{2\pi}(x_{ij}^\mathcal{S})^3} \exp\left(-\frac{\left(1 - I^\mathcal{S} \exp\left\{\left(\boldsymbol{\phi}^\mathcal{S}\right)^\top \mathbf{b}\left(s_{i(j-1)}^\mathcal{S}\right)\right\} x_{ij}^\mathcal{S}\right)^2}{2(\sigma^\mathcal{S})^2 x_{ij}^\mathcal{S}}\right), \quad (9)$$

for $i = 1, \dots, N^\mathcal{S}$, $j = 1, \dots, n_i^\mathcal{S}$, and $\mathcal{S} = A, B$. Here, we let $\boldsymbol{\theta}$ denote the set of parameters $\{I^A, I^B, \sigma^A, \sigma^B, \delta, \boldsymbol{\phi}^A, \boldsymbol{\phi}^B\}$. Using these specified probabilistic models for the single-stimulus response, we can use Equation 6 and Equation 7 to specify the joint distribution of the latent labels, L_{ij}^{AB} , and the observed ISIs, X_{ij}^{AB} , for $i = 1, \dots, N^{AB}$ and $j = 1, \dots, n_i^{AB}$.

A hierarchical shrinkage prior is placed on the $\boldsymbol{\phi}^\mathcal{S}$ parameters to promote shrinkage of the basis coefficients toward zero. Specifically, we will assume that

$$\boldsymbol{\phi}^\mathcal{S} \sim \mathcal{N}_P(\mathbf{0}, \tau^\mathcal{S} \mathbf{I}) \quad \text{and} \quad \sqrt{\tau^\mathcal{S}} \sim t^+(\nu, \gamma), \quad (10)$$

for $\mathcal{S} = A, B$, where $t^+(\nu, \gamma)$ denotes the half-t distribution with ν degrees of freedom and scale parameter γ . Compared to using an inverse-gamma prior on $\tau^\mathcal{S}$, the half-Cauchy distribution has been shown to be more flexible, to have better behavior near the shrinkage point, and less sensitive to the choice of hyperparameter γ (Gelman, 2006; Polson and Scott, 2012). The use of a half-Cauchy prior also leads to conditionally conjugate sampling schemes (Wand et al., 2011), leading to simple and efficient sampling schemes. Compared to using an inverse-gamma prior on $\tau^\mathcal{S}$, we found that the half-Cauchy distribution led to better behavior when the firing rates were time-homogeneous. Through simulation, we found that setting $\gamma = 2$ and $\nu = 5$ led to good results in both time-homogeneous and time-inhomogeneous settings; however, the results were relatively robust to the choice of γ and ν .

Weakly informative priors are utilized for the remaining parameters in $\boldsymbol{\theta}$. Specifically, we have that

$$I^{\mathcal{S}} \sim IG(\alpha_I, \beta_I), \quad \sigma^{\mathcal{S}} \sim IG(\alpha_\sigma, \beta_\sigma), \quad \text{and} \quad \delta \sim \Gamma(\alpha_\delta, \beta_\delta), \quad (11)$$

for $\mathcal{S} = A, B$, where $\Gamma(\alpha, \beta)$ denotes the Gamma distribution with shape α and rate β . To achieve weakly informative priors, we set $\alpha_I = 40$, $\beta_I = 1$, $\alpha_\sigma = \sqrt{40}$, $\beta_\sigma = 1$, $\alpha_\delta = 0.01$, $\beta_\delta = 0.1$. Thus, we have a fully specified Bayesian model to model the spike trains generated from the triplet of conditions.

3 Posterior Inference and Model Comparison

3.1 Posterior Inference

Posterior inference is performed using an efficient Markov chain Monte Carlo (MCMC) algorithm to obtain samples from the posterior distribution. Sampling from the conditional posterior distributions of the sets of parameters $\{I^A, I^B, \sigma^A, \sigma^B\}$ and $\{\phi^A, \phi^B\}$ is carried out using Hamiltonian Monte Carlo (HMC) (Neal et al., 2011). The parameters I^A, I^B, σ^A , and σ^B are transformed to remove positivity constraints, and HMC is carried out in the transformed space. The gradients of the potential energy are obtained through automatic differentiation (Baydin et al., 2018) and the Hamiltonian dynamics are approximated using the leapfrog method (Hockney and Eastwood, 2021; Neal et al., 2011). Although the number of leapfrog steps is user-specified, the step size and diagonal mass matrix used in the HMC sampling scheme are learned in the initial warm-up blocks of the MCMC. Additional details on the implementation of the HMC can be found in the Supplementary Materials.

Although δ is a continuous variable with support on \mathbb{R}^+ , HMC is not a suitable method to obtain samples from the posterior distribution due to bad posterior geometry. Furthermore, due to the strong dependence between δ and the labels, L_{ij} , a joint sampler is needed to achieve an efficient MCMC sampler with good mixing. We will first start by specifying an efficient MCMC algorithm for sampling from the posterior distribution of the labels.

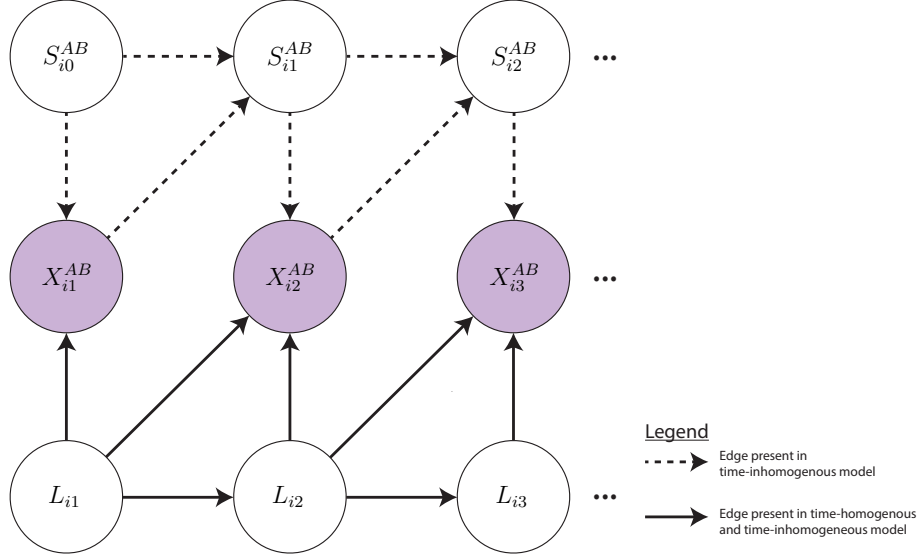


Figure 4: Directed acyclic graph (DAG) characterizing the dependence between the labels (L_{ij}), the observed ISIs (X_{ij}^{AB}), and the spike times (S_{ij}^{AB}).

Although the simplest MCMC scheme would consist of local updates, updating each L_{ij} at a time, the complicated dependency among the labels and the addition of a time delay make this MCMC scheme unsuitable. Specifically, a label change from A to B can occur only when the ISI is greater than δ . Additionally, if the following label is A , then the following ISI needs to be greater than δ since local updates would only update one label at a time. Therefore, an MCMC scheme that simultaneously updates all the labels from a spike train is needed to have an efficient sampler. From Figure 4, it is apparent that our model is not a Markov model, as there is dependence between the previous label and the current ISI. However, the commonly used MCMC method known as the forward-backward algorithm (Baum et al., 1970, 1972; Chib, 1996), also known as forward filtering backward sampling (FFBS), can be adapted to sample from the posterior distribution of the labels.

The FFBS algorithm starts with the forward filtering step; where the objective is to calculate the marginal probabilities $P(L_{ij} = \mathcal{S} \mid \{x_{ik}^{AB}\}_{k=1}^j, \boldsymbol{\theta})$ for $j = 1, \dots, n_i^{AB}$ and $i = 1, \dots, N^{AB}$. While $P(L_{i1} = \mathcal{S} \mid x_{i1}^{AB}, \boldsymbol{\theta})$ is given from Equation 6, we recursively

calculate $P(L_{ij} = \mathcal{S} \mid \{x_{ik}^{AB}\}_{k=1}^j, \boldsymbol{\theta})$ given that

$$P(L_{ij} = \mathcal{S} \mid \{x_{ik}^{AB}\}_{k=1}^j, \boldsymbol{\theta}) \propto \sum_{\mathcal{S}'=\{A,B\}} \left[P(L_{i(j-1)} = \mathcal{S}' \mid \{x_{ik}^{AB}\}_{k=1}^{j-1}, \boldsymbol{\theta}) \right. \\ \left. \times f_{X^{AB},L}(x_{ij}^{AB}, \mathcal{S} \mid L_{i(j-1)} = \mathcal{S}', \boldsymbol{\theta}, s_{i(j-1)}^{AB}) \right], \quad (12)$$

for $j = 2, \dots, n_i^{AB}$ and $i = 1, \dots, N^{AB}$. Once we have calculated all marginal probabilities, we can then sample directly from the posterior distribution using the backward sampling step. We can obtain a sample, denoted $\{\tilde{l}_{ij}\}_{j=1}^{n_i^{AB}}$, from $P(\mathbf{L}_i = \mathbf{l}_i \mid \mathbf{x}_i^{AB}, \boldsymbol{\theta})$ as follows:

Algorithm 1. Let $P(L_{ij} = \mathcal{S} \mid \{x_{ik}^{AB}\}_{k=1}^j, \boldsymbol{\theta})$ be calculated in the forward filtering step (Equation 12) for $i = 1, \dots, N^{AB}$ and $j = 1, \dots, n_i^{AB}$. For $i = 1, \dots, N^{AB}$ repeat the following:

1. Set $\tilde{l}_{in_i^{AB}} = \mathcal{S}$ with probability $P(L_{in_i^{AB}} = \mathcal{S} \mid \{x_{ik}^{AB}\}_{k=1}^{n_i^{AB}}, \boldsymbol{\theta})$ for $\mathcal{S} \in \{A, B\}$,
2. For $j = n_i^{AB} - 1, \dots, 1$, set $\tilde{l}_{ij} = \mathcal{S}$ ($\mathcal{S} \in \{A, B\}$) with probability $w_{ij}^{\mathcal{S}}$, where

$$w_{ij}^{\mathcal{S}} = \frac{P(L_{ij} = \mathcal{S} \mid \{x_{ik}^{AB}\}_{k=1}^j, \boldsymbol{\theta}) f_{X^{AB},L}(x_{i(j+1)}^{AB}, \tilde{l}_{i(j+1)} \mid L_{ij} = \mathcal{S}, \boldsymbol{\theta}, s_{i(j-1)}^{AB})}{\sum_{\mathcal{S}'=A,B} P(L_{ij} = \mathcal{S}' \mid \{x_{ik}^{AB}\}_{k=1}^j, \boldsymbol{\theta}) f_{X^{AB},L}(x_{i(j+1)}^{AB}, \tilde{l}_{i(j+1)} \mid L_{ij} = \mathcal{S}', \boldsymbol{\theta}, s_{i(j-1)}^{AB})} \\ = P(L_{ij} = \mathcal{S} \mid \{x_{ik}^{AB}\}_{k=1}^{j+1}, \{\tilde{l}_{ik}\}_{k=j+1}^{n_i^{AB}}, \boldsymbol{\theta}).$$

Although the FFBS algorithm provides an efficient way to sample from $P(\mathbf{L}_i = \mathbf{l}_i \mid \mathbf{x}_i^{AB}, \boldsymbol{\theta})$, updating the labels and δ separately leads to poor mixing results, as described in detail in the Supplementary Materials. Therefore, we propose a method to efficiently sample from $f(\delta, \{\mathbf{l}_i\}_{i=1}^{N^{AB}} \mid \{\mathbf{x}_i^{AB}\}_{i=1}^{N^{AB}}, \boldsymbol{\theta}_{-\delta}, \alpha_\delta, \beta_\delta)$, where $\boldsymbol{\theta}_{-\delta} := \boldsymbol{\theta} \setminus \{\delta\}$. Let $q_\delta(\delta)$ be a probability density on \mathbb{R}^+ such that $q_\delta(\delta) > 0$ whenever $f(\delta \mid \{\mathbf{x}_i^{AB}\}_{i=1}^{N^{AB}}, \boldsymbol{\theta}) > 0$. Then, a Markov chain $\left(\{(\delta^s, \{\mathbf{l}_i^s\}_{i=1}^{N^{AB}}) : s \in \mathbb{N}\} \right)$ with stationary distribution $f(\delta, \{\mathbf{l}_i\}_{i=1}^{N^{AB}} \mid \{\mathbf{x}_i^{AB}\}_{i=1}^{N^{AB}}, \boldsymbol{\theta}_{-\delta}, \alpha_\delta, \beta_\delta)$ can be constructed as follows:

Algorithm 2. Given the data $\{\mathbf{x}_i^{AB}\}_{i=1}^{N^{AB}}$ and parameters $\boldsymbol{\theta}_{-\delta}$, generate a Markov chain $\left(\{(\delta^s, \{\mathbf{l}_i^s\}_{i=1}^{N^{AB}}) : s \in \mathbb{N}\} \right)$ as follows:

1. Start with some δ^0 and $\{\mathbf{l}_i^0\}_{i=1}^{N^{AB}}$.

2. For $s = 1, 2, \dots$ repeat the following:

- (a) Set $\hat{\delta}_0 = \delta^{s-1}$ and randomly generate $\hat{\delta}_1, \dots, \hat{\delta}_{M_\delta}$ from $q_\delta(\delta)$ ($M_\delta \geq 2$).
- (b) Letting $\hat{\boldsymbol{\theta}}_m = \{I^A, I^B, \sigma^A, \sigma^B, \hat{\delta}_m, \boldsymbol{\phi}^A, \boldsymbol{\phi}^B\}$, use the forward filtration step calculate $P(L_{ij} = \mathcal{S} \mid \{x_{ik}^{AB}\}_{k=1}^j, \hat{\boldsymbol{\theta}}_m)$ in Equation 12 for $m = 0, \dots, M_\delta$, $j = 1, \dots, n_i^{AB}$, and $i = 1, \dots, N^{AB}$. During the forward filtration step, calculate $f(x_{i1}^{AB} \mid \hat{\boldsymbol{\theta}}_m)$ and $f(x_{ij}^{AB} \mid \{x_{ik}^{AB}\}_{k=1}^{j-1}, \hat{\boldsymbol{\theta}}_m)$ for $m = 0, \dots, M_\delta$, $j = 2, \dots, n_i^{AB}$, $i = 1, \dots, N^{AB}$, which can be obtained via the normalizing constants in Equation 12.
- (c) Set $\delta^s = \hat{\delta}_m$ with probability $w_\delta(\hat{\delta}_m)$ ($m = 0, \dots, M$), where

$$w_\delta(\hat{\delta}_m) \propto \frac{\prod_{i=1}^{N^{AB}} f(x_{i1}^{AB} \mid \hat{\boldsymbol{\theta}}_m) \prod_{j=2}^{n_i^{AB}} f(x_{ij}^{AB} \mid \{x_{ik}^{AB}\}_{k=1}^j, \hat{\boldsymbol{\theta}}_m) \pi_\delta(\hat{\delta}_m \mid \alpha_\delta, \beta_\delta)}{q_\delta(\hat{\delta}_m)} \\ \propto \frac{f(\hat{\delta}_m \mid \{\mathbf{x}_i^{AB}\}_{i=1}^{N^{AB}}, \boldsymbol{\theta}_{-\delta}, \alpha_\delta, \beta_\delta)}{q_\delta(\hat{\delta}_m)},$$

where $\pi_\delta(\delta \mid \alpha_\delta, \beta_\delta)$ is the prior probability distribution function of δ .

- (d) Let \tilde{m} denote the chosen index such that $\delta^s = \hat{\delta}_{\tilde{m}}$. Given δ^s and $P(L_{ij} = \mathcal{S} \mid \{x_{ik}^{AB}\}_{k=1}^j, \hat{\boldsymbol{\theta}}_{\tilde{m}})$ obtained from the forward filtration step for $j = 1, \dots, n_i^{AB}$ and $i = 1, \dots, N^{AB}$, obtain $\{\mathbf{l}_i^s\}_{i=1}^{N^{AB}}$ through the backward sampling step (Algorithm 1).

Lemma 3.1. *The Markov chain $\left(\{(\delta^s, \{\mathbf{l}_i^s\}_{i=1}^{N^{AB}}) : s \in \mathbb{N}\}\right)$ generated from Algorithm 2 satisfies detailed balance with respect to $f(\delta, \{\mathbf{l}_i\}_{i=1}^{N^{AB}} \mid \{\mathbf{x}_i^{AB}\}_{i=1}^{N^{AB}}, \boldsymbol{\theta}_{-\delta}, \alpha_\delta, \beta_\delta)$.*

The proof of Lemma 3.1 can be found in the Supplementary Materials. The efficiency of the proposed sampling strategy is highly dependent on the choice of the proposal distribution $q_\delta(\delta)$. Following Gåsemyr (2003), we choose an adaptive proposal as a mixture of distributions such that

$$q_\delta(\delta \mid \alpha_\delta, \beta_\delta) = \alpha \pi_\delta(\delta \mid \alpha_\delta, \beta_\delta) + (1 - \alpha) f_\delta(\delta \mid \boldsymbol{\psi}_\delta),$$

for some $\alpha \in (0, 1)$, where $\pi_\delta(\cdot \mid \alpha_\delta, \beta_\delta)$ is the prior density function of δ , and $\boldsymbol{\psi}_\delta$ is a set of parameters. In our implementation, we choose $f_\delta(\delta \mid \boldsymbol{\psi}_\delta)$ to be the probability density function of a log-normal distribution with $\boldsymbol{\psi}_\delta = (\mu, \sigma)$. The parameters μ and σ are chosen so that the moments of the log-normal distribution match the moments of the posterior distribution of δ . To do this, we periodically update the values of μ and σ in the MCMC warm-up period using posterior samples.

Using the method discussed in this section, we have an efficient MCMC sampling scheme, allowing us to conduct posterior inference. A comparison of the proposed sampling strategy with other sampling methods, together with comprehensive details on the implementation of MCMC adaptation, is available in the Supplementary Materials.

3.2 Model Comparison

To ascertain tenable evidence of multiplexing, we will conduct model comparison between our multiplexing model and a flexible alternative model that encompasses a wide class of alternative neural encoding theories to determine whether the data favor multiplexing over alternative theories of neural encoding. To conduct Bayesian model comparison, we propose using the widely applicable information criterion (WAIC) ([Watanabe and Opper, 2010](#); [Watanabe, 2013](#)) to conduct model comparison. The alternative model, which will be referred to as the inhomogeneous inverse Gaussian point process (IIGPP) model, represents a wide class of alternative theories of neural encoding at a higher level of abstraction than the proposed mechanistic model formulated for multiplexing. As seen in [Table 1](#), the competition model and IIGPP model assume the same model for the spike trains under the *A* and *B* conditions, however, the IIGPP model assumes that the *AB* condition ISIs are also inverse Gaussian distributed with parameters specific to the *AB* condition.

WAIC has been shown to be asymptotically equivalent to leave-one-out cross-validation in Bayesian estimation ([Watanabe and Opper, 2010](#)), and is relatively easy to calculate for most statistical models. WAIC is calculated by first calculating the log pointwise predictive density (lppd) and then adjusting for the effective number of parameters (p_θ). Following

IIGPP Model	Competition Model
$X_{ij}^A \sim IG \left(\frac{1}{I^A \exp\{(\phi^A)^\top \mathbf{b}(s_{i(j-1)}^A)\}}, \left(\frac{1}{\sigma^A}\right)^2 \right)$ [Eq 9]	$X_{ij}^A \sim IG \left(\frac{1}{I^A \exp\{(\phi^A)^\top \mathbf{b}(s_{i(j-1)}^A)\}}, \left(\frac{1}{\sigma^A}\right)^2 \right)$ [Eq 9]
$X_{ij}^B \sim IG \left(\frac{1}{I^B \exp\{(\phi^B)^\top \mathbf{b}(s_{i(j-1)}^B)\}}, \left(\frac{1}{\sigma^B}\right)^2 \right)$ [Eq 9]	$X_{ij}^B \sim IG \left(\frac{1}{I^B \exp\{(\phi^B)^\top \mathbf{b}(s_{i(j-1)}^B)\}}, \left(\frac{1}{\sigma^B}\right)^2 \right)$ [Eq 9]
$X_{ij}^{AB} \sim IG \left(\frac{1}{I^{AB} \exp\{(\phi^{AB})^\top \mathbf{b}(s_{i(j-1)}^{AB})\}}, \left(\frac{1}{\sigma^{AB}}\right)^2 \right)$ [Eq 9]	$f_{X^{AB}}(x_{ij}^{AB} \mid l_{i(j-1)}, l_{ij}, \boldsymbol{\theta}, s_{i(j-1)}^{AB})$ [Eq 8]

Table 1: Specification of the Inhomogeneous Inverse Gaussian Point Process model (IIGPP model) and the Competition Model.

Gelman et al. (2014), the computed log pointwise predictive density is defined as

$$\text{lppd} = \sum_{\mathcal{H} \in \{A, B, AB\}} \sum_{i=1}^{N^{\mathcal{H}}} \sum_{j=1}^{n_i^{\mathcal{H}}} \log \left(\frac{1}{S} \sum_{s=1}^S f_{X^{\mathcal{H}}}(x_{ij}^{\mathcal{H}} \mid \boldsymbol{\theta}^s) \right), \quad (13)$$

and the computed effective number of parameters is defined as

$$p_{\boldsymbol{\theta}} = \sum_{\mathcal{H} \in \{A, B, AB\}} \sum_{i=1}^{N^{\mathcal{H}}} \sum_{j=1}^{n_i^{\mathcal{H}}} \text{Var}_{s=1}^S (\log f_{X^{\mathcal{H}}}(x_{ij}^{\mathcal{H}} \mid \boldsymbol{\theta}^s)), \quad (14)$$

where $\boldsymbol{\theta}^s$ denotes the s^{th} posterior draw of $\boldsymbol{\theta}$ and $\text{Var}_{s=1}^S(x_s) = \frac{1}{S-1} \sum_{s=1}^L (x_s - \bar{x})^2$. Once the log pointwise predictive density and effective number of parameters are estimated, the WAIC estimate is defined as

$$\text{WAIC} = -2(\text{lppd} - p_{\boldsymbol{\theta}}). \quad (15)$$

Using Equation 15 to define WAIC, the preferable model is the one with the smallest WAIC.

From Table 1, it is apparent that the likelihood for the IIGPP model is available in closed form, making the estimated WAIC relatively straightforward to obtain. Alternatively, in the competition framework, the conditional likelihood for the spike trains generated by the AB condition is not available in closed form. To approximate the conditional likelihood, we derived sampling-based algorithms (Algorithm 3 and Algorithm 4) and compared the performance of the algorithms with numerical quadrature approaches (Algorithm 5). Through simulation studies, we found that both sampling-based algorithms obtained very accurate approximations of WAIC, yet Algorithm 3 was able to obtain the WAIC approximations in less than half the time of comparable numerical quadrature approaches. Unlike the conditional likelihood, the likelihood with the labels marginalized out can be calculated in closed

form by using Algorithm 6. We will refer to conditional WAIC and marginal WAIC as the WAIC obtained by using the conditional and marginal likelihoods, respectively. The specification of the algorithms used to calculate WAIC, along with simulation studies exploring the performance of the algorithms, can be found in the Supplementary Materials.

Although the previous literature has suggested that marginal versions of WAIC are more informative than their conditional counterparts (Millar, 2018; Merkle et al., 2019), Du et al. (2023) suggests that the performance of conditional WAIC and marginal WAIC is context dependent. As shown in Watanabe and Opper (2010), WAIC is asymptotically equivalent to Bayesian leave-one-out cross-validation. In the context of this manuscript, conditional WAIC is akin to leave-one-spike-out cross-validation, while marginal WAIC is akin to leave-one-spike-train-out cross-validation.

A simulation study was conducted to determine how informative conditional WAIC and marginal WAIC are in model selection. To evaluate the performance of the information criteria, we generated 100 datasets from the competition framework and 100 datasets from the IIGPP framework, each with different parameters. In each of the 100 datasets generated from the competition framework, both the marginal WAIC and the conditional WAIC suggested that the competition model was preferable to the IIGPP model. Alternatively, when the datasets were generated from the IIGPP model, the marginal WAIC and the conditional WAIC suggested that the IIGPP model was preferable to the competition model 100% and 98% of the time, respectively. The results of the simulation study suggest that both marginal WAIC and conditional WAIC are predictive in model selection, yet provide different insights into model fit (spike level versus spike train level). Additional details on the computation, accuracy, and predictive performance of the information criteria discussed can be found in Section 3 of the Supplementary Materials.

4 Simulation Study: Empirical Convergence

In this subsection, we study the empirical convergence properties of the parameters in our model, the coverage of the credible intervals, and the empirical convergence properties of various posterior predictive distributions of scientific interest. Specifically, we are interested

in inferring the posterior predictive distribution of the number of switches, the time spent encoding stimulus A , and the number of spikes generated in a trial under the AB condition. In this simulation study, we are primarily interested in evaluating model performance as the number of spike trains observed changes ($N^A = N^B = N^{AB} = 25, 50, 100$). For each of the three sample sizes, 100 datasets were generated from the competition framework.

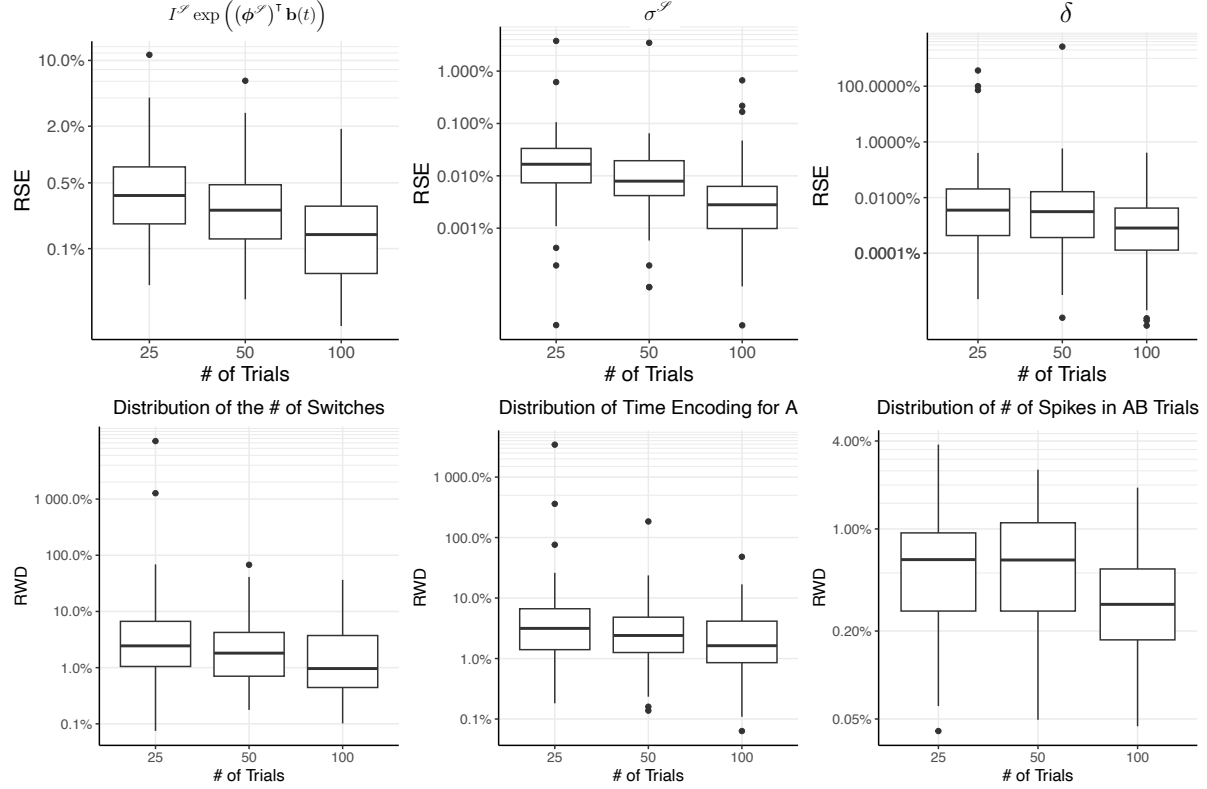


Figure 5: Performance metrics for the recovery of model parameters and posterior predictive distributions of interest, quantified by the relative squared error (RSE) and relative Wasserstein distance (RWD). The performance metrics (RSE and RWD) are plotted on a log scale for ease of visualization.

To evaluate how well we can recover the model parameters and posterior predictive distributions of interest, we calculate the relative squared error (RSE) and the relative Wasserstein distance (RWD), respectively. For a parameter θ , the relative squared error is calculated as $\text{RSE} = \frac{\|\hat{\theta} - \theta\|_2^2}{\|\theta\|_2^2}$, where $\hat{\theta}$ is defined to be the posterior median estimate. The RSE for functional parameters, such as $I^{\mathcal{S}} \exp\left((\phi^{\mathcal{S}})^{\top} \mathbf{b}(t)\right)$, were evaluated on a dense

finite-dimensional grid over $\mathcal{T} = [0, 1]$ prior to the calculation of RSE. The Wasserstein distance between two probability measures μ and ν characterizes the minimum amount of “mass” that must be moved to reconfigure μ into ν (Panaretos and Zemel, 2019); leading to the alternate name of “Earth mover’s distance”. We will characterize the relative Wasserstein distances in terms of empirical measures μ_n and ν_n . Let X_1, \dots, X_n be the posterior predictive samples with empirical measure μ_n and let Y_1, \dots, Y_n be the samples generated under the true model with empirical measure ν_n . The relative Wasserstein distance is calculated as $\text{RWD}(\mu_n, \nu_n) = \frac{\sum_{i=1}^n |X_{(i)} - Y_{(i)}|}{\sum_{i=1}^n |Y_{(i)}|}$, where $X_{(i)}$ and $Y_{(i)}$ are the respective order statistics. For this simulation study, $n = 10,000$ was used to calculate the relative Wasserstein distance.

Figure 5 contains the RSE and RWD obtained in this simulation study. Even with only 25 trials for each condition, we can see that we have good recovery of the parameters and that the error tends to decrease as we add more trials, indicating empirical convergence. Looking at the recovery of δ when we have 25 or 50 trials per condition, we can see that the observed distribution of RSE has long tails. This occurs when δ is relatively large and a switch may not have occurred in any of the observed trials. This leads to an overestimation of δ , causing large RSE values. As more trials are added, the probability of not observing a switch in any of the trials decreases, leading to better recovery of δ in these cases. The confidence interval coverage for the model parameters was found to be nominal for all three sample sizes, and the average 95% credible interval area decreased as the number of trials increased. Table 1 in the Supplementary Materials provides information on the observed coverage of the credible intervals and the relative area of the credible intervals.

Overall, this simulation study provides empirical evidence that our sampling methods do an effective job of exploring the posterior distribution; leading to nominal credible interval coverage and signs of empirical posterior convergence. Furthermore, this simulation study demonstrates that we can recover posterior predictive distributions of scientific interest, with evidence of empirical convergence to the true distributions. Detailed information on how the simulation study was conducted can be found in Section 4 of the Supplementary Materials.

5 Case Study: Inferior Colliculus Neural Recordings under Auditory Stimuli

In this section, we analyze neural spike trains recorded from the inferior colliculus (IC) of macaque monkeys during sound localization tasks, with data initially collected and analyzed by [Caruso et al. \(2018\)](#). The IC is an early station along the auditory pathway ([Adams, 1979](#); [Moore and Goldberg, 1963](#)) that is believed to encode the location of auditory signals, as the level of neural activity has been shown to be highly correlated with the location of the sound ([Groh et al., 2003](#); [McAlpine and Grothe, 2003](#); [Grothe et al., 2010](#)). Considering this, [Caruso et al. \(2018\)](#) focused on understanding how the brain retains information from various auditory stimuli originating from different locations and investigated whether the brain employs multiplexing to preserve information from these distinct stimuli. This data set has also been analyzed at the trial-wise spike count level ([Chen et al., 2024](#)) and at a more granular level (50ms bins) using the dynamic admixture point process (DAPP) model ([Glynn et al., 2021](#)); allowing for a comparison of previous results with the results obtained through the framework described in this manuscript.

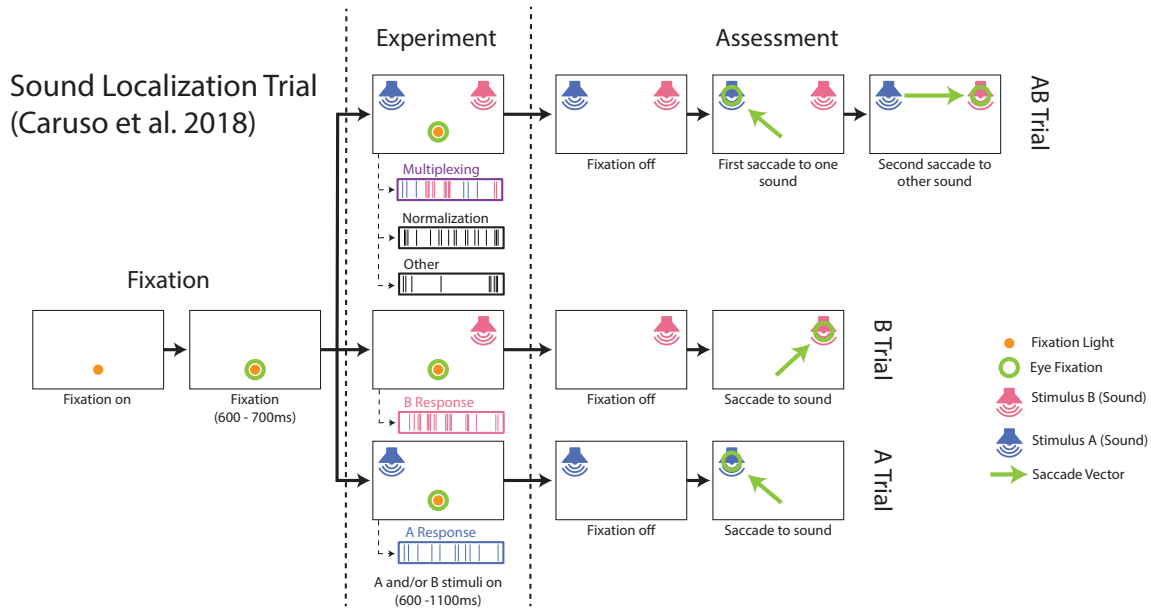


Figure 6: Visualization of the sound localization task conducted in [Caruso et al. \(2018\)](#).

As described throughout the manuscript, the experimental setup consists of recordings under various triplets of conditions; consisting of trials under an A condition (A stimulus only), trials under a B condition (B stimulus only), and trials under an AB condition (A and B stimulus simultaneously). For each triplet, one of the stimuli (A or B) consisted of a bandpass noise with a 742 Hz center frequency at -24, -6, 6, or 24 degrees horizontally. The other stimulus consisted of a bandpass noise with center frequency of 500 Hz, 609 Hz, 903 Hz, 1100 Hz, 1340 Hz, 1632 Hz, or 1988 Hz located 30 degrees from the 742 Hz stimulus (-24, -6, 6, or 24 degrees horizontally). A trial would start with a visual fixation period of 600-700 ms, after which either the single-sound (A or B stimulus) or the dual-sound (A and B stimulus simultaneously), along with the visual stimulus, would be on for 600-1100 ms. After this, the visual fixation light would extinguish, and the macaque would have to visually identify where the sound or sounds were originating from; ensuring that the auditory stimuli were correctly perceived. The data analyzed in this section was recorded when the sound(s) and fixation light were both present, represented by the “Experiment” section in Figure 6. To avoid potential interdependence between trials, the conditions (A , B , and AB) and stimuli from the various triplets were randomly interleaved.

The dataset collected by Caruso et al. (2018) contained 2225 triplets recorded from two different female macaques, consisting of 166 different neurons and a varying number of trials for each of the three conditions. As in Caruso et al. (2018), we will require that each condition in the triplet contains at least five successful trials, leaving us with 1241 triplets. We will add two additional requirements for inclusion in the analysis: (1) single-stimulus spike trains can be represented by a time-inhomogeneous inverse Gaussian point process (Equation 9), and (2) distinguishably different distributions of spike trains for the A and B conditions. The first condition will exclude cases where the single-stimulus spike trains appear to be generated from a mixture of distributions or multiplexing itself, and is carried out by calculating posterior p-values (Meng, 1994; Gelman et al., 1996), allowing us to calculate the discrepancy between the observed spike trains and the spike trains generated from the fitted model that assumes a time-inhomogeneous inverse Gaussian point process. The second condition removes cases where the A and B conditions are indistinguishable

from each other, and is carried out by comparing the pointwise predictive distribution under a joint model of the A and B conditions with the pointwise predictive distribution under separate models for the A and B conditions. After excluding triplets that do not meet these requirements, we have 563 triplets, which is more than the 159 triplets analyzed in the DAPP analysis (Glynn et al., 2021), but less than the 809 triplets analyzed in the spike count analysis conducted by Chen et al. (2024). Additional details on the inclusion criteria can be found in Section 5.1 of the Supplementary Materials.

Chen et al. (2024) proposed two classes of multiplexing: slow juggling and fast juggling. Slow juggling consists of triplets in which the neuron switches between encodings from trial to trial but rarely switches within a trial, while fast juggling consists of triplets where the neuron often switches between encodings within a trial. Slow juggling can be thought of as cases where the switching times are longer than the trial duration, making it unlikely that we would observe a switch between encodings within a single trial. Similarly, we will also define two classes of multiplexing: slow switching and fast switching. In this manuscript, we will define slow switching as cases where the posterior predictive mean number of switches in an AB trial is less than 0.5, and fast switching as cases where the posterior predictive mean number of switches in an AB trial greater than or equal to 0.5.

In this analysis, we consider three main encoding scenarios: multiplexing, winner-take-all (Chen, 2017), and alternative encoding strategies represented by the IIGPP model (normalization (Carandini and Heeger, 2012), subadditivity (Goris et al., 2024), etc.). The winner-take-all encoding scheme assumes that under the dual stimuli trials, a neuron encodes only the A stimulus or the B stimulus for all trials and therefore can be represented by the IIGPP model where the spike trains generated under the AB condition share parameters with one of the single-stimulus condition parameters (i.e. $\sigma^{AB} = \sigma^{\mathcal{S}}$, $I^{AB} = I^{\mathcal{S}}$, and $\phi^{AB} = \phi^{\mathcal{S}}$ for $\mathcal{S} \in \{A, B\}$). Thus, the winner-take-all and IIGPP models can be considered nested models, allowing us to utilize the model comparison methods discussed in Section 3.2. Using WAIC, we will categorize the triplets into one of the following categories: (1) IIGPP, (2) WINNER-TAKE-ALL (PREFERRED) – denoting winner-take-all scenarios where the neuron under the AB condition encodes the stimulus that elicits the higher

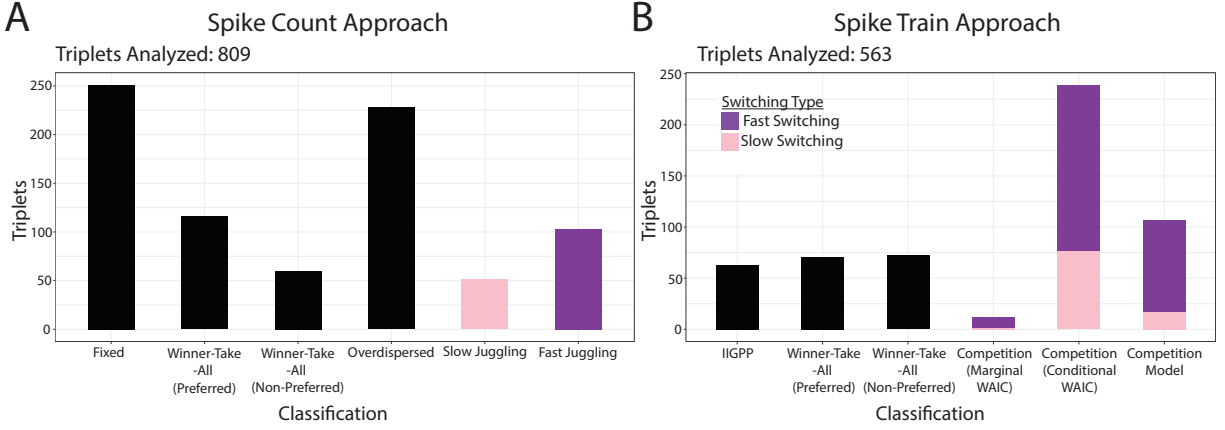


Figure 7: (Subfigure A) Classification results obtained by using the spike count approach discussed in [Chen et al. \(2024\)](#) (Subfigure B) Results obtained from the proposed spike train approach.

overall firing rate between the two stimuli, (3) WINNER-TAKE-ALL (NON-PREFERRED) – denoting winner-take-all scenarios where the neuron under the AB condition encodes the stimulus that elicits the higher overall firing rate between the two stimuli, (4) COMPETITION (MARGINAL WAIC) – denoting scenarios where only the marginal WAIC suggests the competition model (conditional WAIC suggests either winner-take-all or IIGPP), (5) COMPETITION (CONDITIONAL WAIC) – denoting scenarios where only the conditional WAIC suggests the competition model, and (6) COMPETITION MODEL – denoting scenarios where both marginal and conditional WAIC suggest the competition model over all considered alternatives.

As shown in Subfigure B of Figure 7, 18.8% (106) of the triplets exhibited behavior consistent with multiplexing. Among the 106 triplets, 16.0% (17) of the triplets had neurons that exhibited slow switching behavior and 84.0% (89) of the triplets had neurons that displayed fast switching behavior. Similarly, the analysis conducted by [Chen et al. \(2024\)](#) found that 19% (154) of the triplets analyzed had spike count characteristics consistent with multiplexing; however, closer examination revealed a notable proportion of triplets in which the two statistical frameworks showed discrepancies. In 44.6% (329) of the triplets, only one of the WAIC (marginal or conditional WAIC) suggested the competition framework.

These triplets tended to have some trials that exhibited multiplexing characteristics in some trials, but not for all trials under the AB condition. An in-depth discussion on when only Conditional WAIC suggested the competition framework can be found in Section 5.3 of the Supplementary Materials. For the remainder of this section, we will focus on the 249 triplets in which the neuron exhibited behavior consistent with multiplexing.

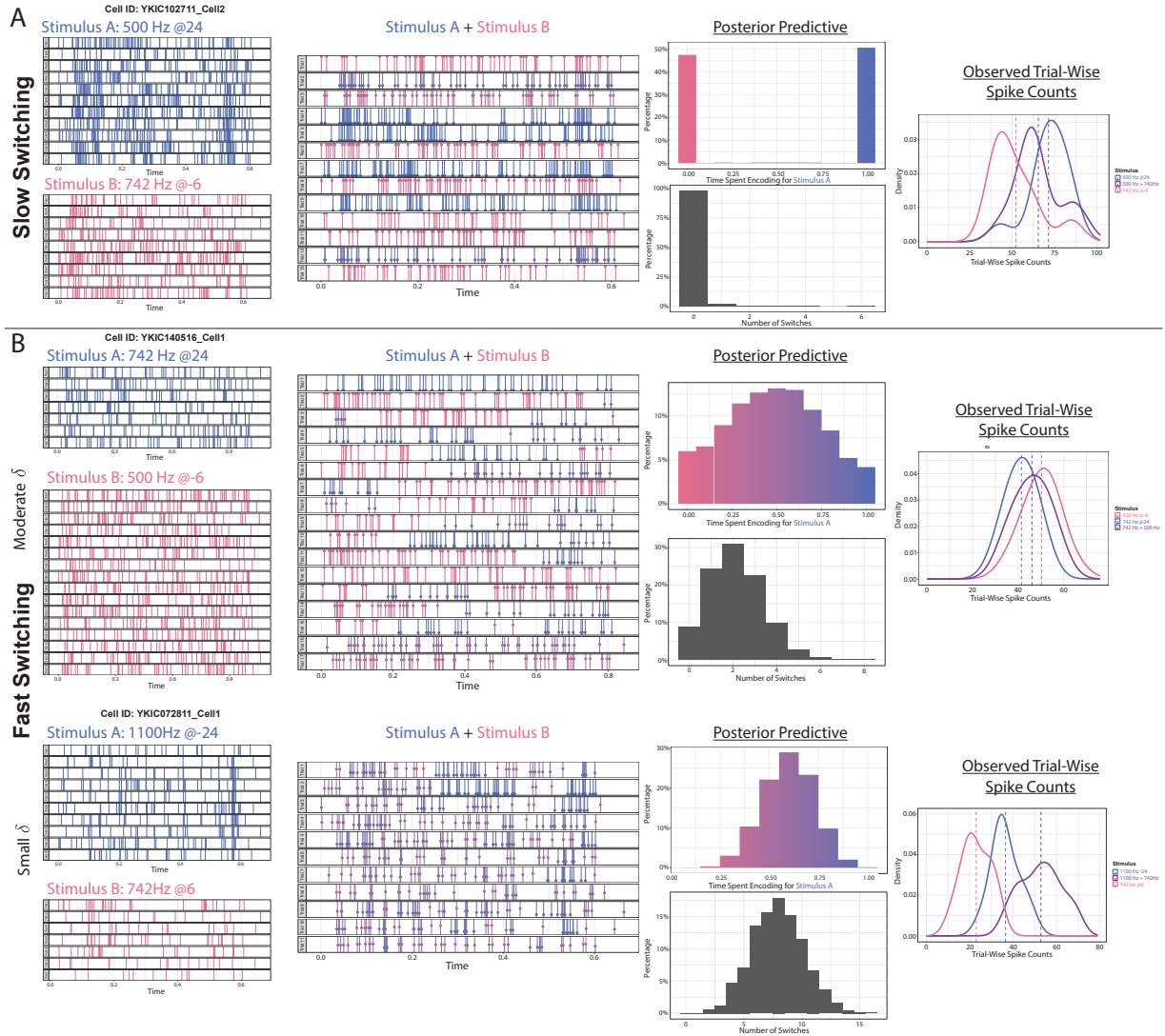


Figure 8: (Subfigure A) Results from a “Slow Switching” triplet. (Subfigure B) Results from two “Fast Switching” triplets; one having a moderate δ , and the other having a small δ leading to an almost additive process. The circles (and color) on the AB condition spikes denote the posterior probability of belonging to A or B .

Due to the mechanistic nature of our competition model representing multiplexing, we are able to gain novel insight into spike-level information that cannot be obtained from spike count analyses or even in the more granular DAPP analysis. Figure 8 exemplifies three different examples of triplets in which the neuron exhibited behavior consistent with multiplexing. Subfigure A illustrates a case of slow switching, where the neuron was unlikely to switch encodings within a trial but often switched between the two encodings between trials. This can also be seen in the posterior predictive distribution for the time encoding for stimulus A in a trial and in the posterior predictive distribution for the number of switches within a trial. Subfigure B contains a visualization of two triplets in which the neuron displays characteristics of fast switching; one with a moderate δ and the other with a small δ . In the moderate δ case, we commonly observe switching between the encodings within the trials; however, it is also not uncommon to see an entire trial in which the neuron encodes only one for one stimulus. In particular, while we can see a distinct difference when looking at the spike-level information for the moderate δ and the slow switching examples, the observed trial-wise spike count look quite similar; illustrating the added benefit from conducting a more granular level of analysis. In the small δ case, we can see an almost additive effect in the spike counts. In almost every trial, the neuron spends some time encoding each stimulus. Although we may not necessarily be able to recover which spikes encode which stimulus, both marginal and conditional WAIC still suggested the competition framework over the IIGPP model; which, based on our simulations in Section 3.6 of the Supplementary Materials, were very informative in model selection, even if δ was zero. In fact, we were unable to recover which spikes encode which stimulus when simulating data from the competition model with $\delta = 0$ (more details can be found in Section 5.4 of the Supplementary Materials).

Overall, this model allows for novel insight into spike-level dynamics and provides compelling evidence that neurons sometimes employ multiplexing to preserve information from multiple stimuli in the receptive field. Compared to Glynn et al. (2021) and Chen et al. (2024), our model relaxes the Poisson distributional assumptions, allowing for the analysis of more triplets and a more flexible model that allows for burstier neurons and more regular

neurons. Compared to Glynn et al. (2021), we developed a more mechanistic approach, allowing us to clearly define behavior consistent with multiplexing. Lastly, our framework allows us to view subadditivity (Goris et al., 2024) as potentially a special case of multiplexing (small δ); broadening the previous thought that the firing rate of a multiplexing neuron should lie between the single-stimulus firing rates of the neuron (Caruso et al., 2018; Glynn et al., 2021; Chen et al., 2024; Groh et al., 2024).

6 Discussion

In this manuscript, we have specified a mechanistic model for multiplexing; a neural encoding theory that posits that individual neurons can temporally switch between encoding different stimuli over time (Groh et al., 2024). As discussed in Section 2, the proposed model is closely related to integrate-and-fire models and accumulator models, both of which are well-established models in computation neuroscience. In Section 3, we derived fast and efficient sampling schemes and techniques for model comparison, allowing us to acquire novel evidence of multiplexing by analyzing 891 triplets obtained in the IC of two macaque monkeys in Section 5. The IC data was also analyzed by Chen et al. (2024) in a trial-wise spike count analysis; however, as illustrated in Figure 2, it is often hard to determine if multiplexing occurs from spike count data alone. The more granular spike train analysis conducted in Section 5 provides more tenable evidence of multiplexing and suggests that multiplexing may actually occur at a higher rate than previously thought in Chen et al. (2024).

The IC data was also analyzed by Glynn et al. (2021) using the DAPP model, in a more granular analysis using 50ms time bins. The model models the A and B condition spike trains as inhomogeneous Poisson processes and posits that the AB condition spike trains are modeled as an admixture of the single-stimulus inhomogeneous Poisson processes. Under the DAPP model, neural variability could not be modeled (assumed ISI-CV of 1), and it was assumed that the AB condition firing rate was bounded between the A and B condition firing rates. These assumptions are relatively strong, as neural coding theory posits that information is encoded in neural variability (Stein et al., 2005), and the assumptions led

to many triplets being excluded from the analysis. Furthermore, determining whether a neuron was multiplexing from this model was nontrivial, as partial mixtures of the A and B encodings cannot necessarily be interpreted as multiplexing, normalization, or other well-established encoding theories. Rather, the DAPP model is a statistical model whose primary purpose is to capture second-order stochasticity, making it difficult to determine whether a neuron is multiplexing. However, [Glynn et al. \(2021\)](#) suggested that there is a non-negligible amount of second-order stochastic variation in the IC dataset. Although our model is relatively flexible, we did not assume any second-order stochastic variation; leading to a potential extension of our framework. The additional flexibility obtained by modeling second-order stochasticity could lead to insight into what is occurring in the triplets where only the conditional WAIC suggested the competition framework.

Although the competition framework offers scientists a method to accumulate evidence of multiplexing in single-neuron spike train recordings, a deeper understanding of how neurons encode stimuli requires inference on a large population of simultaneously recorded neurons. As discussed in [Saxena and Cunningham \(2019\)](#) and [Ebitz and Hayden \(2021\)](#), coordination between neurons is a crucial part of how neurons encode stimuli. As simultaneous recording techniques become more common, there is an increasing need for the development of mechanistic population-level statistical models to understand how the brain encodes multiple stimuli. In addition, we would also like to know under what conditions a neuron employs multiplexing and if it depends on larger-scale neural circuits, the location of the stimuli in the receptive field, the brain region, the species of animal, or the stimuli presented. To gain insight into these scientific questions requires the development of large complex statistical models and the collection of simultaneously recorded neurons in a variety of species of animals and conditions. This manuscript provides a single neuron model for multiplexing that can be used as the basis for a population-level model, and provides empirical support for the existence of multiplexing; warranting further research into when multiplexing occurs and how multiplexing is regulated.

7 Funding Acknowledgments

The authors gratefully acknowledge funding from NIH awards R01 DC013096 and R01 DC016363.

8 Disclosure

The authors report that there are no competing interests to declare.

References

- Adams, J.C., 1979. Ascending projections to the inferior colliculus. *Journal of Comparative Neurology* 183, 519–538.
- Adrian, E.D., Zotterman, Y., 1926. The impulses produced by sensory nerve-endings: Part ii. the response of a single end-organ. *The Journal of physiology* 61, 151.
- Baum, L.E., Petrie, T., Soules, G., Weiss, N., 1970. A maximization technique occurring in the statistical analysis of probabilistic functions of markov chains. *The annals of mathematical statistics* 41, 164–171.
- Baum, L.E., et al., 1972. An inequality and associated maximization technique in statistical estimation for probabilistic functions of markov processes. *Inequalities* 3, 1–8.
- Baydin, A.G., Pearlmutter, B.A., Radul, A.A., Siskind, J.M., 2018. Automatic differentiation in machine learning: a survey. *Journal of Machine Learning Research* 18, 1–43.
- Burkitt, A.N., 2006. A review of the integrate-and-fire neuron model: I. homogeneous synaptic input. *Biological cybernetics* 95, 1–19.
- Carandini, M., Heeger, D.J., 1994. Summation and division by neurons in primate visual cortex. *Science* 264, 1333–1336.
- Carandini, M., Heeger, D.J., 2012. Normalization as a canonical neural computation. *Nature reviews neuroscience* 13, 51–62.

- Caruso, V.C., Mohl, J.T., Glynn, C., Lee, J., Willett, S.M., Zaman, A., Ebihara, A.F., Estrada, R., Freiwald, W.A., Tokdar, S.T., et al., 2018. Single neurons may encode simultaneous stimuli by switching between activity patterns. *Nature communications* 9, 2715.
- Chen, Y., 2017. Mechanisms of winner-take-all and group selection in neuronal spiking networks. *Frontiers in computational neuroscience* 11, 20.
- Chen, Y., Groh, J.M., Tokdar, S.T., 2024. Spike count analysis for multiplexing inference (scampi). *bioRxiv* URL: <https://www.biorxiv.org/content/early/2024/09/15/2024.09.14.613077>, doi:10.1101/2024.09.14.613077, arXiv:<https://www.biorxiv.org/content/early/2024/09/15/2024.09.14.613077.full.pdf>.
- Chib, S., 1996. Calculating posterior distributions and modal estimates in markov mixture models. *Journal of Econometrics* 75, 79–97.
- Chorev, E., Epsztein, J., Houweling, A.R., Lee, A.K., Brecht, M., 2009. Electrophysiological recordings from behaving animals—going beyond spikes. *Current opinion in neurobiology* 19, 513–519.
- Du, H., Keller, B., Alacam, E., Enders, C., 2023. Comparing dic and waic for multilevel models with missing data. *Behavior Research Methods* , 1–20.
- Ebitz, R.B., Hayden, B.Y., 2021. The population doctrine in cognitive neuroscience. *Neuron* 109, 3055–3068.
- Efron, B., 1992. Bootstrap methods: another look at the jackknife, in: *Breakthroughs in statistics: Methodology and distribution*. Springer, pp. 569–593.
- Eilers, P.H., Marx, B.D., 1996. Flexible smoothing with b-splines and penalties. *Statistical science* 11, 89–121.
- Folks, J.L., Chhikara, R.S., 1978. The inverse gaussian distribution and its statistical application—a review. *Journal of the Royal Statistical Society Series B: Statistical Methodology* 40, 263–275.

- G  sem  r, J., 2003. On an adaptive version of the metropolis–hastings algorithm with independent proposal distribution. *Scandinavian Journal of Statistics* 30, 159–173.
- Geisler, C.D., Goldberg, J.M., 1966. A stochastic model of the repetitive activity of neurons. *Biophysical journal* 6, 53–69.
- Gelman, A., 2006. Prior distributions for variance parameters in hierarchical models (comment on article by Browne and Draper). *Bayesian Analysis* 1, 515 – 534. URL: <https://doi.org/10.1214/06-BA117A>, doi:10.1214/06-BA117A.
- Gelman, A., Hwang, J., Vehtari, A., 2014. Understanding predictive information criteria for bayesian models. *Statistics and computing* 24, 997–1016.
- Gelman, A., Meng, X.L., Stern, H., 1996. Posterior predictive assessment of model fitness via realized discrepancies. *Statistica sinica* , 733–760.
- Glynn, C., Tokdar, S.T., Zaman, A., Caruso, V.C., Mohl, J.T., Willett, S.M., Groh, J.M., 2021. Analyzing second order stochasticity of neural spiking under stimuli-bundle exposure. *The annals of applied statistics* 15, 41.
- Gold, J.I., Shadlen, M.N., 2007. The neural basis of decision making. *Annu. Rev. Neurosci.* 30, 535–574.
- Goris, R.L., Coen-Cagli, R., Miller, K.D., Priebe, N.J., Lengyel, M., 2024. Response sub-additivity and variability quenching in visual cortex. *Nature Reviews Neuroscience* , 1–16.
- Groh, J.M., Kelly, K.A., Underhill, A.M., 2003. A monotonic code for sound azimuth in primate inferior colliculus. *Journal of Cognitive Neuroscience* 15, 1217–1231.
- Groh, J.M., Schmehl, M.N., Caruso, V.C., Tokdar, S.T., 2024. Signal switching may enhance processing power of the brain. *Trends in Cognitive Sciences* .
- Grothe, B., Pecka, M., McAlpine, D., 2010. Mechanisms of sound localization in mammals. *Physiological reviews* 90, 983–1012.

- Hockney, R.W., Eastwood, J.W., 2021. Computer simulation using particles. crc Press.
- Jun, N.Y., Ruff, D.A., Kramer, L.E., Bowes, B., Tokdar, S.T., Cohen, M.R., Groh, J.M., 2022. Coordinated multiplexing of information about separate objects in visual cortex. *Elife* 11, e76452.
- Kass, R.E., Eden, U.T., Brown, E.N., et al., 2014. Analysis of neural data. volume 491. Springer.
- Kayser, C., Montemurro, M.A., Logothetis, N.K., Panzeri, S., 2009. Spike-phase coding boosts and stabilizes information carried by spatial and temporal spike patterns. *Neuron* 61, 597–608.
- Liu, Y.H., Wang, X.J., 2001. Spike-frequency adaptation of a generalized leaky integrate-and-fire model neuron. *Journal of computational neuroscience* 10, 25–45.
- Mackay, D.J.C., 1998. Introduction to monte carlo methods, in: *Learning in graphical models*. Springer, pp. 175–204.
- McAlpine, D., Grothe, B., 2003. Sound localization and delay lines—do mammals fit the model? *Trends in neurosciences* 26, 347–350.
- Meng, X.L., 1994. Posterior predictive p -values. *The annals of statistics* 22, 1142–1160.
- Merkle, E.C., Furr, D., Rabe-Hesketh, S., 2019. Bayesian comparison of latent variable models: Conditional versus marginal likelihoods. *Psychometrika* 84, 802–829.
- Millar, R.B., 2018. Conditional vs marginal estimation of the predictive loss of hierarchical models using waic and cross-validation. *Statistics and Computing* 28, 375–385.
- Mohl, J.T., Caruso, V.C., Tokdar, S.T., Groh, J.M., 2020. Sensitivity and specificity of a bayesian single trial analysis for time varying neural signals. *Neurons, behavior, data analysis and theory* 3.
- Moore, R., Goldberg, J., 1963. Ascending projections of the inferior colliculus in the cat. *Journal of Comparative Neurology* 121, 109–135.

- Neal, R.M., et al., 2011. Mcmc using hamiltonian dynamics. *Handbook of markov chain monte carlo* 2, 2.
- Noguchi, A., Ikegaya, Y., Matsumoto, N., 2021. In vivo whole-cell patch-clamp methods: recent technical progress and future perspectives. *Sensors* 21, 1448.
- Panaretos, V.M., Zemel, Y., 2019. Statistical aspects of wasserstein distances. *Annual review of statistics and its application* 6, 405–431.
- Paninski, L., Brown, E.N., Iyengar, S., Kass, R.E., 2009. Statistical models of spike trains. *Stochastic methods in neuroscience* 24, 278–303.
- Paulon, G., Llanos, F., Chandrasekaran, B., Sarkar, A., 2021. Bayesian semiparametric longitudinal drift-diffusion mixed models for tone learning in adults. *Journal of the American Statistical Association* 116, 1114–1127.
- Polson, N.G., Scott, J.G., 2012. On the Half-Cauchy Prior for a Global Scale Parameter. *Bayesian Analysis* 7, 887 – 902. URL: <https://doi.org/10.1214/12-BA730>, doi:10.1214/12-BA730.
- Ratcliff, R., McKoon, G., 2008. The diffusion decision model: theory and data for two-choice decision tasks. *Neural computation* 20, 873–922.
- Ratcliff, R., Smith, P.L., 2004. A comparison of sequential sampling models for two-choice reaction time. *Psychological review* 111, 333.
- Roy, B.K., Smith, D.R., 1969. Analysis of the exponential decay model of the neuron showing frequency threshold effects. *The Bulletin of mathematical biophysics* 31, 341–357.
- Saxena, S., Cunningham, J.P., 2019. Towards the neural population doctrine. *Current opinion in neurobiology* 55, 103–111.
- Schmehl, M.N., Caruso, V.C., Chen, Y., Jun, N.Y., Willett, S.M., Mohl, J.T., Ruff, D.A., Cohen, M., Ebihara, A.F., Freiwald, W.A., et al., 2024. Multiple objects evoke fluctuating responses in several regions of the visual pathway. *Elife* 13, e91129.

- Shi, Y., Bi, D., Hesse, J.K., Lanfranchi, F.F., Chen, S., Tsao, D.Y., 2023. Rapid, concerted switching of the neural code in inferotemporal cortex. *bioRxiv* , 2023–12.
- Stein, R.B., Gossen, E.R., Jones, K.E., 2005. Neuronal variability: noise or part of the signal? *Nature Reviews Neuroscience* 6, 389–397.
- Teeter, C., Iyer, R., Menon, V., Gouwens, N., Feng, D., Berg, J., Szafer, A., Cain, N., Zeng, H., Hawrylycz, M., et al., 2018. Generalized leaky integrate-and-fire models classify multiple neuron types. *Nature communications* 9, 709.
- Tokdar, S.T., Kass, R.E., 2010. Importance sampling: a review. *Wiley Interdisciplinary Reviews: Computational Statistics* 2, 54–60.
- Uhlenbeck, G.E., Ornstein, L.S., 1930. On the theory of the brownian motion. *Physical review* 36, 823.
- Wand, M.P., Ormerod, J.T., Padoan, S.A., Frühwirth, R., 2011. Mean Field Variational Bayes for Elaborate Distributions. *Bayesian Analysis* 6, 847 – 900. URL: <https://doi.org/10.1214/11-BA631>, doi:10.1214/11-BA631.
- Watanabe, S., 2013. A widely applicable bayesian information criterion. *The Journal of Machine Learning Research* 14, 867–897.
- Watanabe, S., Opper, M., 2010. Asymptotic equivalence of bayes cross validation and widely applicable information criterion in singular learning theory. *Journal of machine learning research* 11.

Supplemental Materials: Modeling Neural Switching via Drift-Diffusion Models

1 Proofs

1.1 Lemma 3.1

We would like to show that the Markov chain $\left((\delta^t, \{\mathbf{l}_i^t\}_{i=1}^{N^{AB}}) : t \in \mathbb{N} \right)$ generated from Algorithm 2 in the manuscript satisfies detailed balance with respect to $f(\delta, \{\mathbf{l}_i\}_{i=1}^{N^{AB}} \mid \{\mathbf{x}_i^{AB}\}_{i=1}^{N^{AB}}, \boldsymbol{\theta}_{-\delta}, \alpha_\delta, \beta_\delta)$. Thus, we would like to show that

$$f\left(\delta^t, \{\mathbf{l}_i^t\}_{i=1}^{N^{AB}} \mid \{\mathbf{x}_i^{AB}\}_{i=1}^{N^{AB}}, \boldsymbol{\theta}_{-\delta}, \alpha_\delta, \beta_\delta\right) T\left((\delta^t, \{\mathbf{l}_i^t\}_{i=1}^{N^{AB}}) \longrightarrow (\delta^{t+1}, \{\mathbf{l}_i^{t+1}\}_{i=1}^{N^{AB}})\right) = \\ f\left(\delta^{t+1}, \{\mathbf{l}_i^{t+1}\}_{i=1}^{N^{AB}} \mid \{\mathbf{x}_i^{AB}\}_{i=1}^{N^{AB}}, \boldsymbol{\theta}_{-\delta}, \alpha_\delta, \beta_\delta\right) T\left((\delta^{t+1}, \{\mathbf{l}_i^{t+1}\}_{i=1}^{N^{AB}}) \longrightarrow (\delta^t, \{\mathbf{l}_i^t\}_{i=1}^{N^{AB}})\right),$$

where $T\left((\delta^t, \{\mathbf{l}_i^t\}_{i=1}^{N^{AB}}) \longrightarrow (\delta^{t+1}, \{\mathbf{l}_i^{t+1}\}_{i=1}^{N^{AB}})\right)$ denotes the probability density of moving from $(\delta^t, \{\mathbf{l}_i^t\}_{i=1}^{N^{AB}})$ to $(\delta^{t+1}, \{\mathbf{l}_i^{t+1}\}_{i=1}^{N^{AB}})$.

Suppose that $\delta^t \neq \delta^{t+1}$. Then we have that

$$f\left(\delta^t, \{\mathbf{l}_i^t\}_{i=1}^{N^{AB}} \mid \{\mathbf{x}_i^{AB}\}_{i=1}^{N^{AB}}, \boldsymbol{\theta}_{-\delta}, \alpha_\delta, \beta_\delta\right) T\left((\delta^t, \{\mathbf{l}_i^t\}_{i=1}^{N^{AB}}) \longrightarrow (\delta^{t+1}, \{\mathbf{l}_i^{t+1}\}_{i=1}^{N^{AB}})\right) \\ = f\left(\delta^t, \{\mathbf{l}_i^t\}_{i=1}^{N^{AB}} \mid \{\mathbf{x}_i^{AB}\}_{i=1}^{N^{AB}}, \boldsymbol{\theta}_{-\delta}, \alpha_\delta, \beta_\delta\right) \left[M_\delta q_\delta(\delta^{t+1}) \int \cdots \int \frac{w_\delta(\delta^{t+1})}{w_\delta(\delta^{t+1}) + w_\delta(\delta^t) + \sum_{m=2}^{M_\delta} w_\delta(\hat{\delta}_m)} \prod_{m=2}^{M_\delta} q_\delta(\hat{\delta}_m) d\hat{\delta}_m \right] \\ \times T\left(\{\mathbf{l}_i^t\}_{i=1}^{N^{AB}} \longrightarrow \{\mathbf{l}_i^{t+1}\}_{i=1}^{N^{AB}} \mid \delta^{t+1}\right),$$

where the fact that $\hat{\delta}_m$ for $m = 1, \dots, M_\delta$ are exchangeable is used. Using the fact that FFBS step used to sample the labels (described in A.1-A.2 in the main manuscript) is an independent draw from the posterior distribution, we have that

$$T\left(\{\mathbf{l}_i^t\}_{i=1}^{N^{AB}} \longrightarrow \{\mathbf{l}_i^{t+1}\}_{i=1}^{N^{AB}} \mid \delta^{t+1}\right) = \prod_{i=1}^{N^{AB}} P\left(\mathbf{l}_i = \mathbf{l}_i^{t+1} \mid \mathbf{x}_i^{AB}, \boldsymbol{\theta}_{-\delta}, \delta^{t+1}\right).$$

Thus, using the definition of $w_\delta(\delta)$, we have

$$f\left(\delta^t, \{\mathbf{l}_i^t\}_{i=1}^{N^{AB}} \mid \{\mathbf{x}_i^{AB}\}_{i=1}^{N^{AB}}, \boldsymbol{\theta}_{-\delta}, \alpha_\delta, \beta_\delta\right) T\left((\delta^t, \{\mathbf{l}_i^t\}_{i=1}^{N^{AB}}) \longrightarrow (\delta^{t+1}, \{\mathbf{l}_i^{t+1}\}_{i=1}^{N^{AB}})\right) \quad (1)$$

$$= \left[M_\delta f\left(\delta^{t+1} \mid \{\mathbf{x}_i^{AB}\}_{i=1}^{N^{AB}}, \boldsymbol{\theta}_{-\delta}, \alpha_\delta, \beta_\delta\right) \int \cdots \int \frac{f\left(\{\mathbf{x}_i^{AB}\}_{i=1}^{N^{AB}} \mid \boldsymbol{\theta}_{-\delta}, \alpha_\delta, \beta_\delta\right)}{w_\delta(\delta^{t+1}) + w_\delta(\delta^t) + \sum_{m=2}^{M_\delta} w_\delta(\hat{\delta}_m)} \prod_{m=2}^{M_\delta} q_\delta(\hat{\delta}_m) d\hat{\delta}_m \right] \quad (2)$$

$$\times f\left(\delta^t, \{\mathbf{l}_i^t\}_{i=1}^{N^{AB}} \mid \{\mathbf{x}_i^{AB}\}_{i=1}^{N^{AB}}, \boldsymbol{\theta}_{-\delta}, \alpha_\delta, \beta_\delta\right) \left[\prod_{i=1}^{N^{AB}} P(\mathbf{L}_i = \mathbf{l}_i^{t+1} \mid \mathbf{x}_i^{AB}, \boldsymbol{\theta}_{-\delta}, \delta^{t+1}) \right] \\ = \left[M_\delta \int \cdots \int \frac{f\left(\{\mathbf{x}_i^{AB}\}_{i=1}^{N^{AB}} \mid \boldsymbol{\theta}_{-\delta}, \alpha_\delta, \beta_\delta\right)}{w_\delta(\delta^{t+1}) + w_\delta(\delta^t) + \sum_{m=2}^{M_\delta} w_\delta(\hat{\delta}_m)} \prod_{m=2}^{M_\delta} q_\delta(\hat{\delta}_m) d\hat{\delta}_m \right] \quad (3)$$

$$\times f\left(\delta^t, \{\mathbf{l}_i^t\}_{i=1}^{N^{AB}} \mid \{\mathbf{x}_i^{AB}\}_{i=1}^{N^{AB}}, \boldsymbol{\theta}_{-\delta}, \alpha_\delta, \beta_\delta\right) f\left(\delta^{t+1}, \{\mathbf{l}_i^{t+1}\}_{i=1}^{N^{AB}} \mid \{\mathbf{x}_i^{AB}\}_{i=1}^{N^{AB}}, \boldsymbol{\theta}_{-\delta}, \alpha_\delta, \beta_\delta\right) \\ = f\left(\delta^{t+1}, \{\mathbf{l}_i^{t+1}\}_{i=1}^{N^{AB}} \mid \{\mathbf{x}_i^{AB}\}_{i=1}^{N^{AB}}, \boldsymbol{\theta}_{-\delta}, \alpha_\delta, \beta_\delta\right) T\left((\delta^{t+1}, \{\mathbf{l}_i^{t+1}\}_{i=1}^{N^{AB}}) \longrightarrow (\delta^t, \{\mathbf{l}_i^t\}_{i=1}^{N^{AB}})\right), \quad (4)$$

where the last equality can be seen by the symmetry of $(\delta^t, \{\mathbf{l}_i^t\}_{i=1}^{N^{AB}})$ and $(\delta^{t+1}, \{\mathbf{l}_i^{t+1}\}_{i=1}^{N^{AB}})$ in Equation 3.

If $\delta^t = \delta^{t+1}$, then we have

$$f\left(\delta^t, \{\mathbf{l}_i^t\}_{i=1}^{N^{AB}} \mid \{\mathbf{x}_i^{AB}\}_{i=1}^{N^{AB}}, \boldsymbol{\theta}_{-\delta}, \alpha_\delta, \beta_\delta\right) T\left((\delta^t, \{\mathbf{l}_i^t\}_{i=1}^{N^{AB}}) \longrightarrow (\delta^{t+1}, \{\mathbf{l}_i^{t+1}\}_{i=1}^{N^{AB}})\right) \\ = f\left(\delta^t, \{\mathbf{l}_i^t\}_{i=1}^{N^{AB}} \mid \{\mathbf{x}_i^{AB}\}_{i=1}^{N^{AB}}, \boldsymbol{\theta}_{-\delta}, \alpha_\delta, \beta_\delta\right) T\left(\delta^t \longrightarrow \delta^{t+1}\right) T\left(\{\mathbf{l}_i^t\}_{i=1}^{N^{AB}} \longrightarrow \{\mathbf{l}_i^{t+1}\}_{i=1}^{N^{AB}} \mid \delta^{t+1}\right) \\ = f\left(\delta^t, \{\mathbf{l}_i^t\}_{i=1}^{N^{AB}} \mid \{\mathbf{x}_i^{AB}\}_{i=1}^{N^{AB}}, \boldsymbol{\theta}_{-\delta}, \alpha_\delta, \beta_\delta\right) T\left(\delta^t \longrightarrow \delta^{t+1}\right) \left[\prod_{i=1}^{N^{AB}} P(\mathbf{L}_i = \mathbf{l}_i^{t+1} \mid \mathbf{x}_i^{AB}, \boldsymbol{\theta}_{-\delta}, \delta^{t+1}) \right] \\ = f\left(\delta^t, \{\mathbf{l}_i^t\}_{i=1}^{N^{AB}} \mid \{\mathbf{x}_i^{AB}\}_{i=1}^{N^{AB}}, \boldsymbol{\theta}_{-\delta}, \alpha_\delta, \beta_\delta\right) T\left(\delta^t \longrightarrow \delta^{t+1}\right) \left[\frac{f\left(\delta^{t+1}, \{\mathbf{l}_i^{t+1}\}_{i=1}^{N^{AB}} \mid \{\mathbf{x}_i^{AB}\}_{i=1}^{N^{AB}}, \boldsymbol{\theta}_{-\delta}, \alpha_\delta, \beta_\delta\right)}{f\left(\delta^{t+1} \mid \{\mathbf{x}_i^{AB}\}_{i=1}^{N^{AB}}, \boldsymbol{\theta}_{-\delta}, \alpha_\delta, \beta_\delta\right)} \right] \\ = f\left(\delta^{t+1}, \{\mathbf{l}_i^{t+1}\}_{i=1}^{N^{AB}} \mid \{\mathbf{x}_i^{AB}\}_{i=1}^{N^{AB}}, \boldsymbol{\theta}_{-\delta}, \alpha_\delta, \beta_\delta\right) T\left((\delta^{t+1}, \{\mathbf{l}_i^{t+1}\}_{i=1}^{N^{AB}}) \longrightarrow (\delta^t, \{\mathbf{l}_i^t\}_{i=1}^{N^{AB}})\right),$$

where the last equality can be seen since $\delta^t = \delta^{t+1}$. Thus, we can see that the Markov chain generated by Algorithm 2 satisfies detailed balance with respect to $f(\delta, \{\mathbf{l}_i\}_{i=1}^{N^{AB}} \mid \{\mathbf{x}_i^{AB}\}_{i=1}^{N^{AB}}, \boldsymbol{\theta}_{-\delta}, \alpha_\delta, \beta_\delta)$.

2 Comparison of MCMC Schemes

To efficiently generate samples from the posterior distribution of the proposed model, we proposed using Algorithm 2 in the main manuscript which jointly samples the labels and δ parameter from the conditional posterior distribution. In this section, we compare the

sampling method proposed in Algorithm 2 to a simpler sampling algorithm where the δ parameter and the labels are sampled separately according to their respective conditional posterior distributions.

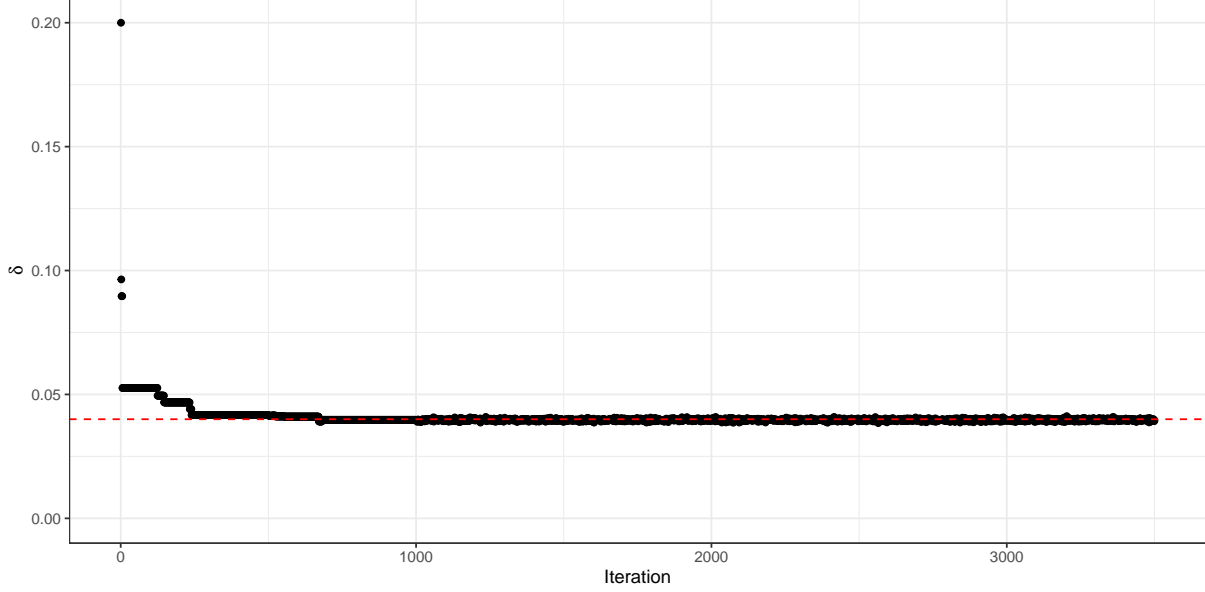


Figure 1: Trace plots of δ using the first sampling scheme (Algorithm 2). The dotted red line represents the value of δ used to generate to data.

In this section, the parameters I^A, I^B, σ^A , and σ^B will be sampled in one block using HMC, and the parameters ϕ^A and ϕ^B will be sampled in an additional block using HMC. The differences in the two sampling schemes compared in this section will be in how we sample from the conditional posterior distribution of the label and the δ parameter. In the first sampling scheme, we will use the sampling scheme in Algorithm 2 to jointly sample the labels and the δ parameter. In the second sampling scheme, we will use Algorithm 1 to sample the labels from the conditional posterior distribution $f(\mathbf{l}_i | I^A, I^B, \sigma^A, \sigma^B, \delta, \phi^A, \phi^B, \mathbf{x}_i^{AB})$, and we will use random walk metropolis to generate samples from the conditional posterior of δ , $f(\delta | I^A, I^B, \sigma^A, \sigma^B, \delta, \phi^A, \phi^B, \{\mathbf{x}_i^{AB}\}_{i=1}^{N^{AB}}, \{\mathbf{l}_i\}_{i=1}^{N^{AB}})$.

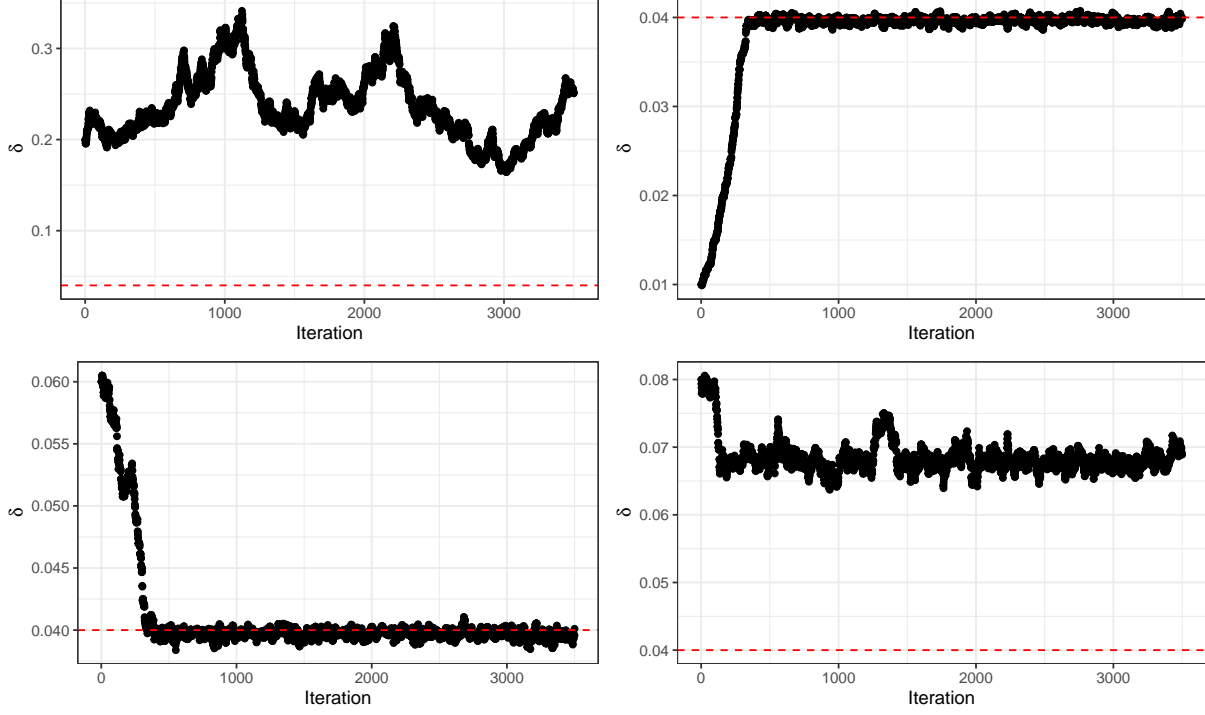


Figure 2: Trace plots of δ using the second sampling scheme (δ and the labels are sampled separately). The dotted red line represents the value of δ used to generate the data.

Figure 1 contains a trace plot of δ using the first sampling scheme (Algorithm 2). From this figure, we can see that the chain quickly converges to the conditional posterior distribution of δ . Alternatively, from Figure 2, we can see that the convergence of the Markov chain depends greatly on the starting value of δ . We can see that if we pick a value too large, the Markov chain does not converge in the 3500 iterations for which the Markov chain was run. Looking at the bottom right panel of Figure 2, we can see that the Markov chain appears to have converged; however, looking at Figure 3, we can see that the Markov chain got stuck in a local mode and was unable to get out of the local mode. We note that adjusting the step size in the random walk did not affect the sampler's ability to leave the local mode, as the labels were not jointly sampled with δ . Thus, we can see that Algorithm 2 provides an efficient sampler that converges relatively fast, regardless of the starting position of the Markov chain.

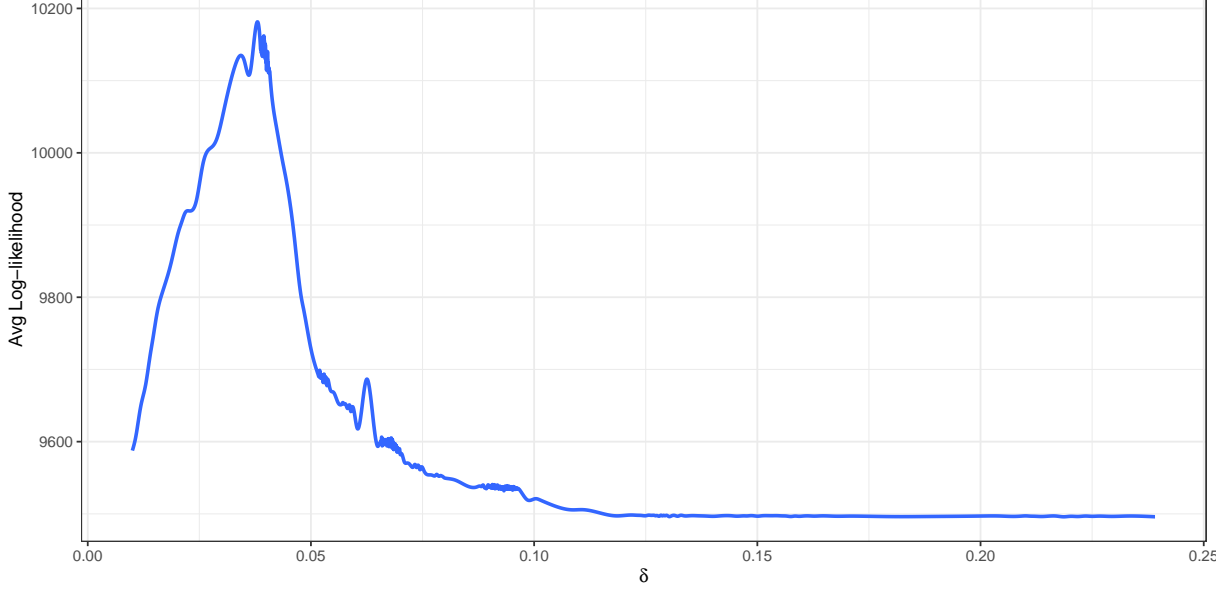


Figure 3: Plot of the log profile likelihood as a function of δ .

3 Estimation of WAIC for the Competition Model

To perform model comparison, we use the widely applicable information criterion (WAIC) (Watanabe and Opper, 2010; Watanabe, 2013) to compare the proposed competition model with a simpler inverse Gaussian process model. Following Gelman et al. (2014), we have that

$$\text{lppd} = \sum_{\mathcal{H} \in \{A, B, AB\}} \sum_{i=1}^{N^{\mathcal{H}}} \sum_{j=1}^{n_i^{\mathcal{H}}} \log \left(\frac{1}{S} \sum_{s=1}^S f_{X^{\mathcal{H}}} (x_{ij}^{\mathcal{H}} | \boldsymbol{\theta}^s) \right), \quad (5)$$

and the computed effective number of parameters is defined as

$$p_{\boldsymbol{\theta}} = \sum_{\mathcal{H} \in \{A, B, AB\}} \sum_{i=1}^{N^{\mathcal{H}}} \sum_{j=1}^{n_i^{\mathcal{H}}} \text{Var}_{s=1}^S (\log f_{X^{\mathcal{H}}} (x_{ij}^{\mathcal{H}} | \boldsymbol{\theta}^s)), \quad (6)$$

where $\boldsymbol{\theta}$ denotes the model parameters and $\boldsymbol{\theta}^s$ denotes the s^{th} posterior draw, and $\text{Var}_{s=1}^S(x_s) = \frac{1}{S-1} \sum_{s=1}^S (x_s - \bar{x})^2$. From this we can calculate the WAIC estimate, which is defined as

$$\text{WAIC} = \text{lppd} - p_{\boldsymbol{\theta}}. \quad (7)$$

Since $f_{X^{AB}}(x_{ij}^{AB} | \boldsymbol{\theta}^s)$ is cannot be written in analytic form, approximation methods must be used. In this section, we outline four different methods for calculating WAIC.

3.1 Fast Sampling

To approximate WAIC, we propose a fast sampling-based scheme to approximate WAIC. The WAIC estimate is slightly biased using this method; however, the bias is relatively small and is unlikely to substantially influence the model comparison results. An empirical study showing this is conducted in Section 3.5. The core idea of this fast sampling scheme is to directly approximate $\int_0^\infty f_{X^{AB},L}(x, L_{ij} = \mathcal{S} \mid \boldsymbol{\theta}, l_{i(j-1)}, s_{i(j-1)}^{AB}) dx$ by Monte Carlo integration. Due to the extra variation created by approximating the likelihood, the effective number of parameters will have to be corrected so that we do not overestimate the effective number of parameters. Algorithm 3 gives a detailed outline of how WAIC can be approximated using this idea.

Algorithm 3. Given the observed data $\{\mathbf{x}_i^A\}_{i=1}^{N^A}, \{\mathbf{x}_i^B\}_{i=1}^{N^B}, \{\mathbf{x}_i^{AB}\}_{i=1}^{N^{AB}}, M_{\tilde{X}}, R$, and posterior samples $\boldsymbol{\theta}^s$ and \mathbf{l}_i^s for $i = 1, \dots, N^{AB}$ and $s = 1, \dots, S$, an estimate of WAIC can be obtained as follows:

1. Calculate $f_{X^{\mathcal{S}}}(x_{ij}^{\mathcal{S}} \mid \boldsymbol{\theta}^s, s_{i(j-1)}^{\mathcal{S}})$ using Equation 9 in the main manuscript for $\mathcal{S} = A, B, s = 1, \dots, S, i = 1, \dots, N^{\mathcal{S}},$ and $j = 1, \dots, n_i^{\mathcal{S}}.$
2. For $s = 1, \dots, S, i = 1, \dots, N^{AB},$ and $j = 2, \dots, n_i^{AB}$ repeat the following:
 - (a) For $r = 1, \dots, R$ repeat the following:

- i. Draw samples \tilde{x}_{ijmr} ($m = 1, \dots, M_{\tilde{X}}$) from $f_{X^{\mathcal{S}}}(x_{ij}^{AB} \mid \boldsymbol{\theta}^s, s_{i(j-1)}^{AB})$ (specified in Equation 5 in the main manuscript), where $l_{ij}^s = \mathcal{S}.$
- ii. If $l_{i(j-1)}^s = \mathcal{S}^c$, set $\tilde{x}_{ijmr} = \tilde{x}_{ijmr} + \delta.$
- iii. Calculate $\left[1 - F_{X^{\mathcal{S}^c}}(\tilde{x}_{ijmr} - \delta \mathbb{1}\{l_{i(j-1)}^s = \mathcal{S}\} \mid \boldsymbol{\theta}^s, s_{i(j-1)}^{AB})\right]$
- iv. Approximate $\int_0^\infty f_{X^{AB},L}(x, L_{ij} = \mathcal{S} \mid \boldsymbol{\theta}^s, l_{i(j-1)}^s, s_{i(j-1)}^{AB}) dx$ by

$$\hat{f}_L = \sum_{m=1}^{M_{\tilde{X}}} \left[1 - F_{X^{\mathcal{S}^c}}(\tilde{x}_{ijmr} - \delta \mathbb{1}\{l_{i(j-1)}^s = \mathcal{S}\} \mid \boldsymbol{\theta}^s, s_{i(j-1)}^{AB})\right]$$

- v. Approximate $f_{X^{AB}}(x_{ij}^{AB} \mid l_{ij}^s, l_{i(j-1)}^s, \boldsymbol{\theta}^s, s_{i(j-1)}^{AB})$ by

$$\hat{f}_{X^{AB}}^r(x_{ij}^{AB} \mid l_{ij}^s, l_{i(j-1)}^s, \boldsymbol{\theta}^s, s_{i(j-1)}^{AB}) = \frac{f_{X^{AB},L}(x_{ij}^{AB}, L_{ij} = \mathcal{S} \mid \boldsymbol{\theta}^s, l_{i(j-1)}^s, s_{i(j-1)}^{AB})}{\hat{f}_L}$$

(b) Calculate $\hat{\sigma}_{f_{ij}^s}^2 = \text{Var}_{r=1}^R \left(\log \left(\hat{f}_{X^{AB}}^r \left(x_{ij}^{AB} \mid l_{ij}^s, l_{i(j-1)}^s, \boldsymbol{\theta}^s, s_{i(j-1)}^{AB} \right) \right) \right)$.

3. For $s = 1, \dots, S$ and $i = 1, \dots, N^{AB}$ repeat the following:

(a) For $r = 1, \dots, R$ repeat the following:

i. Draw samples \tilde{x}_{i1mr} ($m = 1, \dots, M_{\tilde{X}}$) from $f_{X^{\mathcal{S}}} (x_{i1}^{AB} \mid \boldsymbol{\theta}^s, s_{i0}^{AB})$ (specified in Equation 5 in the main manuscript), where $l_{i1}^s = \mathcal{S}$.

ii. Calculate $[1 - F_{X^{\mathcal{S}C}} (\tilde{x}_{i1mr} \mid \boldsymbol{\theta}^s, s_{i0}^{AB})]$

iii. Approximate $\int_0^\infty f_{X^{AB},L} (x, L_{i1} = \mathcal{S} \mid \boldsymbol{\theta}^s, s_{i0}^{AB}) dx$ by

$$\hat{f}_L = \sum_{m=1}^{M_{\tilde{X}}} [1 - F_{X^{\mathcal{S}C}} (\tilde{x}_{i1mr} \mid \boldsymbol{\theta}^s, s_{i0}^{AB})]$$

iv. Approximate $f_{X^{AB}} (x_{i1}^{AB} \mid l_{i1}^s, \boldsymbol{\theta}^s, s_{i0}^{AB})$ by

$$\hat{f}_{X^{AB}}^r (x_{i1}^{AB} \mid l_{i1}^s, \boldsymbol{\theta}^s, s_{i0}^{AB}) = \frac{f_{X^{AB},L} (x_{i1}^{AB}, L_{i1} = \mathcal{S} \mid \boldsymbol{\theta}^s, s_{i0}^{AB})}{\hat{f}_L}$$

(b) Calculate $\hat{\sigma}_{f_{i1}^s}^2 = \text{Var}_{r=1}^R \left(\log \left(\hat{f}_{X^{AB}}^r (x_{i1}^{AB} \mid l_{i1}^s, \boldsymbol{\theta}^s, s_{i0}^{AB}) \right) \right)$.

4. Approximate the log pointwise predictive density by

$$\begin{aligned} \hat{\text{lpd}} = & \sum_{\mathcal{S} \in \{A,B\}} \sum_{i=1}^{N^{\mathcal{S}}} \sum_{j=1}^{n_i^{\mathcal{S}}} \log \left(\frac{1}{S} \sum_{s=1}^S f_{X^{\mathcal{S}}} (x_{ij}^{\mathcal{S}} \mid \boldsymbol{\theta}^s, s_{i(j-1)}^{\mathcal{S}}) \right) \\ & + \sum_{i=1}^{N^{AB}} \sum_{j=2}^{n_i^{AB}} \log \left(\frac{1}{S} \sum_{s=1}^S \hat{f}_{X^{AB}}^1 (x_{ij}^{AB} \mid l_{ij}^s, l_{i(j-1)}^s, \boldsymbol{\theta}^s, s_{i(j-1)}^{AB}) \right) \\ & + \sum_{i=1}^{N^{AB}} \log \left(\frac{1}{S} \sum_{s=1}^S \hat{f}_{X^{AB}}^1 (x_{i1}^{AB} \mid l_{i1}^s, \boldsymbol{\theta}^s, s_{i0}^{AB}) \right). \end{aligned}$$

5. Approximate the effective number of parameters by

$$\begin{aligned} \hat{p}_{\boldsymbol{\theta}} = & \sum_{\mathcal{S} \in \{A,B\}} \sum_{i=1}^{N^{\mathcal{S}}} \sum_{j=1}^{n_i^{\mathcal{S}}} \text{Var}_{s=1}^S (\log f_{X^{\mathcal{S}}} (x_{ij}^{\mathcal{S}} \mid \boldsymbol{\theta}^s, s_{i(j-1)}^{\mathcal{S}})) \\ & + \sum_{i=1}^{N^{AB}} \sum_{j=1}^{n_i^{AB}} \left[\text{Var}_{s=1}^S \left(\log \hat{f}_{X^{AB}}^1 (x_{ij}^{AB} \mid l_{ij}^s, l_{i(j-1)}^s, \boldsymbol{\theta}^s, s_{i(j-1)}^{AB}) \right) - \frac{1}{S} \sum_{s=1}^S \hat{\sigma}_{f_{ij}^s}^2 \right] \\ & + \sum_{i=1}^{N^{AB}} \left[\text{Var}_{s=1}^S \left(\log \hat{f}_{X^{AB}}^1 (x_{i1}^{AB} \mid l_{i1}^s, \boldsymbol{\theta}^s, s_{i0}^{AB}) \right) - \frac{1}{S} \sum_{s=1}^S \hat{\sigma}_{f_{i1}^s}^2 \right]. \end{aligned}$$

6. Approximate WAIC by $\hat{\text{WAIC}} = \hat{\text{lpd}} - \hat{p}_{\boldsymbol{\theta}}$.

3.2 Sampling

In this subsection, we describe another sampling-based approach that is more accurate than the approach specified in 3. This sampling approach provides unbiased estimates of the pointwise predictive density and slightly biased, yet accurate approximations of the log pointwise predictive density and WAIC.

The general idea behind the proposed sampling-based approach to calculate WAIC is that the likelihood is easy to evaluate if we observe the hitting time of the second diffusion process to reach the boundary. Let Y_{ij}^{AB} be the hitting time of the second diffusion process to reach the boundary for $i = 1, \dots, N^{AB}$ and $j = 1, \dots, n_i^{AB}$. Thus, for $i = 1, \dots, N^{AB}$ and $j = 2, \dots, n_i^{AB}$, we have

$$f_{X^{AB}}(x_{ij}^{AB} \mid l_{ij}, l_{i(j-1)}, \boldsymbol{\theta}, s_{i(j-1)}^{AB}, y_{ij}^{AB}) = \frac{f_{X^{\mathcal{S}}}(x_{ij}^{AB} - \delta \mathbb{1}\{l_{i(j-1)} \neq l_{ij}\} \mid \boldsymbol{\theta}, s_{i(j-1)}^{AB})}{\int_0^{y_{ij}^{AB} - \delta \mathbb{1}\{l_{i(j-1)} \neq l_{ij}\}} f_{X^{\mathcal{S}}}(x \mid \boldsymbol{\theta}, s_{i(j-1)}^{AB}) dx}, \quad (8)$$

and

$$f_{Y^{AB}}(y_{ij}^{AB} \mid l_{ij}, l_{i(j-1)}, \boldsymbol{\theta}, s_{i(j-1)}^{AB}, x_{ij}^{AB}) = \frac{f_{X^{\mathcal{S}^C}}(y_{ij}^{AB} - \delta \mathbb{1}\{l_{i(j-1)} = l_{ij}\} \mid \boldsymbol{\theta}, s_{i(j-1)}^{AB})}{\int_{x_{ij}^{AB} - \delta \mathbb{1}\{l_{i(j-1)} = l_{ij}\}}^{\infty} f_{X^{\mathcal{S}^C}}(y \mid \boldsymbol{\theta}, s_{i(j-1)}^{AB}) dy}, \quad (9)$$

where $f_{X^{\mathcal{S}}}(x \mid \boldsymbol{\theta}, s_{i(j-1)}^{AB})$ is defined in Equation 9 in the main manuscript, $\mathcal{S} \in \{A, B\}$, and $\mathcal{S}^C := \{A, B\} \setminus \mathcal{S}$. Thus, we can see that Equation 8 and Equation 9 are the density of truncated inverse Gaussian distributions that are fast to compute. From this we can use Monte Carlo integration methods (Mackay, 1998) to evaluate the following integral:

$$\int_0^{\infty} w_{ij} \left[f_{X^{AB}}(x_{ij}^{AB} \mid l_{ij}, l_{i(j-1)}, \boldsymbol{\theta}, s_{i(j-1)}^{AB}, Y_{ij}^{AB} = y) \right. \\ \left. \times f_{Y^{AB}}(y \mid l_{ij}, l_{i(j-1)}, \boldsymbol{\theta}, s_{i(j-1)}^{AB}, X_{ij}^{AB} = x_{ij}^{AB}) \right] dy, \quad (10)$$

where $w_{ij} = \frac{f_{Y^{AB}}(y_{ij}^{AB} \mid l_{ij}, l_{i(j-1)}, \boldsymbol{\theta}, s_{i(j-1)}^{AB})}{f_{Y^{AB}}(y_{ij}^{AB} \mid l_{ij}, l_{i(j-1)}, \boldsymbol{\theta}, s_{i(j-1)}^{AB}, X_{ij}^{AB} = x_{ij}^{AB})}$ are similar to the weights used in importance sampling (Tokdar and Kass, 2010). It can be shown that the integral in equation 10 is equal to $f_{X^{AB}}(x_{ij}^{AB} \mid l_{ij}, l_{i(j-1)}, \boldsymbol{\theta}, s_{i(j-1)}^{AB})$ for $i = 1, \dots, N^{AB}$ and $j = 2, \dots, n_i^{AB}$. Similarly, an integral of similar form as Equation 10 can be constructed for $f_{X^{AB}}(x_{i1}^{AB} \mid l_{i1}, \boldsymbol{\theta})$ by removing the effect of δ in Equation 8 and Equation 9. It is important to note that

$f_{Y^{AB}} \left(y \mid l_{ij}, l_{i(j-1)}, \boldsymbol{\theta}, s_{i(j-1)}^{AB} \right)$ in the definition of w_{ij} must be approximated by Monte Carlo integration. Since the likelihood can be approximated using Monte Carlo integration methods, we can use this idea to estimate WAIC for the competition model. However, since the likelihood is approximated through Monte Carlo integration, the extra variation due to the approximation must be taken into account when computing the effective number of parameters.

Algorithm 4. Given the observed data $\{\mathbf{x}_i^A\}_{i=1}^{N^A}, \{\mathbf{x}_i^B\}_{i=1}^{N^B}, \{\mathbf{x}_i^{AB}\}_{i=1}^{N^{AB}}$, $M_{\tilde{Y}}$, $M_{\tilde{X}}$, R , and posterior samples $\boldsymbol{\theta}^s$ and \mathbf{l}_i^s for $i = 1, \dots, N^{AB}$ and $s = 1, \dots, S$, an estimate of WAIC can be obtained as follows:

1. Calculate $f_{X^{\mathcal{S}}} \left(x_{ij}^{\mathcal{S}} \mid \boldsymbol{\theta}^s, s_{i(j-1)}^{\mathcal{S}} \right)$ using Equation 9 in the main manuscript for $\mathcal{S} = A, B$, $s = 1, \dots, S$, $i = 1, \dots, N^{\mathcal{S}}$, and $j = 1, \dots, n_i^{\mathcal{S}}$.
2. For $s = 1, \dots, S$, $i = 1, \dots, N^{AB}$, and $j = 2, \dots, n_i^{AB}$ repeat the following:
 - (a) For $r = 1, \dots, R$ repeat the following:
 - i. Draw samples \tilde{y}_{ijmr} ($m = 1, \dots, M_{\tilde{Y}}$) from $f_{Y^{AB}} \left(y_{ij}^{AB} \mid l_{ij}^s, l_{i(j-1)}^s, \boldsymbol{\theta}^s, s_{i(j-1)}^{AB}, x_{ij}^{AB} \right)$, specified in Equation 17 in the main manuscript.
 - ii. For $m = 1, \dots, M_{\tilde{Y}}$, calculate $f_{X^{AB}} \left(x_{ij}^{AB} \mid l_{ij}^s, l_{i(j-1)}^s, \boldsymbol{\theta}^s, s_{i(j-1)}^{AB}, \tilde{y}_{ijmr} \right)$, specified in Equation 16 in the main manuscript.
 - iii. Approximate $f(\tilde{y}_{ijmr} \mid l_{ij}^s, l_{i(j-1)}^s, \boldsymbol{\theta}^s)$ for $m = 1, \dots, M_{\tilde{Y}}$ as follows:
 - A. Sample $(\tilde{x}_{ijmr})_{m'}$ ($m' = 1, \dots, M_{\tilde{X}}$) from $f_{X^{AB}}(x_{ij}^{AB} \mid l_{ij}^s, l_{i(j-1)}^s, \boldsymbol{\theta}^s)$ which is proportional to Equation 7 in the main manuscript using rejection sampling.
 - B. Calculate $f_{Y^{AB}} \left(\tilde{y}_{ijmr} \mid l_{ij}^s, l_{i(j-1)}^s, \boldsymbol{\theta}^s, s_{i(j-1)}^{AB}, (\tilde{x}_{ijmr})_{m'} \right)$, specified in Equation 17 in the main manuscript.
 - C. Approximate $f(\tilde{y}_{ijmr} \mid l_{ij}^s, l_{i(j-1)}^s, \boldsymbol{\theta}^s)$ by $\hat{f}(\tilde{y}_{ijmr} \mid l_{ij}^s, l_{i(j-1)}^s, \boldsymbol{\theta}^s)$

$$= \frac{1}{M_{\tilde{X}}} \sum_{m'=1}^{M_{\tilde{X}}} f_{Y^{AB}} \left(\tilde{y}_{ijmr} \mid l_{ij}^s, l_{i(j-1)}^s, \boldsymbol{\theta}^s, s_{i(j-1)}^{AB}, (\tilde{x}_{ijmr})_{m'} \right).$$
 - iv. Calculate $\hat{w}_{ijmr} = \frac{\hat{f}(\tilde{y}_{ijmr} \mid l_{ij}^s, l_{i(j-1)}^s, \boldsymbol{\theta}^s)}{f_{Y^{AB}}(\tilde{y}_{ijmr} \mid l_{ij}^s, l_{i(j-1)}^s, \boldsymbol{\theta}^s, s_{i(j-1)}^{AB}, x_{ij}^{AB})}$.

- v. Approximate the likelihood by $\hat{f}_{X^{AB}}^r \left(x_{ij}^{AB} \mid l_{ij}^s, l_{i(j-1)}^s, \boldsymbol{\theta}^s, s_{i(j-1)}^{AB} \right)$
 $= \frac{1}{M_{\tilde{Y}}} \sum_{m=1}^{M_{\tilde{Y}}} \hat{w}_{ijmr} f_{X^{AB}} \left(x_{ij}^{AB} \mid l_{ij}^s, l_{i(j-1)}^s, \boldsymbol{\theta}^s, s_{i(j-1)}^{AB}, \tilde{y}_{ijmr} \right).$
- (b) Calculate $\hat{\sigma}_{f_{ij}^s}^2 = \text{Var}_{r=1}^R \left(\log \left(\hat{f}_{X^{AB}}^r \left(x_{ij}^{AB} \mid l_{ij}^s, l_{i(j-1)}^s, \boldsymbol{\theta}^s, s_{i(j-1)}^{AB} \right) \right) \right).$
3. For $s = 1, \dots, S$ and $i = 1, \dots, N^{AB}$ repeat the following:
- (a) For $r = 1, \dots, R$ repeat the following:
- Draw samples \tilde{y}_{i1mr} ($m = 1, \dots, M_{\tilde{Y}}$) from $f_{Y^{AB}} \left(y_{i1}^{AB} \mid l_{i1}^s, \boldsymbol{\theta}^s, s_{i0}^{AB}, x_{i1}^{AB} \right).$
 - For $m = 1, \dots, M_{\tilde{Y}}$, calculate $f_{X^{AB}} \left(x_{i1}^{AB} \mid l_{i1}^s, \boldsymbol{\theta}^s, s_{i0}^{AB}, \tilde{y}_{i1mr} \right)$, specified in Equation 16 in the main manuscript.
 - Approximate $f(\tilde{y}_{i1mr} \mid l_{i1}^s, \boldsymbol{\theta}^s, s_{i0}^{AB})$ for $m = 1, \dots, M_{\tilde{Y}}$ as follows:
 - Sample $(\tilde{x}_{i1mr})_{m'}$ ($m' = 1, \dots, M_{\tilde{X}}$) from $f_{X^{AB}}(x_{i1}^{AB} \mid l_{i1}^s, \boldsymbol{\theta}^s, s_{i0}^{AB})$ using rejection sampling.
 - Calculate $f_{Y^{AB}} \left(\tilde{y}_{i1mr} \mid l_{i1}^s, \boldsymbol{\theta}^s, s_{i0}^{AB}, (\tilde{x}_{i1mr})_{m'} \right).$
 - Approximate $f(\tilde{y}_{i1mr} \mid l_{i1}^s, \boldsymbol{\theta}^s, s_{i0}^{AB})$ by

$$\hat{f}(\tilde{y}_{i1mr} \mid l_{i1}^s, \boldsymbol{\theta}^s, s_{i0}^{AB}) = \frac{1}{M_{\tilde{X}}} \sum_{m'=1}^{M_{\tilde{X}}} f_{Y^{AB}} \left(\tilde{y}_{i1mr} \mid l_{i1}^s, \boldsymbol{\theta}^s, s_{i0}^{AB}, (\tilde{x}_{i1mr})_{m'} \right).$$

- Calculate $\hat{w}_{i1mr} = \frac{\hat{f}(\tilde{y}_{i1mr} \mid l_{i1}^s, \boldsymbol{\theta}^s, s_{i0}^{AB})}{f_{Y^{AB}}(\tilde{y}_{i1mr} \mid l_{i1}^s, \boldsymbol{\theta}^s, s_{i0}^{AB}, x_{i1}^{AB})}.$
 - Approximate the likelihood by $\hat{f}_{X^{AB}}^r \left(x_{i1}^{AB} \mid l_{i1}^s, \boldsymbol{\theta}^s \right)$
 $= \frac{1}{M_{\tilde{Y}}} \sum_{m=1}^{M_{\tilde{Y}}} \hat{w}_{i1mr} f_{X^{AB}} \left(x_{i1}^{AB} \mid l_{i1}^s, \boldsymbol{\theta}^s, s_{i0}^{AB}, \tilde{y}_{i1mr} \right).$
- (b) Calculate $\hat{\sigma}_{f_{i1}^s}^2 = \text{Var}_{r=1}^R \left(\log \left(\hat{f}_{X^{AB}}^r \left(x_{i1}^{AB} \mid l_{i1}^s, \boldsymbol{\theta}^s, s_{i0}^{AB} \right) \right) \right).$

4. Approximate the log pointwise predictive density by

$$\begin{aligned} \hat{\text{lpd}} = & \sum_{\mathcal{S} \in \{A, B\}} \sum_{i=1}^{N^{\mathcal{S}}} \sum_{j=1}^{n_i^{\mathcal{S}}} \log \left(\frac{1}{S} \sum_{s=1}^S f_{X^{\mathcal{S}}} \left(x_{ij}^{\mathcal{S}} \mid \boldsymbol{\theta}^s, s_{i(j-1)}^{\mathcal{S}} \right) \right) \\ & + \sum_{i=1}^{N^{AB}} \sum_{j=2}^{n_i^{AB}} \log \left(\frac{1}{S} \sum_{s=1}^S \hat{f}_{X^{AB}}^1 \left(x_{ij}^{AB} \mid l_{ij}^s, l_{i(j-1)}^s, \boldsymbol{\theta}^s, s_{i(j-1)}^{AB} \right) \right) \\ & + \sum_{i=1}^{N^{AB}} \log \left(\frac{1}{S} \sum_{s=1}^S \hat{f}_{X^{AB}}^1 \left(x_{i1}^{AB} \mid l_{i1}^s, \boldsymbol{\theta}^s, s_{i0}^{AB} \right) \right). \end{aligned}$$

5. Approximate the effective number of parameters by

$$\begin{aligned}\hat{p}_{\boldsymbol{\theta}} = & \sum_{\mathcal{S} \in \{A, B\}} \sum_{i=1}^{N^{\mathcal{S}}} \sum_{j=1}^{n_i^{\mathcal{S}}} \text{Var}_{s=1}^S \left(\log f_{X^{\mathcal{S}}} (x_{ij}^{\mathcal{S}} \mid \boldsymbol{\theta}^s, s_{i(j-1)}^{\mathcal{S}}) \right) \\ & + \sum_{i=1}^{N^{AB}} \sum_{j=1}^{n_i^{AB}} \left[\text{Var}_{s=1}^S \left(\log \hat{f}_{X^{AB}}^1 (x_{ij}^{AB} \mid l_{ij}^s, l_{i(j-1)}^s, \boldsymbol{\theta}^s, s_{i(j-1)}^{AB}) \right) - \frac{1}{S} \sum_{s=1}^S \hat{\sigma}_{f_{ij}^s}^2 \right] \\ & + \sum_{i=1}^{N^{AB}} \left[\text{Var}_{s=1}^S \left(\log \hat{f}_{X^{AB}}^1 (x_{i1}^{AB} \mid l_{i1}^s, \boldsymbol{\theta}^s, s_{i0}^{AB}) \right) - \frac{1}{S} \sum_{s=1}^S \hat{\sigma}_{f_{i1}^s}^2 \right].\end{aligned}$$

6. Approximate WAIC by $\hat{\text{WAIC}} = \text{lppd} - \hat{p}_{\boldsymbol{\theta}}$.

We can see that Algorithm 4 accounts for the extra variation in the lppd caused by the Monte Carlo integration Algorithm when estimating the effective number of parameters. Although this is not an unbiased estimate of the effective number of parameters, simulation studies show that it does a good job of recovering the effective number of parameters, especially when using smaller $M_{\tilde{X}}$ and $M_{\tilde{Y}}$ which will be less computationally intensive. Although we cannot achieve unbiased estimates of lppd or $p_{\boldsymbol{\theta}}$ using Algorithm 4, it does produce unbiased estimates of the pointwise predictive density. Specifically, we have

$$\mathbb{E} \left[\frac{1}{S} \sum_{s=1}^S \hat{f}_{X^{AB}}^1 (x_{ij}^{AB} \mid l_{ij}^s, l_{i(j-1)}^s, \boldsymbol{\theta}^s, s_{i(j-1)}^{AB}) \right] = \frac{1}{S} \sum_{s=1}^S f_{X^{AB}} (x_{ij}^{AB} \mid l_{ij}^s, l_{i(j-1)}^s, \boldsymbol{\theta}^s, s_{i(j-1)}^{AB}). \quad (11)$$

This can be seen as follows:

$$\mathbb{E}_{\tilde{X}} [\hat{w}_{ijmr}] = \frac{\mathbb{E}_{\tilde{x}_{ijmr}} \left[\hat{f}_{Y^{AB}} \left(\tilde{y}_{ijmr} \mid l_{ij}^s, l_{i(j-1)}^s, \boldsymbol{\theta}^s, s_{i(j-1)}^{AB} \right) \right]}{f_{Y^{AB}} \left(\tilde{y}_{ijmr} \mid l_{ij}^s, l_{i(j-1)}^s, \boldsymbol{\theta}^s, s_{i(j-1)}^{AB}, x_{ij}^{AB} \right)}$$

Thus we have that $\mathbb{E}_{\tilde{X}} \left[\hat{f}_{Y^{AB}} \left(\tilde{y}_{ijmr} \mid l_{ij}^s, l_{i(j-1)}^s, \boldsymbol{\theta}^s, s_{i(j-1)}^{AB} \right) \right]$ can be written as

$$\begin{aligned}
& \mathbb{E} \left[\frac{1}{M_{\tilde{X}}} \sum_{m'=1}^{M_{\tilde{X}}} f_{Y^{AB}} \left(\tilde{y}_{ijmr} \mid l_{ij}^s, l_{i(j-1)}^s, \boldsymbol{\theta}^s, s_{i(j-1)}^{AB}, (\tilde{x}_{ijmr})_{m'} \right) \right] \\
&= \int \cdots \int \left[\frac{1}{M_{\tilde{X}}} \sum_{m'=1}^{M_{\tilde{X}}} f_{Y^{AB}} \left(\tilde{y}_{ijmr} \mid l_{ij}^s, l_{i(j-1)}^s, \boldsymbol{\theta}^s, s_{i(j-1)}^{AB}, (\tilde{x}_{ijmr})_{m'} \right) \right. \\
&\quad \left. \times f_{X^{AB}}((\tilde{x}_{ijmr})_{m'} \mid l_{ij}^s, l_{i(j-1)}^s, \boldsymbol{\theta}^s, s_{i(j-1)}^{AB}) \right] \prod d(\tilde{x}_{ijmr})_{m'} \\
&= \int \cdots \int \frac{1}{M_{\tilde{X}}} \sum_{m'=1}^{M_{\tilde{X}}} f \left(\tilde{y}_{ijmr}, (\tilde{x}_{ijmr})_{m'} \mid l_{ij}^s, l_{i(j-1)}^s, \boldsymbol{\theta}^s, s_{i(j-1)}^{AB} \right) \prod d(\tilde{x}_{ijmr})_{m'} \\
&= \frac{1}{M_{\tilde{X}}} \sum_{m'=1}^{M_{\tilde{X}}} f_{Y^{AB}} \left(\tilde{y}_{ijmr} \mid l_{ij}^s, l_{i(j-1)}^s, \boldsymbol{\theta}^s, s_{i(j-1)}^{AB} \right) \\
&= f_{Y^{AB}} \left(\tilde{y}_{ijmr} \mid l_{ij}^s, l_{i(j-1)}^s, \boldsymbol{\theta}^s, s_{i(j-1)}^{AB} \right)
\end{aligned}$$

Thus we have that

$$\mathbb{E}_{\tilde{X}} [\hat{w}_{ijmr}] = \frac{f_{Y^{AB}} \left(\tilde{y}_{ijmr} \mid l_{ij}^s, l_{i(j-1)}^s, \boldsymbol{\theta}^s, s_{i(j-1)}^{AB} \right)}{f_{Y^{AB}} \left(\tilde{y}_{ijmr} \mid l_{ij}^s, l_{i(j-1)}^s, \boldsymbol{\theta}^s, s_{i(j-1)}^{AB}, x_{ij}^{AB} \right)}. \quad (12)$$

Next, we have that

$$\begin{aligned}
&= \mathbb{E}_{\tilde{Y}} \left[\mathbb{E}_{\tilde{X}} \left[\frac{1}{M_{\tilde{Y}}} \sum_{m=1}^{M_{\tilde{Y}}} \hat{w}_{ijmr} f_{X^{AB}} \left(x_{ij}^{AB} \mid l_{ij}^s, l_{i(j-1)}^s, \boldsymbol{\theta}^s, s_{i(j-1)}^{AB}, \tilde{y}_{ijmr} \right) \right] \right] \\
&= \frac{1}{M_{\tilde{Y}}} \sum_{m=1}^{M_{\tilde{Y}}} \int \left[\mathbb{E}_{\tilde{X}} [\hat{w}_{ijmr}] f_{X^{AB}} \left(x_{ij}^{AB} \mid l_{ij}^s, l_{i(j-1)}^s, \boldsymbol{\theta}^s, s_{i(j-1)}^{AB}, \tilde{y}_{ijmr} \right) \right. \\
&\quad \left. \times f_{Y^{AB}} \left(\tilde{y}_{ijmr}^{AB} \mid l_{ij}^s, l_{i(j-1)}^s, \boldsymbol{\theta}^s, s_{i(j-1)}^{AB}, x_{ij}^{AB} \right) \right] d\tilde{y}_{ijmr}^{AB} \\
&= \frac{1}{M_{\tilde{Y}}} \sum_{m=1}^{M_{\tilde{Y}}} \int \left[f_{X^{AB}} \left(x_{ij}^{AB} \mid l_{ij}^s, l_{i(j-1)}^s, \boldsymbol{\theta}^s, s_{i(j-1)}^{AB}, \tilde{y}_{ijmr} \right) \right. \\
&\quad \left. \times f_{Y^{AB}} \left(\tilde{y}_{ijmr}^{AB} \mid l_{ij}^s, l_{i(j-1)}^s, \boldsymbol{\theta}^s, s_{i(j-1)}^{AB} \right) \right] d\tilde{y}_{ijmr}^{AB} \\
&= \frac{1}{M_{\tilde{Y}}} \sum_{m=1}^{M_{\tilde{Y}}} \int \left[f \left(x_{ij}^{AB}, \tilde{y}_{ijmr} \mid l_{ij}^s, l_{i(j-1)}^s, \boldsymbol{\theta}^s, s_{i(j-1)}^{AB} \right) \right] d\tilde{y}_{ijmr}^{AB} \\
&= \frac{1}{M_{\tilde{Y}}} \sum_{m=1}^{M_{\tilde{Y}}} f \left(x_{ij}^{AB} \mid l_{ij}^s, l_{i(j-1)}^s, \boldsymbol{\theta}^s, s_{i(j-1)}^{AB} \right) = f \left(x_{ij}^{AB} \mid l_{ij}^s, l_{i(j-1)}^s, \boldsymbol{\theta}^s, s_{i(j-1)}^{AB} \right).
\end{aligned}$$

Thus, we have shown that Equation 11 holds using Algorithm 4 for $j \geq 2$. Although we showed that Equation 11 holds for $j \geq 2$, it can be shown that Equation 11 holds for $j = 1$ in a similar way. Thus, we have shown that we can obtain unbiased samples of the pointwise predictive density. However, from Jensen's inequality, we know that $\hat{\text{llpd}} \geq \text{llpd}$. However, from simulation studies we will show that the bias is relatively small and has negligible effects on model comparison.

3.3 Numerical Approximation

One standard approach may be to use quadrature to approximate

$\int_0^\infty f_{X^{AB},L}(x, L_{ij} = \mathcal{S} \mid \boldsymbol{\theta}^s, l_{i(j-1)}^s, s_{i(j-1)}^{AB}) dx$. When calculating WAIC, we need to approximate integrals of this form $S \times \left(\sum_{i=1}^{N^{AB}} n_i^{AB} \right)$ times, where S is the number of MCMC samples considered when calculating WAIC. From numerical simulations, we found that using composite Simpson's 3/8 rule, we needed around 3000 evaluations of the function to get accurate approximations of integrals of that form. Therefore, evaluating $S \times \left(\sum_{i=1}^{N^{AB}} n_i^{AB} \right)$ is often not computationally tractable.

Often in these types of experiments, the duration of the AB trials is bounded. Thus, we can specify a time interval $\mathcal{T} := [0, T]$ such that $S_{ij}^{AB} \in \mathcal{T}$ for $i = 1, \dots, N^{AB}$ and $j = 1, \dots, n_i^{AB}$. To reduce the computational burden, we can specify a uniform grid of \tilde{p} points such that $\tilde{t}_1 = 0$ and $\tilde{t}_{\tilde{P}} = T$. Using these grid-points, we can calculate $\int_0^\infty f_{X^{AB},L}(x, L_{ij} = \mathcal{S} \mid \boldsymbol{\theta}^s, l_{i(j-1)}^s, \tilde{t}_p) dx$ for $p = 1, \dots, \tilde{P}$ and $s = 1, \dots, S$. Estimates of $\int_0^\infty f_{X^{AB},L}(x, L_{ij} = \mathcal{S} \mid \boldsymbol{\theta}^s, l_{i(j-1)}^s, s_{i(j-1)}^{AB}) dx$ can be obtained by using linear interpolation of the \tilde{P} evaluations across the uniform grid. An approximation of WAIC can be obtained using Algorithm 5.

Algorithm 5. Given the observed data $\{\mathbf{x}_i^A\}_{i=1}^{N^A}, \{\mathbf{x}_i^B\}_{i=1}^{N^B}, \{\mathbf{x}_i^{AB}\}_{i=1}^{N^{AB}}, \tilde{P}, \mathcal{T} := [0, T], N_{\text{simp}}$, and posterior samples $\boldsymbol{\theta}^s$ and \mathbf{l}_i^s for $i = 1, \dots, N^{AB}$ and $s = 1, \dots, S$, an approximation of WAIC can be obtained as follows:

1. Calculate $f_{X^{\mathcal{S}}}(x_{ij}^{\mathcal{S}} \mid \boldsymbol{\theta}^s, s_{i(j-1)}^{\mathcal{S}})$ using Equation 9 in the main manuscript for $\mathcal{S} = A, B, s = 1, \dots, S, i = 1, \dots, N^{\mathcal{S}},$ and $j = 1, \dots, n_i^{\mathcal{S}}$.

2. Let $\tilde{t}_p = \frac{(i-1)T}{\tilde{P}-1}$ ($p = 1, \dots, \tilde{P}$) create a uniform grid over \mathcal{T} . Let $\tilde{f}(L_{ij} = \mathcal{S} \mid \boldsymbol{\theta}^s, l_{i(j-1)}^s, \tilde{t}_p)$ be the approximation of $\int_0^\infty f_{X^{AB},L}(x, L_{ij} = \mathcal{S} \mid \boldsymbol{\theta}^s, l_{i(j-1)}^s, \tilde{t}_p) dx$ using composite Simpson's 3/8 rule with N_{simp} subintervals ($p = 2, \dots, \tilde{P}$ and $\mathcal{S} = A, B$). Similarly, for \tilde{t}_1 , let $\tilde{f}(L_{ij} = \mathcal{S} \mid \boldsymbol{\theta}^s, \tilde{t}_1)$ be the approximation of $\int_0^\infty f_{X^{AB},L}(x, L_{ij} = \mathcal{S} \mid \boldsymbol{\theta}^s, \tilde{t}_1) dx$.

3. For $s = 1, \dots, S$, $i = 1, \dots, N^{AB}$, and $j = 2, \dots, n_i^{AB}$ repeat the following:

- (a) Let $\tilde{f}_L(L_{ij} = \mathcal{S} \mid l_{i(j-1)}^s, \boldsymbol{\theta}^s, s_{i(j-1)}^{AB})$ be the approximation of $\int_0^\infty f_{X^{AB},L}(x, L_{ij} = \mathcal{S} \mid \boldsymbol{\theta}^s, l_{i(j-1)}^s, s_{i(j-1)}^{AB}) dx$ such that

$$\begin{aligned} \tilde{f}_L(L_{ij} = \mathcal{S} \mid l_{i(j-1)}^s, \boldsymbol{\theta}^s, s_{i(j-1)}^{AB}) &= \tilde{f}(L_{ij} = \mathcal{S} \mid \boldsymbol{\theta}^s, l_{i(j-1)}^s, \tilde{t}_{p*}) \\ &+ \frac{(s_{i(j-1)}^{AB} - \tilde{t}_{p*}) \left(\tilde{f}(L_{ij} = \mathcal{S} \mid \boldsymbol{\theta}^s, l_{i(j-1)}^s, \tilde{t}_{p*+1}) - \tilde{f}(L_{ij} = \mathcal{S} \mid \boldsymbol{\theta}^s, l_{i(j-1)}^s, \tilde{t}_{p*}) \right)}{\tilde{t}_{p*+1} - \tilde{t}_{p*}}, \end{aligned}$$

where $p*$ is such that $\tilde{t}_{p*} \leq s_{i(j-1)}^{AB} \leq \tilde{t}_{p*+1}$.

- (b) Approximate $f_{X^{AB}}(x_{ij}^{AB} \mid l_{ij}^s, l_{i(j-1)}^s, \boldsymbol{\theta}^s, s_{i(j-1)}^{AB})$ with

$$\tilde{f}_{X^{AB}}(x_{ij}^{AB} \mid l_{ij}^s, l_{i(j-1)}^s, \boldsymbol{\theta}^s, s_{i(j-1)}^{AB}) = \frac{f_{X^{AB},L}(x, L_{ij} = \mathcal{S} \mid \boldsymbol{\theta}^s, l_{i(j-1)}^s, s_{i(j-1)}^{AB})}{\tilde{f}_L(L_{ij} = \mathcal{S} \mid l_{i(j-1)}^s, \boldsymbol{\theta}^s, s_{i(j-1)}^{AB})}$$

4. For $s = 1, \dots, S$ and $i = 1, \dots, N^{AB}$ repeat the following:

- (a) Approximate $f_{X^{AB}}(x_{i1}^{AB} \mid l_{i1}^s, \boldsymbol{\theta}^s, s_{i0}^{AB})$ with

$$\tilde{f}_{X^{AB}}(x_{i1}^{AB} \mid l_{i1}^s, \boldsymbol{\theta}^s, s_{i0}^{AB}) = \frac{f_{X^{AB},L}(x, L_{i1} = \mathcal{S} \mid \boldsymbol{\theta}^s, s_{i0}^{AB})}{\tilde{f}(L_{i1} = \mathcal{S} \mid \boldsymbol{\theta}^s, \tilde{t}_1)}$$

5. Approximate the log pointwise predictive density by

$$\begin{aligned} \text{lpd} &= \sum_{\mathcal{S} \in \{A, B\}} \sum_{i=1}^{N^{\mathcal{S}}} \sum_{j=1}^{n_i^{\mathcal{S}}} \log \left(\frac{1}{S} \sum_{s=1}^S f_{X^{\mathcal{S}}}(x_{ij}^{\mathcal{S}} \mid \boldsymbol{\theta}^s) \right) \\ &+ \sum_{i=1}^{N^{AB}} \sum_{j=2}^{n_i^{AB}} \log \left(\frac{1}{S} \sum_{s=1}^S \tilde{f}_{X^{AB}}(x_{ij}^{AB} \mid l_{ij}^s, l_{i(j-1)}^s, \boldsymbol{\theta}^s, s_{i(j-1)}^{AB}) \right) \\ &+ \sum_{i=1}^{N^{AB}} \log \left(\frac{1}{S} \sum_{s=1}^S \tilde{f}_{X^{AB}}(x_{i1}^{AB} \mid l_{i1}^s, \boldsymbol{\theta}^s, s_{i0}^{AB}) \right). \end{aligned}$$

6. Approximate the effective number of parameters by

$$\begin{aligned}\tilde{p}_{\boldsymbol{\theta}} = & \sum_{\mathcal{S} \in \{A, B\}} \sum_{i=1}^{N^{\mathcal{S}}} \sum_{j=1}^{n_i^{\mathcal{S}}} \text{Var}_{s=1}^S \left(\log f_{X^{\mathcal{S}}} (x_{ij}^{\mathcal{S}} \mid \boldsymbol{\theta}^s) \right) \\ & + \sum_{i=1}^{N^{AB}} \sum_{j=1}^{n_i^{AB}} \left[\text{Var}_{s=1}^S \left(\log \tilde{f}_{X^{AB}} (x_{ij}^{AB} \mid l_{ij}^s, l_{i(j-1)}^s, \boldsymbol{\theta}^s, s_{i(j-1)}^{AB}) \right) \right] \\ & + \sum_{i=1}^{N^{AB}} \left[\text{Var}_{s=1}^S \left(\log \tilde{f}_{X^{AB}} (x_{i1}^{AB} \mid l_{i1}^s, \boldsymbol{\theta}^s, s_{i0}^{AB}) \right) \right].\end{aligned}$$

7. Approximate WAIC by $\tilde{\text{WAIC}} = \text{llpd} - \tilde{p}_{\boldsymbol{\theta}}$.

It is apparent from Algorithm 5, that most of the computational burden comes from Step 2. Specifically, the choice of N_{simp} and \tilde{P} will greatly impact the computational budget needed to approximate WAIC. Unlike the schemes specified in Algorithm 4 and Algorithm 5, we need to specify a grid of time points which will be used to approximate WAIC. For processes in which $I^{\mathcal{S}} \exp \{(\boldsymbol{\phi}^{\mathcal{S}} \mathbf{b}(t))\}$ ($\mathcal{S} = A, B$) is relatively constant over $t \in \mathcal{T}$, a relatively small \tilde{P} can be used to achieve accurate approximations of WAIC. Alternatively, if the firing rate changes rapidly over \mathcal{T} , a relatively large \tilde{P} may be needed to achieve accurate approximations to WAIC.

3.4 Marginal

A marginal version of WAIC can be calculated and, compared to the previous methods of calculating WAIC, is relatively fast to compute. Specifically, we can consider using the marginal likelihood, marginalizing out the labels (L_{ij}). As shown in [Watanabe and Oppen \(2010\)](#), WAIC is asymptotically equivalent to Bayesian leave-one-out cross-validation. While the previous schemes were akin to leave-one-spike-out cross-validation, the marginal WAIC proposed in this section is similar to leave-one-trial-out cross-validation. The marginal WAIC can be calculated using the normalization constants of Equation 12

in the main manuscript (forward filtration step). Specifically, we have that

$$f_{X^{AB}}(x_{ij}^{AB} \mid \{x_{ik}^{AB}\}_{k=1}^{j-1}, \boldsymbol{\theta}) = \sum_{\mathcal{S} \in \{A, B\}} \sum_{\mathcal{S}' \in \{A, B\}} \left[P(L_{i(j-1)} = \mathcal{S}' \mid \{x_{ik}^{AB}\}_{k=1}^{j-1}, \boldsymbol{\theta}) \right. \\ \left. \times f_{X^{AB}, L}(x_{ij}^{AB}, L_{ij} = \mathcal{S} \mid L_{i(j-1)} = \mathcal{S}', \boldsymbol{\theta}, s_{i(j-1)}^{AB}) \right].$$

From this we have $f_{\mathbf{X}}(\{x_{ik}\}_{k=1}^{n_i^{AB}} \mid \boldsymbol{\theta}) = f_{X^{AB}}(x_{i1}^{AB} \mid \boldsymbol{\theta}) \times \prod_{j=2}^{n_i^{AB}} f_{X^{AB}}(x_{ij}^{AB} \mid \{x_{ik}^{AB}\}_{k=1}^{j-1}, \boldsymbol{\theta})$.

Thus, we can calculate the marginal WAIC using Algorithm 6.

Algorithm 6. Given the observed data $\{\mathbf{x}_i^A\}_{i=1}^{N^A}$, $\{\mathbf{x}_i^B\}_{i=1}^{N^B}$, $\{\mathbf{x}_i^{AB}\}_{i=1}^{N^{AB}}$, and posterior samples $\boldsymbol{\theta}^s$ and \mathbf{l}_i^s for $i = 1, \dots, N^{AB}$ and $s = 1, \dots, S$, the marginal WAIC can be obtained as follows:

1. Calculate $f_{\mathbf{X}^{\mathcal{S}}}(\{x_{ij}^{\mathcal{S}}\}_{j=1}^{n_i^{\mathcal{S}}} \mid \boldsymbol{\theta}^s) = \prod_{j=1}^{n_i^{\mathcal{S}}} f_{X^{\mathcal{S}}}(x_{ij}^{\mathcal{S}} \mid \boldsymbol{\theta}^s, s_{i(j-1)}^{\mathcal{S}})$ using Equation 9 in the main manuscript for $\mathcal{S} = A, B$, $s = 1, \dots, S$ and $i = 1, \dots, N^{\mathcal{S}}$.
2. For $s = 1, \dots, S$ and $i = 1, \dots, N^{AB}$, repeat the following:

(a) Calculate

$$f_{X^{AB}}(x_{i1}^{AB} \mid \boldsymbol{\theta}^s) = \sum_{\mathcal{S} \in \{A, B\}} f_{X^{AB}, L}(x_{i1}^{AB}, L_{i1} = \mathcal{S} \mid \boldsymbol{\theta}^s).$$

(b) Run the forward filtration step, specified in Equation 12 of the main manuscript, to obtain $f_{X^{AB}}(x_{ij}^{AB} \mid \{x_{ik}^{AB}\}_{k=1}^{j-1}, \boldsymbol{\theta}^s)$ ($j = 2, \dots, n_i^{AB}$).

(c) Calculate

$$\tilde{f}_{\mathbf{X}^{AB}}(\{x_{ij}^{AB}\}_{j=1}^{n_i^{AB}} \mid \boldsymbol{\theta}^s) = f_{X^{AB}}(x_{i1}^{AB} \mid \boldsymbol{\theta}^s) \times \prod_{j=2}^{n_i^{AB}} f_{X^{AB}}(x_{ij}^{AB} \mid \{x_{ik}^{AB}\}_{k=1}^{j-1}, \boldsymbol{\theta}^s)$$

3. Calculate the marginal log pointwise predictive density by

$$\text{llpd} = \sum_{\mathcal{S} \in \{A, B\}} \sum_{i=1}^{N^{\mathcal{S}}} \log \left(\frac{1}{S} \sum_{s=1}^S f_{\mathbf{X}^{\mathcal{S}}}(\{x_{ij}^{\mathcal{S}}\}_{j=1}^{n_i^{\mathcal{S}}} \mid \boldsymbol{\theta}^s) \right) \\ + \sum_{i=1}^{N^{AB}} \log \left(\frac{1}{S} \sum_{s=1}^S \tilde{f}_{\mathbf{X}^{AB}}(\{x_{ij}^{AB}\}_{j=1}^{n_i^{AB}} \mid \boldsymbol{\theta}^s) \right).$$

4. Calculate the effective number of parameters by

$$p_{\boldsymbol{\theta}} = \sum_{\mathcal{S} \in \{A, B\}} \sum_{i=1}^{N^{\mathcal{S}}} \text{Var}_{s=1}^S \left(\log f_{\mathbf{X}^{\mathcal{S}}} \left(\{x_{ij}^{\mathcal{S}}\}_{j=1}^{n_i^{\mathcal{S}}} \mid \boldsymbol{\theta}^s \right) \right) \\ + \sum_{i=1}^{N^{AB}} \text{Var}_{s=1}^S \left(\log \tilde{f}_{\mathbf{X}^{AB}} \left(\{x_{ij}^{AB}\}_{j=1}^{n_i^{AB}} \mid \boldsymbol{\theta}^s \right) \right).$$

5. Calculate the marginal WAIC by $\text{WAIC} = \text{llpd} - p_{\boldsymbol{\theta}}$.

3.5 Simulation Study: Accuracy of WAIC Approximations

In this simulation study, we will evaluate the accuracy of the different algorithms proposed to approximate WAIC (Algorithm 3, Algorithm 4, and Algorithm 5). In this simulation, three versions of Algorithm 5 were considered, with $\tilde{P} = 25, 50$, and 100 ($N_{\text{simp}} = 3000$). For this simulation study, we consider the setting in which WAIC is calculated using Algorithm 5 with $\tilde{P} = 100$ to be the gold standard, as the grid of time points are relatively dense in \mathcal{T} . In the setting where we approximate WAIC using Algorithm 4, we set $M_{\tilde{X}} = 30$, $M_{\tilde{Y}} = 5$, and $R = 2$. Lastly, for the settings where we approximated WAIC using Algorithm 5, we set $M_{\tilde{X}} = 100$ and $R = 2$. Throughout this section, we refer to the different schemes as follows:

Method 1: Algorithm 5($\tilde{P} = 25, N_{\text{simp}} = 3000$),

Method 2: Algorithm 5($\tilde{P} = 50, N_{\text{simp}} = 3000$),

Method 3: Algorithm 5($\tilde{P} = 100, N_{\text{simp}} = 3000$),

Method 4: Algorithm 3($M_{\tilde{X}} = 100, R = 2$),

Method 5: Algorithm 4($M_{\tilde{X}} = 30, M_{\tilde{Y}} = 5, R = 2$).

To evaluate the performance of these methods, we generated 50 data sets from our

model by randomly sampling the model parameters in the following way:

$$\begin{aligned}
I^A &\sim \mathcal{N}^+(40, 16), \\
I^B &\sim \mathcal{N}^+(80, 16), \\
\sigma^A &\sim N^+(\sqrt{40}, 4), \\
\sigma^B &\sim N^+(\sqrt{80}, 4), \\
\delta &\sim \text{LogNormal}(-2.5, 0.5), \\
\phi^A &\sim \mathcal{N}_6(\mathbf{0}, 0.09\mathbf{I}_6), \\
\phi^B &\sim \mathcal{N}_6(\mathbf{0}, 0.09\mathbf{I}_6),
\end{aligned}$$

where \mathcal{N}^+ denotes a truncated normal distribution with support on $[0, \infty)$. In this simulation study, we considered $\mathcal{T} = [0, 1]$ and used B splines to capture the time inhomogeneity of the firing rates. Specifically, we used B-splines of degree 3, with boundary knots $(0, 1)$ and internal knots $(0.25, 0.5, 0.75)$. Once the 50 data sets were generated, MCMC was conducted to fit our model, with the 500 iterations for `Warm_Block_1` = 500, `Warm_Block_2` = 2000, and `N_MCMC` = 2000 (the total number of MCMC iterations is 4500). For the purposes of this experiment, the first 2250 MCMC iterations were discarded due to burn-in.

To evaluate the performance of the five schemes considered in this section, we will look at the relative error in the calculation of WAIC, LPPD, and the effective number of parameters. The relative error can be expressed as

$$\text{Relative Error} = \frac{\hat{x} - x}{x},$$

where x is the gold standard, or the “truth”, and \hat{x} is an estimate of x . In this simulation study, the relative errors were multiplied by 100 to be expressed as percentages. Since experiments typically have multiple recordings from different neurons (not simultaneous recordings), we will typically have to fit one model for each neuron, and we need to calculate WAIC for each model. Therefore, the computational cost will also be important when considering how to approximate WAIC.

Figure 4 contains a graphical representation of performance metrics, using Method 3 as the gold standard. As expected, as \tilde{P} increases in Algorithm 5, the accuracy of the

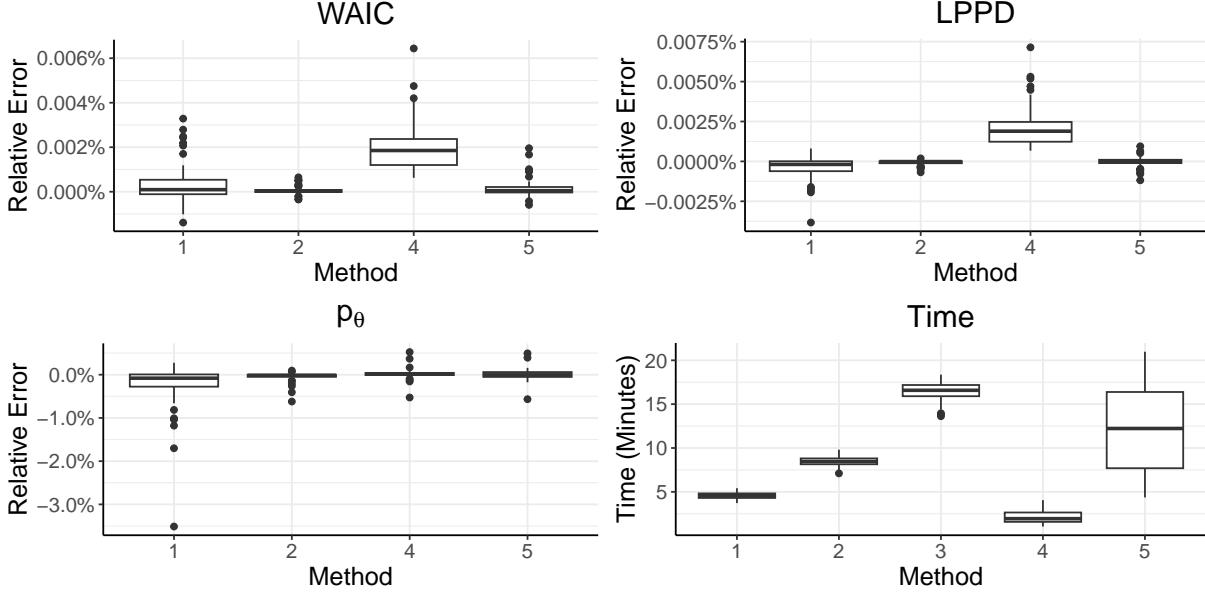


Figure 4: Performance metrics of the five schemes for approximating WAIC over the 50 data sets. The numerical approximation scheme with $\tilde{P} = 100$ (Method 3) was considered to be the gold standard, as was used as the “truth” for the relative error calculations.

approximations of WAIC increases, but the computational time also increases linearly with \tilde{P} . As shown in Section 3.2, the estimate of the pointwise predictive density using Algorithm 4 (Method 5) is unbiased; however, lppd is biased. However, from Figure 4, we can see that the bias is small, and it performs similarly to Method 2. However, Algorithm 4 requires a relatively large $M_{\tilde{X}}$ and/or $M_{\tilde{Y}}$ to obtain estimates of WAIC, making it computationally expensive. In particular, if $M_{\tilde{X}}$ is too small, such that $(\tilde{x}_{ijm1})_{m'} > \tilde{y}_{ijm1}$ for all m' and m ($1 \leq m' \leq M_{\tilde{X}}$ and $1 \leq m \leq M_{\tilde{Y}}$), then $\hat{w}_{ijm1} = 0$ for $1 \leq m \leq M_{\tilde{Y}}$, and $\hat{f}_{X^{AB}}^1(x_{ij}^{AB} | l_{ij}^s, l_{i(j-1)}^s, \theta^s, s_{i(j-1)}^{AB}) = 0$. Thus, the approximated log pointwise predictive density will be $-\infty$. In our simulation study, we experienced this in 10 out of 50 simulations, and these simulations were removed when creating Figure 4. Therefore, in some cases, larger $M_{\tilde{x}}$ and / or $M_{\tilde{y}}$ may be needed, which requires even more computational resources. Moreover, we can see that the distribution of time taken to approximate WAIC using Algorithm 4 (Method 5) has a long tail, meaning that some data sets required significantly longer time to approximate WAIC. This is because the method requires rejection

sampling, which can be inefficient when $[1 - F_{X^{\mathcal{S}^C}}(x_{ij}^{AB} - \delta \mathbb{1}\{l_{i(j-1)} = \mathcal{S}\})]$ is small.

From Figure 4, it is apparent that approximating WAIC using Algorithm 3 (Method 4) is the fastest method out of the five methods considered in this simulation study. Although it results in a biased estimate of WAIC, the relative error is very small, around 0.003%. Compared to Method 3, the median difference in WAIC was -1.13 (range of (-3.96, -0.37)), while the median WAIC calculated using Method 3 was -60172.09 (range of (-90780.41, -43750.57)). This small bias is unlikely to have a significant impact on the results of model selection, making this method a fast and relatively reliable way to estimate WAIC. It is important to note that improved accuracy can be obtained by increasing $M_{\tilde{x}}$.

This simulation study showed that approximating WAIC using Algorithm 5 (Methods 1-3) is reliable and also has some advantages and disadvantages over Algorithm 3 and Algorithm 4. The first advantage is that the computational burden does not really depend on the number of spikes observed. Since we only evaluated $\int_0^\infty f_{X^{AB}, L}(x, L_{ij} = \mathcal{S} \mid \boldsymbol{\theta}^s, l_{i(j-1)}^s, s_p) dx$ over a finite grid of values s_p ($1 \leq p \leq \tilde{P}$), the algorithm can scale well for samples with a large number of observed spikes. On the other hand, the accuracy of this will depend on how rapidly $I^{\mathcal{S}} \exp\{(\boldsymbol{\phi}^{\mathcal{S}} \mathbf{b}(t))\}$ ($\mathcal{S} = A, B$) changes over $t \in \mathcal{T}$. If it changes rapidly, a more dense grid of points may be needed to achieve accurate approximations.

Although each algorithm has advantages and disadvantages, we suggest using Algorithm 3 to approximate WAIC, as it is relatively fast and accurate, and does not require specifying a grid of points over which we will approximate $\int_0^\infty f_{X^{AB}, L}(x, L_{ij} = \mathcal{S} \mid \boldsymbol{\theta}^s, l_{i(j-1)}^s, s_p) dx$. Although the estimates of WAIC are slightly biased, the bias is unlikely to affect the model selection results.

3.6 Simulation Study 2: Marginal vs. Conditional WAIC

In this simulation study, we study how conditional WAIC compares to marginal WAIC in model selection. To approximate conditional WAIC, we will use Algorithm 3 with $M_{\tilde{x}} = 100$. Alternatively, marginal WAIC is available in closed form and can be quickly calculated using Algorithm 6. In this simulation study, we generated 100 data sets from the proposed model, as well as 100 data sets where the spike trains observed under the A , B , and

AB stimuli are generated from separate inverse Gaussian processes. These 200 data sets will be used to evaluate the performance of marginal WAIC and conditional WAIC compared to the WAIC obtained by assuming a model that assumes a separate inverse Gaussian process for spike trains generated from each of the three conditions ($\mathcal{H} = \{A, B, AB\}$). We will refer to the latter version of WAIC as the “IIGPP-WAIC” and the corresponding model as the “IIGPP model” .

The 100 data sets generated from the proposed model were created by randomly sampling the model parameters in the following way:

$$\begin{aligned}
I^A &\sim \mathcal{N}^+(40, 16), \\
I^B &\sim \mathcal{N}^+(80, 16), \\
\sigma^A &\sim N^+(\sqrt{40}, 4), \\
\sigma^B &\sim N^+(\sqrt{80}, 4), \\
\delta &\sim \text{LogNormal}(-2.5, 0.5), \text{ (for 80\% of the data sets)} \\
\delta &= 0, \text{ (for 20\% of the data sets)} \\
\phi^A &\sim \mathcal{N}_6(\mathbf{0}, 0.09\mathbf{I}_6), \\
\phi^B &\sim \mathcal{N}_6(\mathbf{0}, 0.09\mathbf{I}_6),
\end{aligned}$$

where \mathcal{N}^+ denotes a truncated normal distribution with support on $[0, \infty)$. In this simulation study, we considered $\mathcal{T} = [0, 1]$ and used B splines to capture the inhomogeneity of the firing rates over time. Specifically, we used B-splines of degree 3, with boundary knots $(0, 1)$ and internal knots $(0.25, 0.5, 0.75)$. The 100 data sets generated from the three inverse Gaussian processes were created by randomly sampling the model parameters in

the following way:

$$\begin{aligned}
I^A &\sim \mathcal{N}^+(40, 16), \\
I^B &\sim \mathcal{N}^+(80, 16), \\
I^{AB} &\sim \mathcal{N}^+(80, 64), \\
\sigma^A &\sim N^+(\sqrt{40}, 4), \\
\sigma^B &\sim N^+(\sqrt{80}, 4), \\
\sigma^{AB} &\sim N^+(\sqrt{60}, 16), \\
\phi^A &\sim \mathcal{N}_6(\mathbf{0}, 0.09\mathbf{I}_6), \\
\phi^B &\sim \mathcal{N}_6(\mathbf{0}, 0.09\mathbf{I}_6), \\
\phi^{AB} &\sim \mathcal{N}_6(\mathbf{0}, 0.09\mathbf{I}_6).
\end{aligned}$$

From Figure 5 and Figure 6, we can see that both marginal and conditional WAIC were highly informative in suggesting the competition model when the simulated data were generated from the competition model and suggesting the IIGPP model when the data were generated from the IIGPP model. Specifically, both the marginal and conditional WAIC were less than the IIGPP-WAIC for each of the 100 simulations where data were generated from the competition model. Although we used Algorithm 3 to calculate the conditional WAIC which is biased, we can see that the differences between conditional WAIC and IIGPP-WAIC were much larger than the empirically estimated bias in Section 3.5; suggesting that the bias did not significantly affect the results from this simulation study. On average, the conditional WAIC was smaller than the marginal WAIC, especially when δ is small or the number of observed switches is large. When the data were generated from the IIGPP model, the conditional WAIC was less than the IIGPP-WAIC for 98 out of the 100 simulations, while the marginal WAIC was less than the IIGPP-WAIC for all 100 of the simulations. Although both conditional and marginal WAIC were informative in determining whether the data were generated from the competition framework, we suggest using marginal WAIC over conditional WAIC due to the slightly better performance in distinguishing when data were generated from an IIGPP model and because the marginal WAIC can be calculated up to machine precision. We note that while marginal WAIC

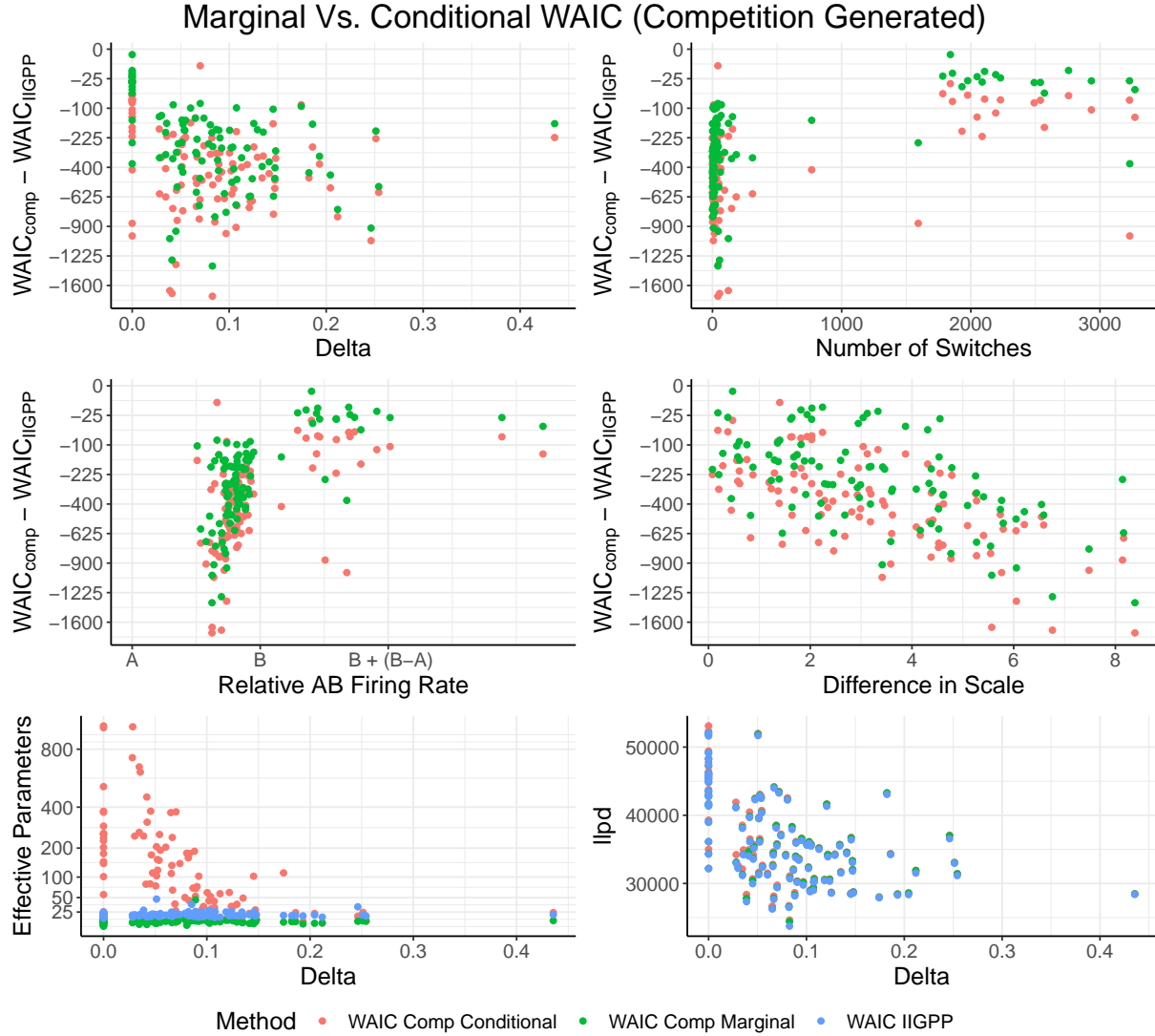


Figure 5: Visualizations of marginal and conditional WAIC compared to IIGPP-WAIC from data generated from the proposed competition model. The top-left panel visualizes the WAIC estimates as a function of the delta used to generate the data. The top-right panel visualizes the WAIC estimates as a function of the true number of switches from the A process to the B process (or vice versa) in the AB spike trains. The middle-left panel visualizes the WAIC estimates as a function of the expected number of spikes in a spike train generated under the AB stimulus, compared to the expected number of spikes generated under the A stimulus or B stimulus alone. The middle-right panel visualizes the WAIC estimates as a function of the distance between σ^A and σ^B . The two bottom panels visualize the effective number of parameters and llpd as a function of the true delta used to generate the data.

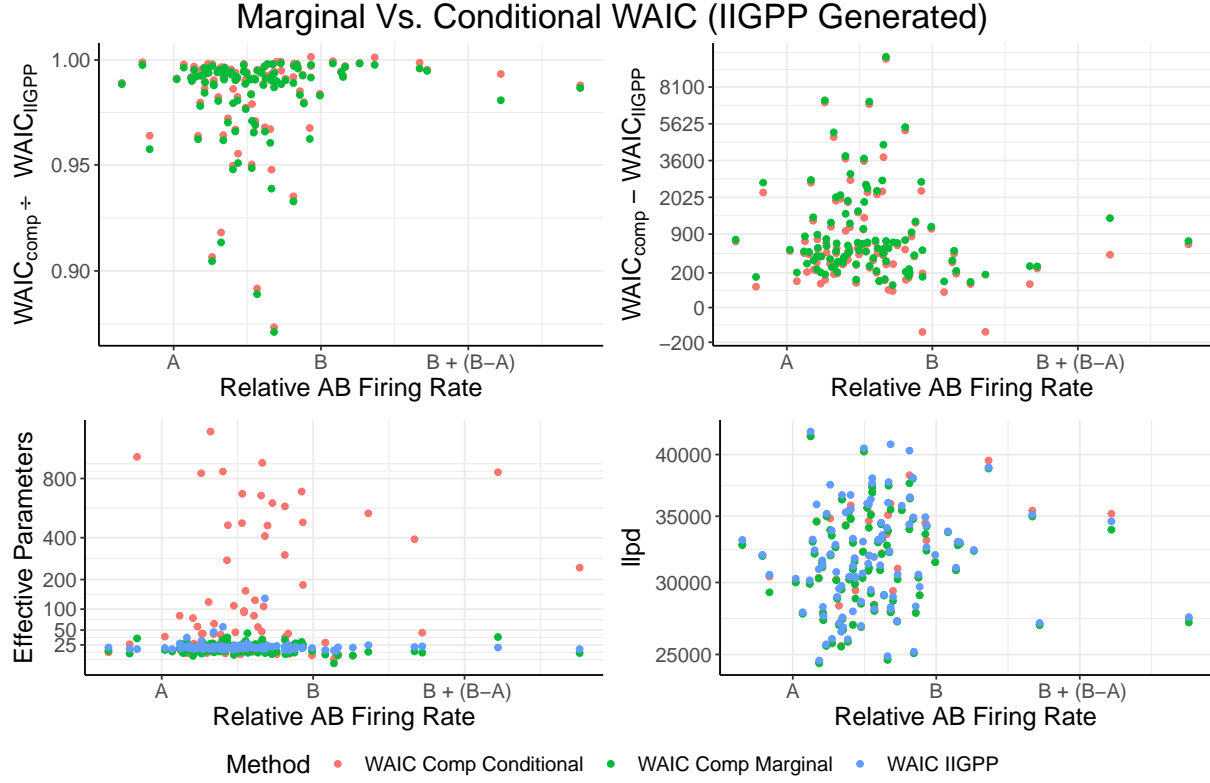


Figure 6: Visualizations of marginal and conditional WAIC compared IIGPP-WAIC from data generated from the IIGPP model. The top panels visualize the how marginal and conditional WAIC compare to IIGPP-WAIC as a function of the expected number of spikes in a spike train generated under the AB stimulus, compared to the expected number of spikes generated under the A stimulus or B stimulus alone. The two bottom panels visualize the effective number of parameters and llpd.

does not need to be approximated, the computational cost to calculate marginal WAIC is similar to approximating conditional WAIC using Algorithm 3.1 with $M_{\hat{X}} = 100$.

This simulation study also shows that when $\delta = 0$, WAIC can be informative in determining whether the AB -stimulus spike trains were generated from the competition process or if the AB -stimulus spike trains follow an inverse Gaussian process. We note that if we assumed a Poisson process, the ISIs would follow an exponential distribution. Thus, the competition process would assume that the ISIs of the AB -stimulus spike trains, which would be the minimum of two random variables that are exponentially distributed, could also be represented as an exponential distribution. Thus, the resulting AB -stimulus spike train could be modeled as a Poisson process when $\delta = 0$. Although this result does not hold for ISIs that have an inverse Gaussian distribution, it was unclear whether the information criteria could differentiate between the competition model and the IIGPP model when $\delta = 0$.

As stated in the main manuscript, conditional WAIC is akin to leave-one-spike-out cross-validation, while marginal WAIC is akin to leave-one-spike-train-out cross-validation. From Figure 5 and Figure 6, we can see that the effective number of parameters for the conditional WAIC increases greatly when δ is small. This increase in the effective number of parameters occurs because there is more switching, meaning there is more heterogeneity in the labels. Alternatively, the marginal calculation did not see a similar increase in the effective number of parameters since the labels were marginalized out.

3.7 Simulation Study 3: WAIC Performance under Partial Switching Behavior

In this section, we are interested in exploring the performance of conditional and marginal WAIC when only a proportion $\alpha \in (0, 1)$ of the observations come from the competition framework, and $(1 - \alpha)$ come from the IIGPP framework. With this simulation study, we aim to shed light on why conditional WAIC suggest the competition model while marginal WAIC suggests the IIGPP model. To study the performance of the information criteria under partial switching behavior, we generated 100 datasets from a mixture of the

IIGPP model and the competition model and calculated the information criteria of interest (Marginal WAIC, Conditional WAIC, IIGPP WAIC). The 100 datasets were generated as follows:

$$\begin{aligned}
I^A &\sim \mathcal{N}^+(40, 16), \\
I^B &\sim \mathcal{N}^+(80, 16), \\
I^{AB} &\sim \mathcal{N}^+(80, 64) \\
\sigma^A &\sim N^+(\sqrt{40}, 4), \\
\sigma^B &\sim N^+(\sqrt{80}, 4), \\
\sigma^{AB} &\sim N^+(\sqrt{60}, 16), \\
\delta &\sim \text{LogNormal}(-2.5, 0.5), \\
\phi^A &\sim \mathcal{N}_6(\mathbf{0}, 0.09\mathbf{I}_6), \\
\phi^B &\sim \mathcal{N}_6(\mathbf{0}, 0.09\mathbf{I}_6), \\
\phi^{AB} &\sim \mathcal{N}_6(\mathbf{0}, 0.09\mathbf{I}_6), \\
N_{Comp}^{AB} &\sim \text{Unif}(\{n \in \mathbb{N} | 2 \leq n \leq 24\}), \\
\mathcal{S}_1^{AB}, \dots, \mathcal{S}_{N_{Comp}^{AB}}^{AB} &\sim \text{Competition Framework}(I^A, I^B, \sigma^A, \sigma^B, \delta), \\
\mathcal{S}_{N_{Comp}^{AB}+1}^{AB}, \dots, \mathcal{S}_{25}^{AB} &\sim \text{IIGPP}(I^{AB}, \sigma^{AB}), \\
\mathcal{S}_1^A, \dots, \mathcal{S}_{25}^A &\sim \text{IIGPP}(I^A, \sigma^A), \\
\mathcal{S}_1^B, \dots, \mathcal{S}_{25}^B &\sim \text{IIGPP}(I^B, \sigma^B).
\end{aligned}$$

Figure 7 contains the results from the simulation study. We can see that on average, conditional WAIC is more likely to recommend the competition framework when compared to marginal WAIC. We can see that there is a significant amount of heterogeneity in the WAIC values, but even with roughly 10% of the observations coming from the competition framework, the marginal WAIC will sometimes recommend the competition framework over the IIGPP framework.

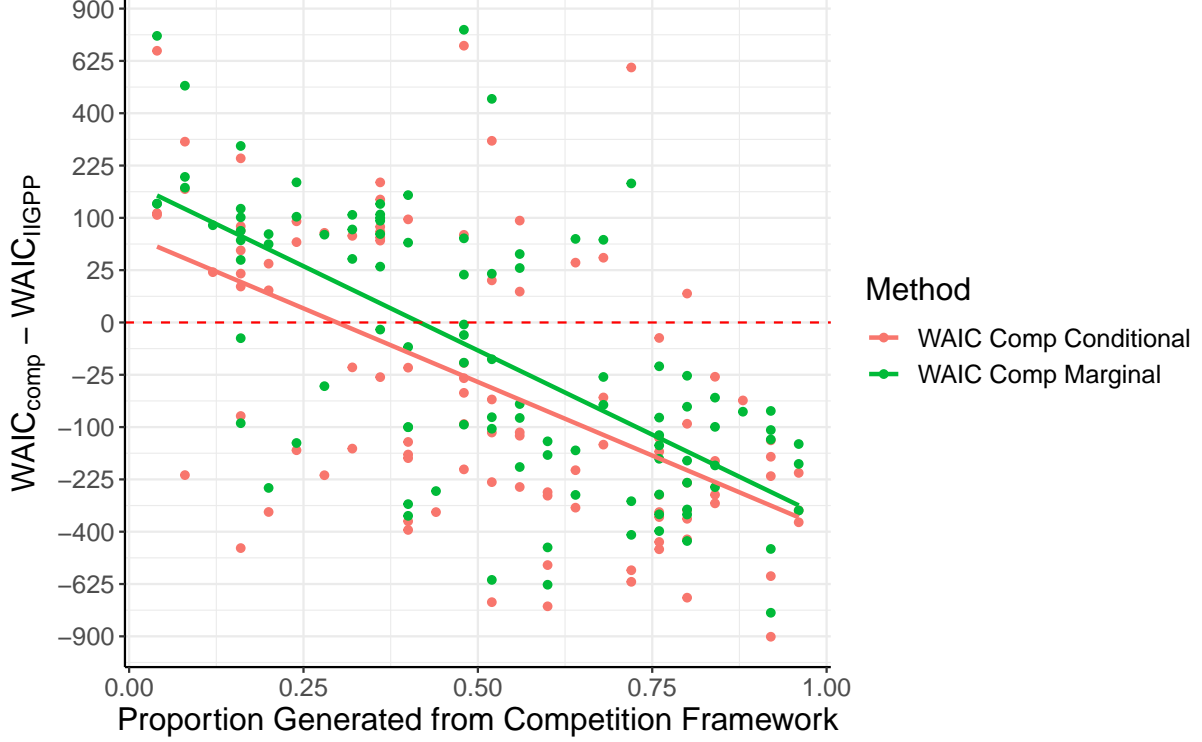


Figure 7: Performance of Marginal and Conditional WAIC when only a subset of the *AB* trials are generated from the competition framework.

4 Simulation Study: Empirical Convergence

Table 1 provides the empirical coverage obtained from the simulation study conducted in Section 4 of the main manuscript. We can see that the coverage of the credible intervals is nominal, covering the true parameter value roughly 95% of the time under the various sample sizes. We can also see that as we gain more information (more spike trains), the width of the credible intervals decreases, as expected.

5 Case Study: Caruso

This section of the Supplementary Materials contains additional information on the analysis of the IC spike trains collected in [Caruso et al. \(2018\)](#).

$N^A = N^B = N^{AB}$	$I^{\mathcal{S}} \exp \left((\boldsymbol{\phi}^{\mathcal{S}})^{\top} \mathbf{b}(t) \right)$	$\sigma^{\mathcal{S}}$	δ
25	96.0% (1)	95% (1)	97.0% (1)
50	95.7% (0.583)	96% (0.696)	93.9% (0.407)
100	92.9% (0.299)	96% (0.489)	97.0% (0.005)

Table 1: Observed empirical coverage for 95% credible intervals of the model parameters, with average relative credible interval lengths (shown in parenthesis). The coverage for $I^{\mathcal{S}} \exp \left((\boldsymbol{\phi}^{\mathcal{S}})^{\top} \mathbf{b}(s) \right)$ is pointwise-coverage, evaluated on a dense finite-dimensional grid over \mathcal{T} .

5.1 Inclusion Criteria

To be included in the analysis, the triplet must satisfy the following conditions:

1. At least five trials for each of the three conditions (A , B , and AB),
2. single-stimulus spike trains can be represented by a time-inhomogeneous inverse Gaussian point process,
3. Distinguishably different distributions of spike trains for the A and B conditions.

The first one ensures that we have a sufficient amount of data for each of the three conditions and is straightforward to implement. The second condition will remove any triplets where the single-stimuli conditions (A or B conditions) are a mixture of processes or multiplexing itself. The screening is done by calculating posterior p-values (Meng, 1994; Gelman et al., 1996) and discarding any triplets where the p-values are less than 0.05 for either the A or B conditions for any of the discrepancy variables. Specifically, the three discrepancy variables we use when calculating the posterior p-values are

1. Average Log-Likelihood – measure of average discrepancy between observed ISIs and the posited distributions of the ISIs under the modeling assumptions.

$$D_{avg-LL}(\{\mathbf{x}_i^{\mathcal{S}}\}_{i=1}^{N^{\mathcal{S}}}, \boldsymbol{\theta}) := \int \left(\prod_{i=1}^{N^{\mathcal{S}}} \prod_{j=1}^{n_i^{\mathcal{S}}} f_{X^{\mathcal{S}}}(x_{ij}^{\mathcal{S}} \mid \boldsymbol{\theta}) \right) f(\boldsymbol{\theta} \mid \{\mathbf{x}_i^{\mathcal{S}}\}_{i=1}^{N^{\mathcal{S}}}) d\boldsymbol{\theta},$$

2. Mean Number of Spike Counts – measure of average discrepancy between the observed mean spike counts and the posited mean spike count under the modeling assumptions.

$$D_{mean-SC}(\{\mathbf{x}_i^{\mathcal{S}}\}_{i=1}^{N^{\mathcal{S}}}, \boldsymbol{\theta}) := \left| \frac{1}{N^{\mathcal{S}}} \sum_{i=1}^{N^{\mathcal{S}}} n_i^{\mathcal{S}} - \mathbb{E}_{\boldsymbol{\theta}}(n^{\mathcal{S}}) \right|,$$

3. Mean Number of Spike Counts – measure of average discrepancy between the sample variance of the spike counts and the posited variance of spike counts under the modeling assumptions.

$$D_{var-SC}(\{\mathbf{x}_i^{\mathcal{S}}\}_{i=1}^{N^{\mathcal{S}}}, \boldsymbol{\theta}) := \left| \frac{1}{N^{\mathcal{S}} - 1} \sum_{i=1}^{N^{\mathcal{S}}} (n_i^{\mathcal{S}} - \overline{n_i^{\mathcal{S}}})^2 - \text{Var}_{\boldsymbol{\theta}}(n^{\mathcal{S}}) \right|,$$

where $\mathbb{E}_{\boldsymbol{\theta}}(n^{\mathcal{S}})$ and $\text{Var}_{\boldsymbol{\theta}}(n^{\mathcal{S}})$ are the expectation and variance of the trial-wise spike count with respect to the fitted model, respectively. Using the defined discrepancy metrics, we can define the tail area to get the corresponding posterior predictive p-value as follows:

$$p(y) = P\left(\{D(\tilde{\mathbf{x}}_i^{\mathcal{S}}\}_{i=1}^{N^{\mathcal{S}}}, \boldsymbol{\theta}) \geq D(\{\mathbf{x}_i^{\mathcal{S}}\}_{i=1}^{N^{\mathcal{S}}}, \boldsymbol{\theta}) \mid \{\mathbf{x}_i^{\mathcal{S}}\}_{i=1}^{N^{\mathcal{S}}}, H\right),$$

where H denotes the model and $\tilde{\mathbf{x}}_i^{\mathcal{S}}$ denotes a spike train generated from the posterior predictive distribution. Algorithm 7 provides an outline of how we calculate the posterior p-values.

Algorithm 7. Given the spike trains recorded under stimulus \mathcal{S} ($\{\mathbf{x}_i^{\mathcal{S}}\}_{i=1}^{N^{\mathcal{S}}}$) and draws from the posterior distribution $\boldsymbol{\theta}^1, \dots, \boldsymbol{\theta}^S$ we can simulate the posterior p-values as follows:

1. Let $K_h(n)$ be a Gaussian kernel with bandwidth h , and let the corresponding Gaussian kernel density estimate be $\hat{f}(n \mid n_1^{\mathcal{S}}, \dots, n_{N^{\mathcal{S}}}^{\mathcal{S}})_h = \sum_{i=1}^{N^{\mathcal{S}}} K_h(n - n_i^{\mathcal{S}})$. Find h_{crit} such that $h_{crit} := \inf\{h \mid \hat{f}(n \mid n_1^{\mathcal{S}}, \dots, n_{N^{\mathcal{S}}}^{\mathcal{S}})_h \text{ is unimodal (i.e. one maxima)}\}$.
2. For $j = 1, \dots, N_{Boot}$, repeat the following:
 - (a) Generate the bootstrapped spike counts $\mathcal{N}_j = \{\tilde{n}_{1j}^{\mathcal{S}}, \dots, \tilde{n}_{N^{\mathcal{S}}j}^{\mathcal{S}}\}$ as follows:

$$\tilde{n}_{ij} = \left\lfloor \bar{n} + [(y - \bar{n} + h_{crit} * z) / \sqrt{2}] \right\rfloor,$$

where $y \sim \mathcal{N}(0, 1)$, $\bar{n} := \frac{1}{N^{\mathcal{S}}} \sum_{i=1}^{N^{\mathcal{S}}} n_i^{\mathcal{S}}$, y is a uniform draw from $\{n_1^{\mathcal{S}}, \dots, n_{N^{\mathcal{S}}}^{\mathcal{S}}\}$, and $\lfloor x \rfloor$ is x rounded to the nearest integer, for $i = 1, \dots, N^{\mathcal{S}}$. Note that this is similar to the method described in [Efron \(1992\)](#).

(b) Calculate $\hat{f}(n | \mathcal{N}_j)$ and set $M_i^{max} = \# \text{ of modes of } \hat{f}(n | \mathcal{N}_j)$.

3. Estimate the p-value as

$$p = \frac{|\{i \mid M_i^{max} > 1\}|}{N_{Boot}},$$

where $|\mathcal{A}|$ is the cardinality of the set \mathcal{A} .

To verify the triplet has distinguishably different distributions of spike trains for the A and B conditions, we fit a joint model and compare the pointwise predictive distributions of the joint model and separate model. Specifically, for the joint model, we assume that

$$f_X^{joint}(x_{ij}^{\mathcal{S}} \mid I, \sigma, \phi, s_{i(j-1)}^{\mathcal{S}}) = \frac{1}{\sigma \sqrt{2\pi}(x_{ij}^{\mathcal{S}})^3} \exp \left(-\frac{\left(1 - I \exp \left\{ (\phi)^{\top} \mathbf{b} \left(s_{i(j-1)}^{\mathcal{S}} \right) \right\} x_{ij}^{\mathcal{S}} \right)^2}{2(\sigma)^2 x_{ij}^{\mathcal{S}}} \right), \quad (13)$$

for $\mathcal{S} = A, B$. Thus we can see that both the A and B distribution of spike trains share the same parameters (I, σ, ϕ) . For the separate models, we have

$$f_{X^A}(x_{ij}^A \mid \boldsymbol{\theta}, s_{i(j-1)}^A) = \frac{1}{\sigma^A \sqrt{2\pi}(x_{ij}^A)^3} \exp \left(-\frac{\left(1 - I^A \exp \left\{ (\phi^A)^{\top} \mathbf{b} \left(s_{i(j-1)}^A \right) \right\} x_{ij}^A \right)^2}{2(\sigma^A)^2 x_{ij}^A} \right), \quad (14)$$

$$f_{X^B}(x_{ij}^B \mid \boldsymbol{\theta}, s_{i(j-1)}^B) = \frac{1}{\sigma^B \sqrt{2\pi}(x_{ij}^B)^3} \exp \left(-\frac{\left(1 - I^B \exp \left\{ (\phi^B)^{\top} \mathbf{b} \left(s_{i(j-1)}^B \right) \right\} x_{ij}^B \right)^2}{2(\sigma^B)^2 x_{ij}^B} \right). \quad (15)$$

We can see that the A and B condition spike trains have there own parameters $(I^{\mathcal{S}}, \sigma^{\mathcal{S}}, \phi^{\mathcal{S}})$. We will conclude that the triplet has distinguishably different distributions of spike trains for the A and B conditions if the following holds:

$$\text{llpd}_{seperate} - \text{llpd}_{joint} > \log(3),$$

where

$$\begin{aligned}\text{llpd}_{joint} &= \sum_{\mathcal{S} \in \{A, B\}} \sum_{i=1}^{N^{\mathcal{S}}} \sum_{j=1}^{n_i^{\mathcal{S}}} \log \left(\frac{1}{S} \sum_{s=1}^S f_X^{joint}(x_{ij}^{\mathcal{S}} \mid I^s, \sigma^s, \phi^s, s_{i(j-1)}^{\mathcal{S}}) \right), \\ \text{llpd}_{seperate} &= \sum_{\mathcal{S} \in \{A, B\}} \sum_{i=1}^{N^{\mathcal{S}}} \sum_{j=1}^{n_i^{\mathcal{S}}} \log \left(\frac{1}{S} \sum_{s=1}^S f_{X^{\mathcal{S}}}(x_{ij}^{\mathcal{S}} \mid \boldsymbol{\theta}^s, s_{i(j-1)}^{\mathcal{S}}) \right),\end{aligned}$$

where S is the number of MCMC samples. From the 2225 triplets recorded in [Caruso et al. \(2018\)](#), 1241 triplets passed the first criterion of at least five trials per condition. From there, 983 of the 1241 triplets passed the second criterion of unimodality of spike counts. Lastly, we arrive at the final number of 891 triplets that fit all three criteria for inclusion.

5.2 Simultaneously Recorded Cells

A subset of the 166 neurons recorded in the [Caruso et al. \(2018\)](#) dataset were recorded simultaneously with another neuron (two neurons recorded at the same time). Thus, we have access to pairs of simultaneously recorded spike trains from two different neurons in the IC. The recording of these spike trains are a very time intensive and skill intensive task, which can lead to potential concerns of shifting of the probes or other artifacts that can influence the spike trains. Thus in this subsection, we will explore whether the results of one neuron seem to be dependent on the results of the other simultaneously recorded neuron. Although dependence could indicate that perhaps a large population of neurons are simultaneously multiplexing and not a result of artificial artifacts, independent results would suggest that the findings are not due to movement of the probe, movement of the monkey, or other artifacts. Table 2 contains the results of the preferred model (competition vs. IIGPP) using WAIC. When performing Fisher’s exact test, we obtain a p-value of 0.384, indicating that we did not observe a significant amount of dependence in the model selection results between the two simultaneously recorded neurons.

		Neuron 1						
		IIGPP	WTA (P)	WTA (NP)	Marg	Cond	Comp	Total
Neuron 2	IIGPP	0	0	1	0	3	0	4
	WTA (P)	0	0	1	0	3	0	4
	WTA (NP)	0	0	0	0	1	1	2
	Marg	0	0	0	0	0	0	0
	Cond	1	2	1	0	3	5	12
	Comp	0	0	4	0	6	4	14
	Total	1	2	7	0	16	10	36

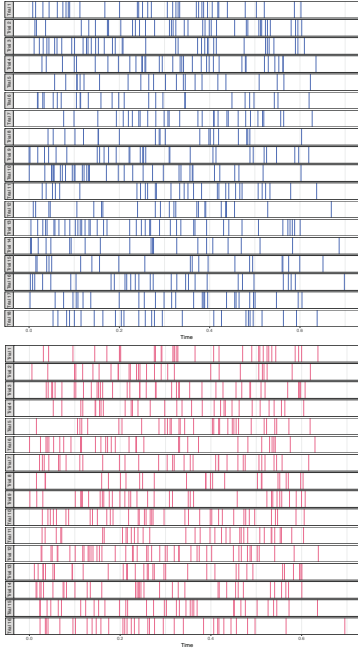
Table 2: Contingency table showing the results of WAIC from the subset of simultaneously recorded neurons (two cells simultaneously recorded). The p-value obtained from performing Fisher’s exact test is 0.504.

5.3 Conditional WAIC Suggests Multiplexing, but not Marginal WAIC

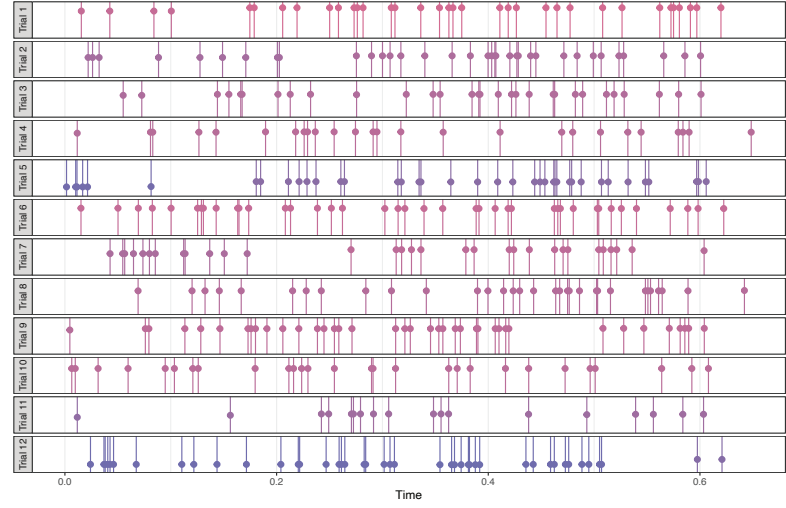
From the main manuscript, we can see that the conditional WAIC suggested the competition model, but the marginal WAIC suggested the IIGPP model for 309 triplets. From Simulation Study 3 in Section 3.7 of the Supplementary Materials, we can see that the conditional WAIC is more likely to suggest the competition model when the neuron multiplexes in only a subset of the trials.

Figure 8 contains the spike trains of two triplets where conditional WAIC suggested the competition model, but marginal WAIC did not. In both of these examples, we can see that slow switching appears to occur in a subset of the AB trials, however, there are trials that appear to be averaging the A and B processes. This suggests that there may be something more complicated going on in a subset of these triplets, which may require a more flexible model. It may be that I^A and I^B should be able to change between trials, which could indicate larger-scale changes in neural circuits. It could be that δ should be able to change between trials, or perhaps multiplexing is not neuron specific and other

A



Cell ID: PSIC031711_cell1
Stimulus A: 1100Hz@6
Stimulus B: 742Hz@-24



B

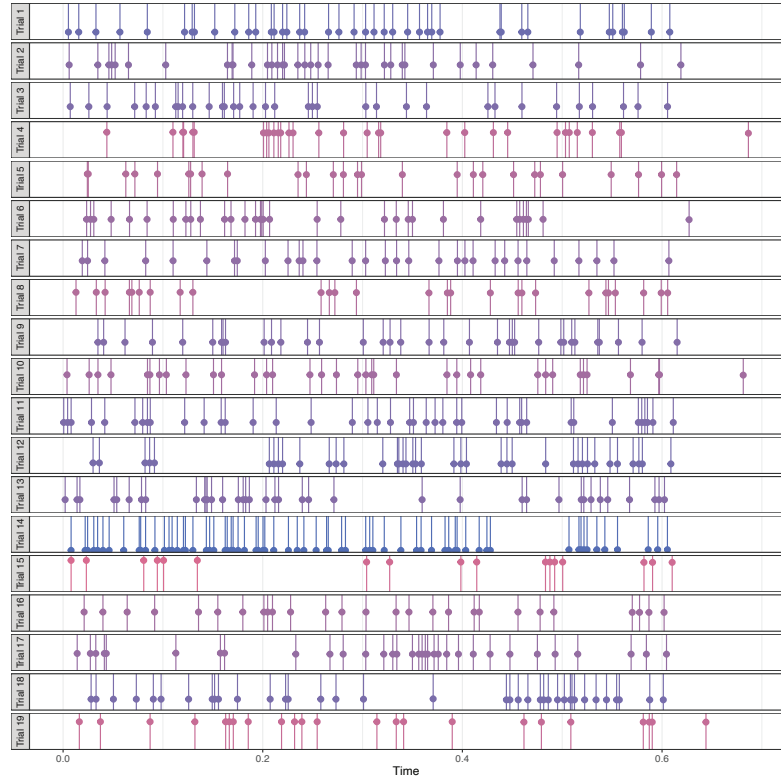
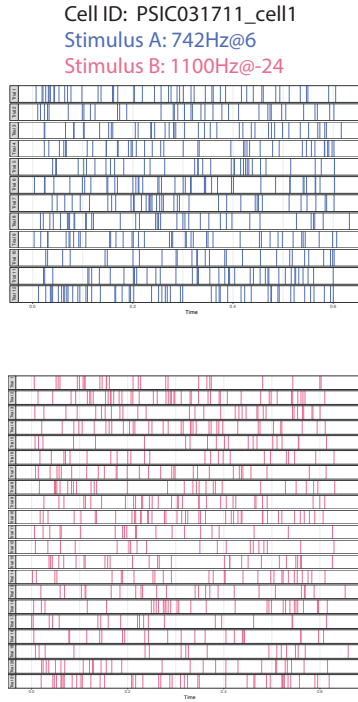


Figure 8: Two examples of Triplets where conditional WAIC suggests the competition model, but marginal WAIC suggests the IIGPP model.

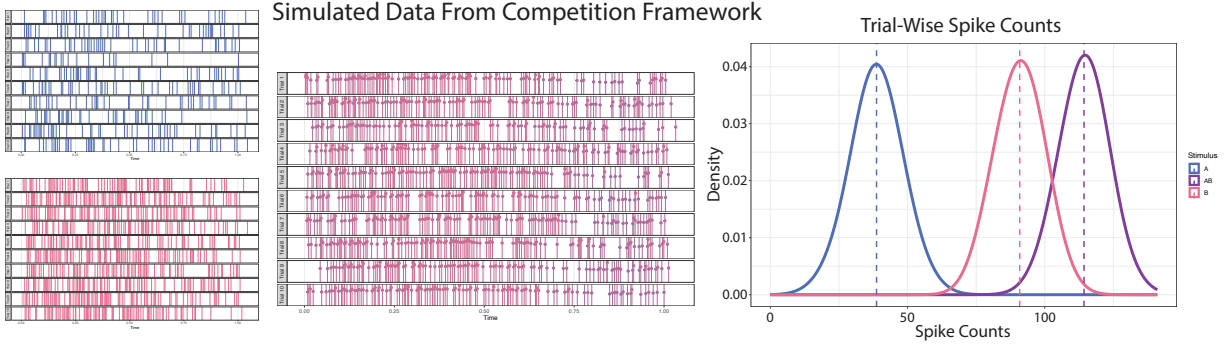


Figure 9: Results from a triplet generated from the competition framework with $\delta = 0$.

conditions (not modeled) influence a neuron’s propensity to multiplex. Future studies including simultaneous recordings may give us insight into some of these questions, leading to more flexible and powerful models. Nevertheless, the cases where conditional WAIC suggested the competition model, but marginal WAIC did not, are of interest and will likely influence future work.

5.4 Can We Recover Which Stimulus is Encoded in a Spike?

As evident from the case study, we are able to recover which stimulus a set of spikes is encoding when δ is large or moderate. However, we can see that we were not able to recover which stimulus a spike was encoding when δ was small in the case study. As δ becomes smaller, recovering the stimulus for which a spike is encoding for becomes a more challenging task. However, as shown in Section 3.6, both Marginal and Conditional WAIC are able to determine whether the data were generated from the Competition Framework or the IIGPP model. From Figure 9, we can see that even under data simulated from the model, we are unable to recover which stimulus a set of spikes is encoding.